2017

BODIPY-based Red Sensitizers for Near-infrared Emission of Lanthanide Complexes

Priyangika Prasadini Senevirathne
Eastern Illinois University

The Graduate School
EASTERN ILLINOIS UNIVERSITY

Thesis Maintenance and Reproduction Certificate

FOR: Graduate Candidates Completing Theses in Partial Fulfillment of the Degree
Graduate Faculty Advisors Directing the Theses

RE: Preservation, Reproduction, and Distribution of Thesis Research

---

Preserving, reproducing, and distributing thesis research is an important part of Booth Library's responsibility to provide access to scholarship. In order to further this goal, Booth Library makes all graduate theses completed as part of a degree program at Eastern Illinois University available for personal study, research, and other not-for-profit educational purposes. Under 17 U.S.C. § 108, the library may reproduce and distribute a copy without infringing on copyright; however, professional courtesy dictates that permission be requested from the author before doing so.

Your signatures affirm the following:

- The graduate candidate is the author of this thesis.
- The graduate candidate retains the copyright and intellectual property rights associated with the original research, creative activity, and intellectual or artistic content of the thesis.
- The graduate candidate certifies her/his compliance with federal copyright law (Title 17 of the U. S. Code) and her/his right to authorize reproduction and distribution of all copyrighted materials included in this thesis.
- The graduate candidate in consultation with the faculty advisor grants Booth Library the non-exclusive, perpetual right to make copies of the thesis freely and publicly available without restriction, by means of any current or successive technology, including by not limited to photocopying, microfilm, digitization, or internet.
- The graduate candidate acknowledges that by depositing her/his thesis with Booth Library, her/his work is available for viewing by the public and may be borrowed through the library's circulation and interlibrary loan departments, or accessed electronically.
- The graduate candidate waives the confidentiality provisions of the Family Educational Rights and Privacy Act (FERPA) (20 U. S. C. § 1232g; 34 CFR Part 99) with respect to the contents of the thesis and with respect to information concerning authorship of the thesis, including name and status as a student at Eastern Illinois University.

I have conferred with my graduate faculty advisor. My signature below indicates that I have read and agree with the above statements, and hereby give my permission to allow Booth Library to reproduce and distribute my thesis. My adviser's signature indicates concurrence to reproduce and distribute the thesis.

Graduate Candidate Signature _____ Faculty Adviser Signature _____

Printed Name _____ Printed Name _____

Master of Science in Chemistry
Graduate Degree Program

5/30/2017
Date

Please submit in duplicate.

BODIPY-based Red Sensitizers for Near-infrared Emission of Lanthanide Complexes

(TITLE)

BY

Priyangika Prasadini Senevirathne

THESIS

SUBMITTED IN PARTIAL FULFILLMENT OF THE REQUREMENTS FOR
THE DEGREE OF

Master of Science in Chemistry

IN THE GRADUATE SCHOOL, EASTERN ILLINOIS UNIVERSITY
CHARLESTON, ILLINOIS

2017
YEAR

I HEREBY RECOMMEND THAT THIS THESIS BE ACCEPTED AS FULFILLING
THIS PART OF THE GRADUATE DEGREE CITED ABOVE

5/22/17
THESIS COMMITTEE CHAIR DATE

DEPARTMENT/SCHOOL CHAIR DATE
OR CHAIR'S DESIGNEE

05/22/2017
THESIS COMMITTEE MEMBER DATE

5/22/17
THESIS COMMITTEE MEMBER DATE

5/22/17
THESIS COMMITTEE MEMBER DATE

BODIPY-based Red Sensitizers for Near-infrared Emission of Lanthanide Complexes

PRIYANGIKA PRASADINI SENEVIRATHNE

Research Advisor: Dr. Hongshan He

Department of Chemistry

Eastern Illinois University

TABLE OF CONTENTS

ABBREVIATIONS

1. NIR – Near-infrared
2. BODIPY – Boron dipyrromethene
3. DDQ – 2,3-Dichloro-5,6-dicyano-1,4-benzoquinone
4. DO3A – 1,4,7,10-Tetraazacyclododecane-1,4,7-triacetic acid
5. NIS – N-Iodosuccinimide
6. DMSO - Dimethyl sulfoxide

ABSTRACT

During the past 20 years there has been a remarkable growth in the use of the fluorescence technique in biological studies. Fluorescence and time-resolved fluorescence spectroscopy are considered primary research tools in the field of biochemistry. Currently, fluorescence spectroscopy is a dominant methodology and used widely in biotechnology and medical diagnosis process. One impediment in using fluorescent probes is the fluorescence of biological substrates and fluorescence of diagnostic probes are significantly overlapped, and it decreases the detection sensitivity. Also, commercially available probes require UV or near-UV light excitation, causing severe degradation of biological substrates. Near-infrared emitting lanthanide complexes can overcome this problem by enhancing the detection sensitivity.

BODIPY dyes have gained significant attention in application of fluorescence sensing and imaging in recent years, because they possess many desirable properties such as high extinction coefficient, narrow absorption and emission bands, high quantum yield and low photobleaching effect. One strategy to overcome the low detection sensitivity of fluorescent dyes is; shift the absorbance and emission of BODIPY precursor towards the longer wavelength regions by increasing the π-conjugation of a sensitizer. BODIPY molecules are especially responsive to this method.

Four BODIPY-based ligands and four Yb(III) lanthanide complexes have been synthesized, which bear 5-ethynyl-5'-methyl-2,2'-N-bipyridine ligand-binding-group (LBG) in the C2 position and either a hydrogen (PH1), an iodine (PH2), an 4-ethynylbenzoic acid (PH3) or an 1-ethynyl-4-isothiocyanatobenzene (PH4) groups in its

C6 position. This study focused to test their ability to sensitize the luminescence of NIR emission of Yb(III) ion. All ligands exhibited broader absorption with high molar absorption coefficients. The PH3 ligand displays maximum absorption at (573 nm). The typical metal centered luminescence is detected at 980 nm for Yb(III) upon excitation at their maximal absorption position in the visible region. All complexes showed similar lifetimes in the NIR region (10.9 – 11.1 μs), which corresponds to emission yield of 0.09%. This study demonstrates that the BODIPY-bipyridine ligands are adequate for sensitizing the luminescence of NIR-emitting lanthanide ions, allowing excitation wavelengths extending into the red region of the visible spectrum.

ACKNOWLEDGEMENTS

It is with the deepest sense of gratitude and appreciation to my supervisor, Dr Hongshan He, for giving me all the valuable guidance, encouragement, motivation and patients throughout this project. At many stages in the course of this research project I benefited from his advice, particularly so when exploring new ideas. His positive attitude and confidence in my research inspired me and gave me confidence to improve my weak points.

I would like to thank Eastern Illinois University, and specifically the Chemistry Department, the Graduate School, National Science Foundation, the College of Science as well as the Chemistry Department stockroom staff for their help. I would also like to thank my thesis committee; Dr. Kraig A. Wheeler, Dr. Radu F. Semeniuc and Dr. Gopal R. Periyannan for their assistance, guidance, and patients during the course of my degree.

I also wish to express my deepest gratitude to Dr. Radu F. Semenuic for giving me valuable guidance while synthesizing the 5-ethynyl-5'-methyl-2,2'-N-bipyridine group and for granting me access to the glovebox facility in his lab. I would like to acknowledge Dr. Kraig A. Wheeler for X-ray diffraction analysis and Dr. Barbara A. Lawrence for NMR training.

I wish to remember my family and loving parents who stand behind me with their encouragement and research colleagues for their positive support and encouragement.

LIST OF FIGURES

LIST OF TABLES

Chapter 1

INTRODUCTION

1.0 General Overview

There has been an increasing demand for luminescence probes with a high sensitivity, low toxicity, and low cost. However, biological substrates have numerous fluorescent active groups.[1] The biological substrate fluorescence and diagnostic probes fluorescence are significantly overlapped. Therefore, it decreases the detection sensitivity.[2] The test sensitivity depends on the ratio of materials and background signals. Also, commercially available probes cause some severe biological degradation due to the UV or near-UV light excitation.[3] Near-infrared emitting organic complexes have overcome this problem. It also has the potential to enhance the detection sensitivity because biological substrates do not exhibit NIR emission. The NIR light luminescent probes can be used in *in-vivo* medical diagnosis process because of its deep tissue penetration capability.[4] Lanthanide ions such as Nd(III), Yb(III), Er(III), Tm(III), Sm(III), Ho(III), and Pr(III) emit in NIR region. NIR emission from lanthanide ions is difficult to obtain by direct excitation because of its weak f-f transition absorption.[5] To solve this problem, chromophores (antenna) are usually attached to lanthanide ions to form coordinated complexes. After absorption of UV light and intersystem crossing, the organic chromophore is excited from its ground state to its excited state. Then the energy transfers to the lanthanide excited state *via* an intramolecular energy transfer process. When lanthanide ion returns to its ground state, produces a characteristic NIR emission. A large number of lanthanide complexes have been studied. However, these complexes only emit under the UV or near

UV light illumination causing severe degradation and poor detection sensitivity.[4-5] In this study, borondipyrromethene (BODIPY) was used as an organic chromophore to sensitize the ytterbium (III) ion, because of its excellent biocompatibility and stability for medical applications.[5] This study focused on Yb(III) ion since it has only one excited state and emits at 980 nm strongly. These complexes were found to be sensitized under long wavelength region.

1.1 Phenomena of Fluorescence

Fluorescence phenomenon was reported by Sir John Frederick William Herschel. He observed fluorescence from a quinine solution under the sunlight in 1845. The development of the first spectrofluorometer appeared in 1950 with the rapid development of fluorescence technology. Luminescence can be categorized into two forms: fluorescence and phosphorescence, which are determined by the nature of the excited state of the compound.[6,7] The molecules which have fluorescent properties are known as fluorophores, and typically they are aromatic compounds (pyrene, quinine, anthracene). Fluorescence spectra are depended upon the chemical structure of the fluorophore and dissolved solvent.[1]

The principles of the absorption and emission are usually illustrated by the Jablonski diagram, which was introduced by Alexander Jablonski.[1] Jablonski is regarded as the father of spectroscopy because of his many achievements in the fluorescence spectroscopic field. The energy levels S0, S1, and S2, are depicted by singlet ground, first and second electronic states, respectively. Several processes usually occur under the light irradiation. The fluorophores are excited to higher vibrational levels, either S1 or S2. Then the molecules rapidly relax to the lowest vibrational level of S1 (Figure 1.0). The

process of internal conversion happens within 10^{-12} s or less that is smaller than the fluorescence lifetimes 10^{-8} s.[8] So this internal conversion process usually completes prior to the fluorescence. The fluorophores in the lowest vibrational state of S1 return to an excited vibrational state at the level of the S0, releasing the energy through emission of photons. This process is known as fluorescence. As a consequence of emission to an excited vibrational state of S0, the emission spectrum acts as a mirror image of an absorption spectrum of the S0 to S1 transition. [1,9] The fluorophores in the excited state of S1 transfer to the triplet state T1 *via* intersystem crossing process between different spin states. The transition process from the T1 to the S0 state is known as phosphorescence, and it has long wavelength emission relative to the fluorescence due to the lower energy level of T1 relative to the S1 state. As a consequence of this, the emission rate of phosphorescence is smaller than that of fluorescence.[10]

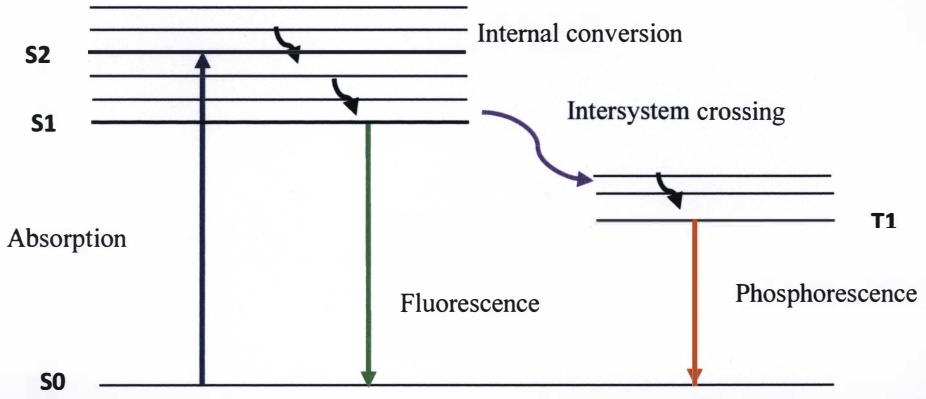

Figure 1.0 One form of a Jablonski diagram: S0; ground state, S1, S2; excited state, T1; triplet state

1.2 Characteristics of Fluorescence

1.2.1 Representation of fluorescence data

Fluorescence data is typically shown as an emission and excitation spectra. The plot is shown as the fluorescence intensity *vs* wavelength (nm). The intensity and the shape of the fluorescence spectrum depends on the chemical structure, solvent, excited states and other factors.[1] The symmetric nature of this excitation and emission exhibits the same transitions in both absorption and emission and also the similar vibrational energy levels S_0 and S_1.

1.2.2 Stokes shift

The Jablonski diagram explains that the energy of emission is always less than the absorption. This reduction is because of the longer wavelength of emission than the absorption (Figure 1.2). In 1852, Sir G. G. Stokes discovered wavelength shift known as the "Stokes shift." The Stoke shift causes further loss of excitation energy by thermalization of excess vibrational energy. The rapid decay to the lowest vibrational level of S1 and decay to the lowest vibrational level of S0 affect the energy loss process. The typical fluorescence spectrum has a broad emission spectrum with mirror image absorption spectrum of S0 - S1 transitions. Fluorescence displays a smaller Stokes shift than the phosphorescence because triplet energy level is lower than the singlet level involved in fluorescence.[1,11]

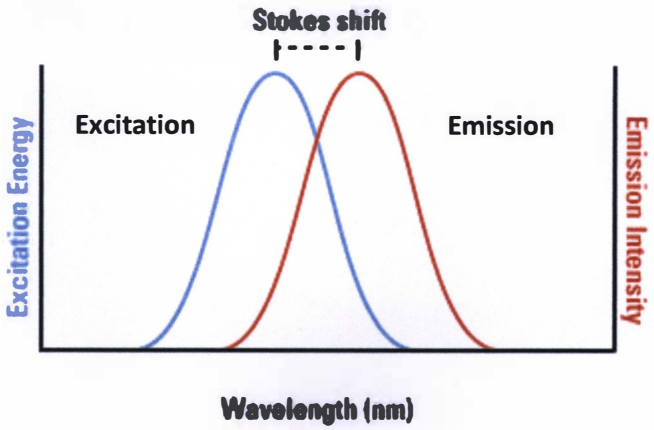

Figure 1.2 Stokes shift[12]

1.3 Applications of Fluorescence

Fluorescence sensing and imaging technology have been growing in various fields of modern science during the past 20 years. This technology has become a very powerful and essential tool in the area of biotechnology, molecular biology, environmental science and clinical diagnostic. This method is more important compared to the traditional methods like electrochemical detection, chemo-absorptive detections, NMR and radio tracing in chemical recognition events, especially for biological sensing and imaging analysis. The biological sensors are an analytical device, used for the detection of an analyte that combines a biological component with a physicochemical detector. The sensitive biological elements like tissue, microorganisms, organelles, cell receptors, enzymes, antibodies and nucleic acid are biologically derived material or biomimetic component that interacts with the analyte under study.[1,12]

1.3.1 Fluorescence sensing and fluorescence probes

Fluorescence sensing is an ideal technology for the biological diagnostic non-invasive processes with ultra-high sensitivity and specificity. It does not consume or destruct analytes surrounding objectives.[13] Also, it has a rapid response time (10^{-8} s), and fluorescence travel without a physical guide as a reference material, which extensively simplifies this technique with low costs.[1] Fluorescence sensing technology has become the most important technique for diagnosis and screening purposes in the medical field.[14] Fluorescent probe is a key component of fluorescence sensing technology because it has some ability to convert chemical events to detectable fluorescent signals. It is also correlated with sensitivity, specificity and response range.

The fluorescence sensing and imaging are dependent on the desired properties of fluorescent probes. The designed fluorescent probes should have an ability to respond selectively and specifically to the analyte of interest without any interference.[8] Brightness of the fluorescence should be sharp as possible because it can obtain high quantum yield and large extinction coefficient at the excitation wavelength. Also, the chemo stability and the photostability of the fluorescent probes should be at a high level. Most of the properties in fluorescent probes suffer from photobleaching due to the instability.[11]

Application of the fluorescent probes inside of living cells or biological tissues is a much more complicated process. Therefore, these probes should have some features to give a proper outcome in the biological sensing and imaging diagnosis process. The size of the fluorescent dyes should be suitable to allow its insertion into the biological system, and the typical size range is from 0.5-2.0 nm. Molar absorptivity of these dyes is around 103-105 $M^{-1}cm^{-1}$ and Stokes shift is short and typically ranges from 10-100 nm. The

maximum excitation wavelength depends on the chemical structure of the fluorescent dyes and spectroscopic techniques being used.[15]

The biological sensing and labeling molecular fluorescent dyes have unique absorption and emission properties relative to the radioactive labeling and electrochemical sensing absorbance based dyes. These chromophores are much more sensitive, non-invasive and more informative compared to the other dyes. Nowadays, scientists have synthesized different types of chromophores that absorb and emit in the visible to near infrared regions. The most important chromophore families are rhodamines, cyanines, fluorescein and BODIPY.[15]

1.4 BODIPY dyes

BODIPY dyes have many advantages compared with the other three fluorescent chromophores mention above. Boron dipyrromethene (BODIPY) dyes are good candidates because of their excellent spectroscopic and chemical properties such as high molar extinction coefficient, high fluorescence quantum yields, excellent photostability, coupled with chemical versatility, color tunability, moderate redox potential, and negligible sensitivity to solvent and temperature. In this research, BODIPY was used as the main skeleton fluorophore to synthesize new BODIPY ligands.[15,16,17]

In 1968, Triebs and Kreuzer first investigated the fluorescent active BODIPY dyes by reacting pyrrole and acetic anhydride. IUPAC name of BODIPY is 4,4-Difluoro-4-bora-3a,4a-diaza-s-indacene. The BODIPY core is formed by linking dipyrromethene ligand through the N-B-N bridge. It delocalized the positive charge *via* resonance equilibrium. According to the X-ray diffraction single crystal structure, BODIPY core has a fused

planar twelve member framework, and two fluorine atoms are bound to the boron atom leading to a tetrahedral geometry.[18] According to the IUPAC numbering system, BODIPY core has eight functional positions and these also label as α-, β- and *meso*-positions (Figure 1.3). The substituted BODIPY dyes are easier to synthesize than unsubstituted dyes because of high stability. Particularly, the hydrogen atoms at the α-positions of the pyrrole ring are substituted by two methyl groups to prevent further electrophilic substitution. The BODIPY dyes can be functionalized using different types of reactions like electrophilic substitution at 2, 6- positions, condensation reactions at 3,5 or 2,6 positions, or nucleophilic substitution at 3,5 or 4 or 8 positions.[15] Researchers have been modifying these π-conjugated molecules for biological sensing and imaging applications. However, they are facing many challenges because of the undesirable characteristics of BODIPY dyes like hydrophobicity, lack of efficient sensing for toxic species and intracellular pH and transition metal ions. Additionally, the short wavelength absorption and emission cause biological degradation to the tissues. To overcome the problem of low sensitivity and biological degradation, researchers have synthesized NIR-emissive BODIPY-lanthanide fluorescent probes for biological sensing and imaging applications.[24]

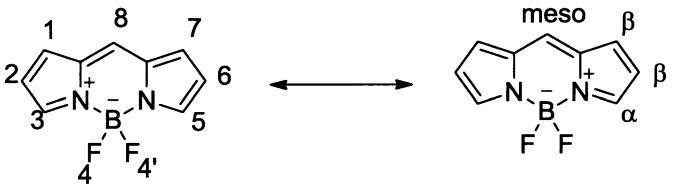

Figure 1.3 Structure of BODIPY core and numbering system

1.4.1 Synthesis of BODIPY dyes

BODIPY dyes can be synthesized using a one pot method *via* the condensation reaction of pyrrole and aldehyde, acid chloride or acid anhydride. The reaction produces two intermediates: dipyrrolmethane and dipyrrin. DDQ (2,3-dichloro-5,6-dicyano-1,4-benzoquinone) is used as an oxidant to synthesize dipyrrin from dipyrrolmethane to synthesize BODIPY using aldehydes (Figure 1.4). Then boron trifluoride diethyl etherate (BF_3•Et_2O) is added to the reaction mixture under basic conditions to synthesize a fluorescent active BODIPY.[15, 23, 24]

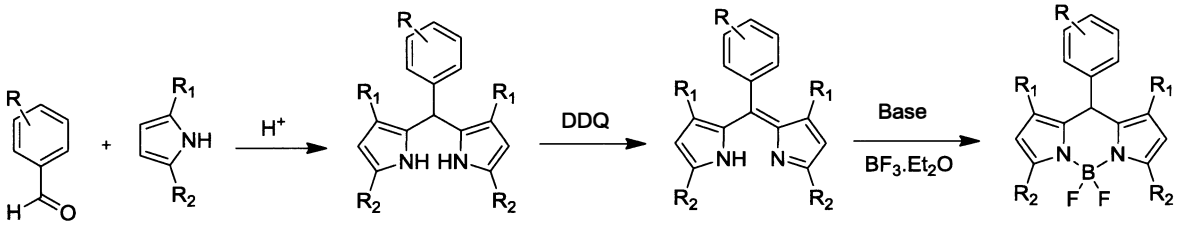

Figure 1.4 Synthetic route of BODIPY dyes using aromatic aldehyde

1.4.2 Modification of BODIPY core

The properties of the BODIPY dye can be altered by modifying the BODIPY core. There are four main positions in the BODIPY core, 3, 2, 8 carbon centers, and 4 boron center. These active positions can be modified by attaching different types of organic fragments to its core structure.[15]

1.4.2.1Functionalization at the 2,6-positions of BODIPY core

A simple examination of the structure (Figure 1.5) reveals that the least positive charge is at the 2- and 6- positions if BODIPY core. This electron rich 2 and 6 positions facilitate the electrophilic substitution reaction like halogenation, formylation, nitration and

sulfonation. The halogenation reaction can undergo iodination reaction by slowly adding a iodine source (NIS) to the BODIPY reaction mixture (Figure 1.6).[19] In this research, iodination reaction was used for the purpose of further modification of BODIPY core. The π- conjugation between the iodine and BODIPY core increases the λ_{abs} and λ_{em} with 20-50 nm from initial BODIPY molecule absorption.

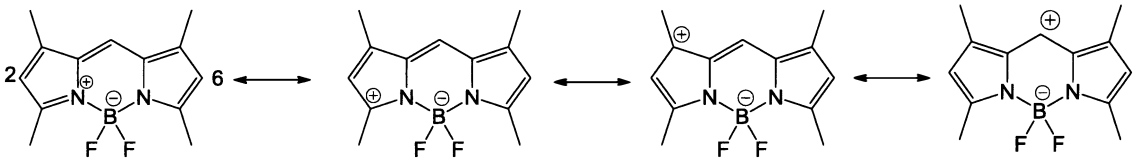

Figure 1.5 Resonance structures of BODIPY core

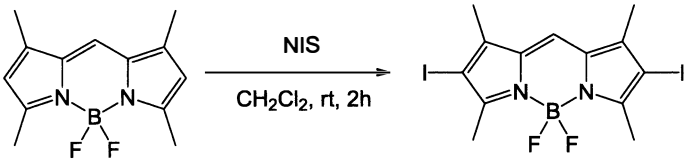

Figure 1.6 Iodination of BODIPY dyes

Quantum yield of the dyes is decreased due to the intersystem crossing of electrons from the excited state to the triplet state of the BODIPY dye because of the "heavy atom" effect from iodine atom.[20,21] Halogenated BODIPY dyes are good starting materials in the synthesis of long conjugated systems through various carbon-carbon cross coupling reactions, like Sonogashira, Heck or Suzuki procedures (Figure 1.7).[15,18]

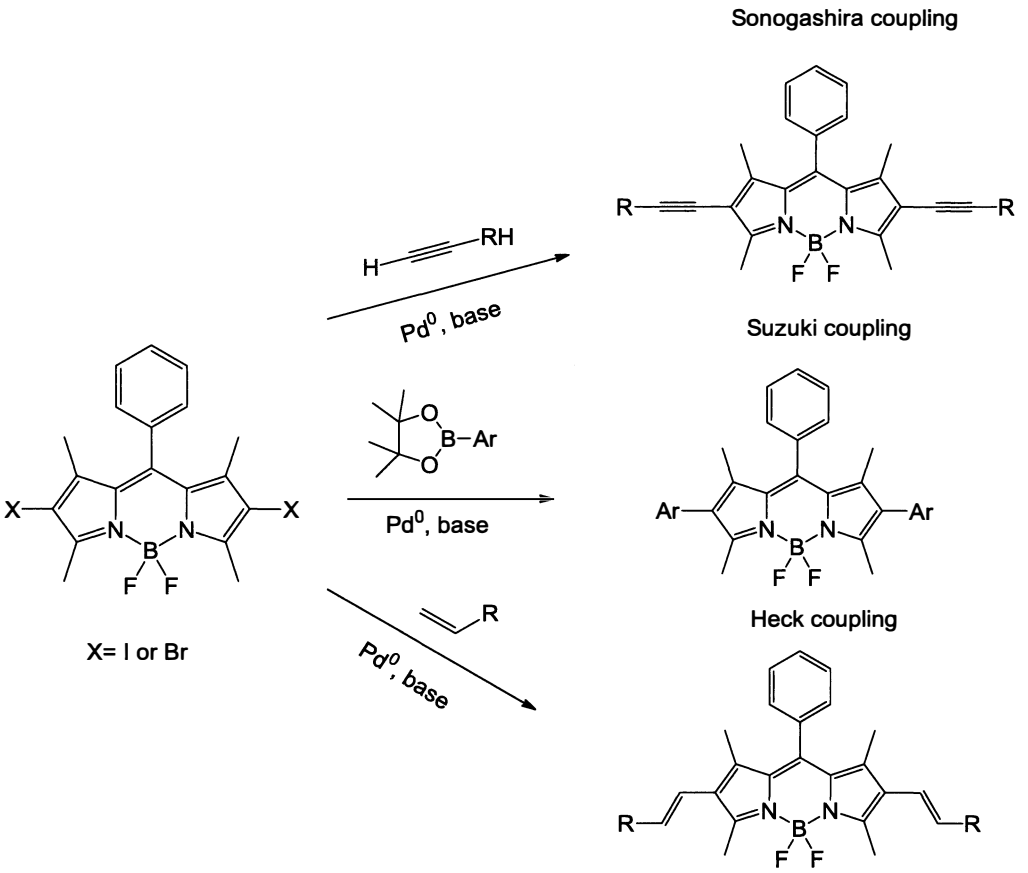

Figure 1.7 Cross-coupling reactions of 2,6- position of BODIPY core

1.4.2.2 Sonogashira coupling reaction

The Sonogashira coupling reaction is one of the most useful cross-coupling methods to form conjugated enynes or aryl alkynes using C-C and C-heteroatom bonds.[22] The reaction is based on a palladium compound used as a catalyst and CuI as a co-catalyst (Figure 1.8). The active palladium catalyst reacts with a halogenated molecule in an oxidative addition step to produce a Pd^{II} intermediate, complex A. The formed complex A undergoes a transmetallation step with the copper acetylide and form out complex B. The CuI is allowed to form the conjugated enynes and aryl alkynes by pairing with a palladium catalyst.[23,24] Complex B is changed from trans to cis to produce complex C. In

the final step, complex C undergoes a reductive elimination process and generates the target alkyne compound with regeneration of the palladium catalyst.

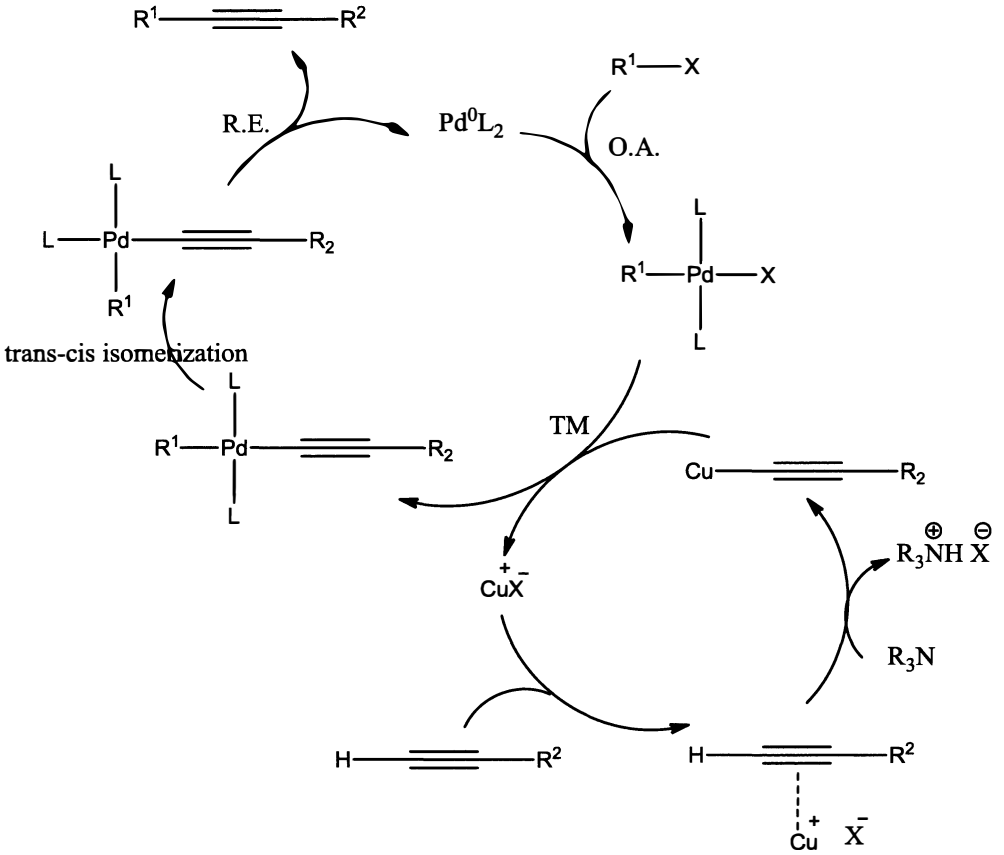

Figure 1.8 Mechanism of Sonogashira cross-coupling reaction

1.5 Lanthanide Luminescence

Lanthanide metals are part of the *f*-block elements and have [Xe]$4f^n5s^25p^6$ electronic configuration. The lanthanide luminescence originates from f-f transitions in the $4f^n$ shell.[25, 26] There are some factors that limit the luminescence at the lanthanide ions. First, the 4f electrons of lanthanide ions are properly shielded from 5s and 5p orbitals by preventing the direct participation in chemical bonding. Absorption and emission spectra show narrow and sharp bands with a low molar absorption coefficient due to the

shielding effect from *5s* and *5p* electrons[27] (Figure 1.9). Lanthanide compounds generate weak luminescence because of the low extinction coefficient. Second, f-f transitions of lanthanide ions are forbidden by spin and the Laporte rule, which affects the long excited state lifetime from millisecond to the microsecond.[28] Also it provides time-gated or time-resolved *in vivo* medical applications. [4]The direct excitation of lanthanide ions is inefficient because of the poor absorption capability of lanthanide ions. Therefore, a strong light source such as laser light has to be used. To enhance the efficiency of the lanthanide luminescence, researchers have introduced an organic molecules as ligands to obtain highly efficient NIR emission.[34,37] In 1940, Weissman introduced sensitized lanthanide luminescence complexes of terbium and samarium metals.[29,30]

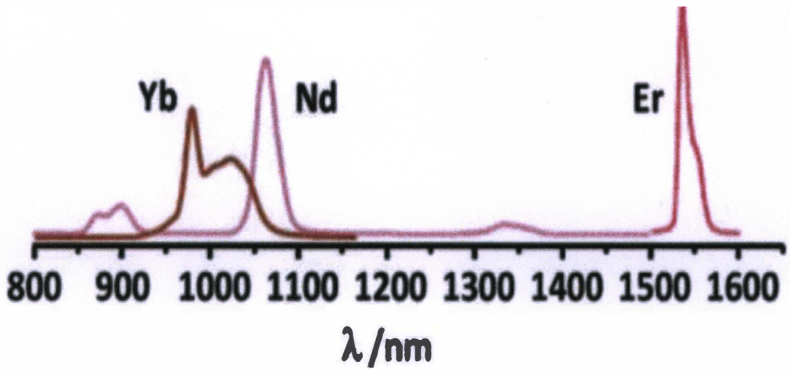

Figure 1.9 Characteristic lanthanide emission peaks for Yb(III), Nd(III), Er(III). Reproduced with permission from ref 30. Copyright 2010 American Chemical Society.

The principle behind the lanthanide probe is known as the antenna effect. The fragment that absorbs the light is called an antenna, and the energy transfer process occurs from the ligand to the lanthanide ions.[30,34,38] First, the antenna ligand is excited to the singlet excited state (S_1) from the ground state (S_0) using absorbed energy, and secondly, the excited state energy transfers to the triplet state (T_1) through intersystem crossing (ISC).

If the lanthanide excited state is close enough to the T_1 state with lower energy, the triplet state energy transfers to the excited state of a lanthanide ion (Figure 1.10).[31]

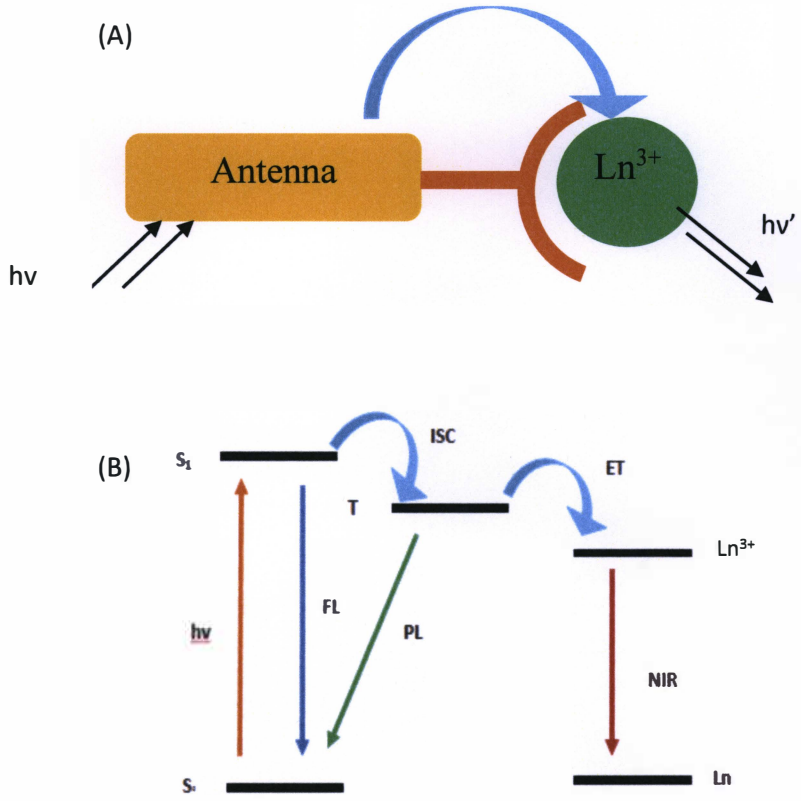

Figure 1.10 (A) Schematic diagram of lanthanide sensitization from organic chromophore. (B)Proposed energy diagram for sensitization process in Ln(III) complexes: S0; ground state, S1; excited state, T; triplet state, Ln^{3+}; lanthanide excited state, FL; fluorescence, PL; phosphorescence, ET; energy transfer

1.5.1 Lanthanide luminescence efficiency

The efficiency of the lanthanide luminescence process can be compromised by fluorescence from a singlet excited state, phosphorescence from triplet state and non-radiative energy loss in either state.[32] If the energy level of the triplet state is lower than the lanthanide excited state, the energy transfer from the triplet state to lanthanide excited

state cannot occur.[33] The coordination of water molecules reduces the excited state lifetime of lanthanide ions by non-radiative energy transfer to the high-frequency O-H vibrational level. The Quantum yield of the lanthanide probes decrease with the number of water molecules.[34]

The selection of lanthanide metals depends on several factors like emission wavelength, luminescence intensity and excited state lifetime of lanthanide ions. Among the lanthanide metals, the Gd(III) ion has the most luminescence, though it emits around 310 nm. Therefore, Gd(III) lanthanide probes are not suitable for biological applications. The most often used lanthanide ions in biological sensitization are Tb(III), Eu(III), Sm(III), Dy(III) and Tm(III) (visible region) and Nd(III), Yb(III), Er(III) and Ho(III) (near infrared region) because of the excited states that exist very close to the ligand triplet state with lower energy. These ions can be excited using a wide variety of antenna ligands.[34,32] In this study, Yb(III) lanthanide metal ion was mainly focused as a metal center of the synthesized ligands. Yb(III) ion emits around 980 nm which is related to $^2F_{5/2} \rightarrow {}^2F_{7/2}$ transition and has the highest emission intensity.

1.5.2 Lanthanide complexes

During the last few decades, researchers have been working with different types of chromophores including β-diketonates,[34,35] porphyrins,[36,37] terphenyl ligands, 8-hydroxyquinoline,[38,39] pyrazolones, 1,4,7,10-tetraazacyclododecane, ferrocene, transition metal complexes and BODIPY. These probes have variable NIR emission efficiencies with different excitation wavelengths.[16] The metal complexes that explained below have short excitation wavelength when compare with the synthesized compounds in this study.

However, these metal complexes have efficient NIR emission with the long conjugated system.

1.5.2.1 Porphyrin based lanthanide complexes

Porphyrins are highly conjugated macrocyclic molecules which are chemically and thermally stable. They are mostly used in photodynamic therapy treatments because of the high absorption in the UV-Vis region. Porphyrins are easy to synthesize and can coordinate to a wide range of metal ions, to obtain variable porphyrin derivatives for different purposes. Porphyrin has a favorable triplet state energy level (15000 cm^{-1}) to sensitize lanthanide metal ions. These features provide suitable electronic and optical properties to porphyrin complexes. Lanthanide porphyrins are mostly used in laser systems, sensing of biological substrates, molecular information storage, magnetic resonance shift reagents and so on.[37,40]

The first lanthanide (III) monoporphyrinate complexes were reported in 1974.[41] Since then only a few studies have reported in the literature. In 2001, Wong and coworkers have reported neutral 3d-4f bi-metallic porphyrinate complexes *via* the interaction of cationic lanthanide (III) (Er(III) and Yb(III)) porphyrinate complexes with sodium (cyclopentadienyl)-tris(diethylphosphito)cobaltate (Figure 1.11). They have observed almost identical UV-Vis absorption (601 nm) and emission at 1531 nm for Er(III) complex and 921 nm for Yb(III) complex. The authors concluded that cationic Ln(III) porphyrinate complexes were good precursors for the preparation of neutral 3d-4f bi-metallic porphyrinate complexes. Also, the porphyrinate ligand efficiently sensitized the Ln(III) ions to produce near-infrared emission by absorbing visible light.[41]

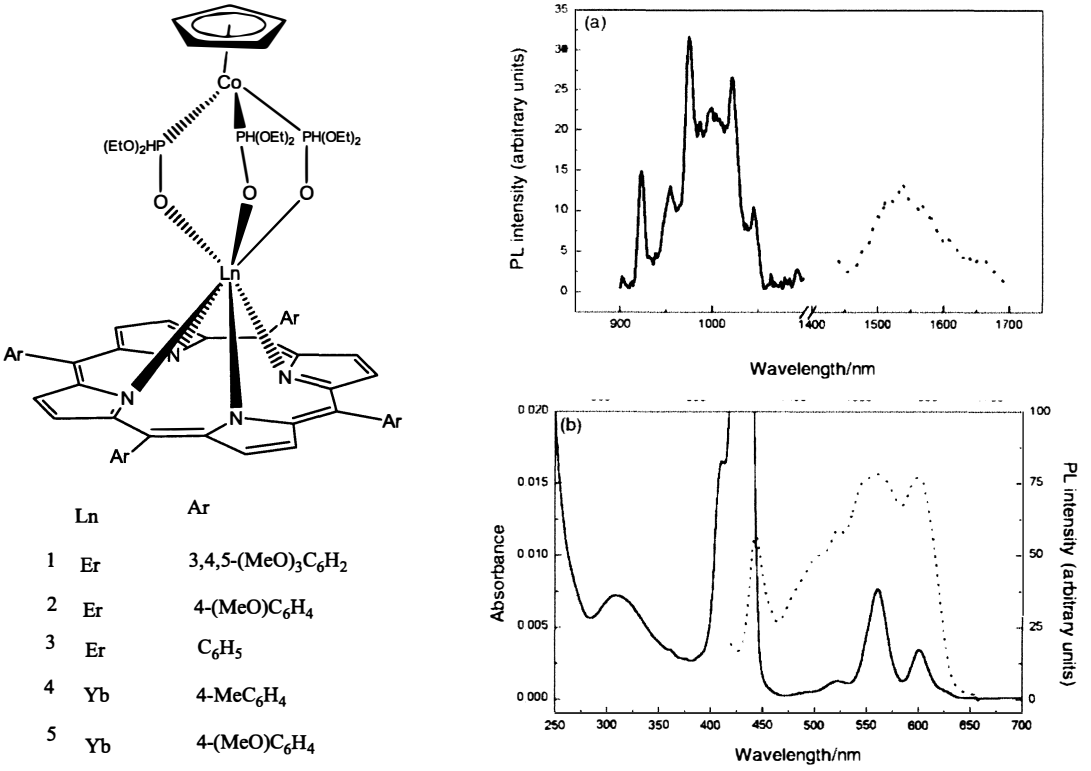

	Ln	Ar
1	Er	3,4,5-$(MeO)_3C_6H_2$
2	Er	4-$(MeO)C_6H_4$
3	Er	C_6H_5
4	Yb	4-MeC_6H_4
5	Yb	4-$(MeO)C_6H_4$

Figure 1.11 (a) NIR luminescence spectra of complex **1** (_ _ _) and **5** (——) in $CHCl_3$upon excitation at 600 nm. (b) Room temperature absorption (——) spectrum and excitation (_ _ _) spectrum (monitored at 921 nm) of complex **5** in $CHCl_3$. Reproduced with permission from ref 41. Copyright 2001 Royal Society of Chemistry.

In 2003, Wong et al. prepared an unsymmetrical diethyl malonate appended porphyrin ligand and its lanthanide complexes (Yb(III), Er(III), Nd(III)) (Figure 1.12). The photophysical properties of compounds are summarized in Table 1.1. The absorption bands at 422,552 and 589 nm and UV-Vis absorption of complexes were almost identical to each other (650 nm). Quantum efficiency of the metalloporphyrin was much lower than that of the appended porphyrin free base ligand ($Ø_{em}$ = 3.56×10^{-2}). The NIR emission of Yb(III) and Er(III) peaks were centered at 980 nm and 1544 nm, respectively. For Nd(III), the emission peak was centered at 853 nm and 890 nm (Figure 1.12). The

authors concluded that the porphyrin ring transferred the absorbed light to the lanthanide metal ions, to generate near-infrared emission of lanthanide ions. Also, they concluded that better donating solvents (DMF) could enhance the luminescence efficiency by replacing the coordinated water molecule (Figure 1.13).[42]

Table 1.1 Photophysical data of compounds a, b and c[42]

Compound	Absorption: λ_{max}/nm	Excitation: λ_{ex}/nm	Emission: λ_{em}/nm (Γ, $\emptyset_{em} \times 10^3$)
(a)	422, 552, 589	422	650 (5.1 ns,0.15), 980 (2.43 μs)
(b)	422, 551, 589	422	650 (3.3 ns, 0.098), 1544
(c)	422, 551, 594	422	650 (8.9 ns, 5.02), 853

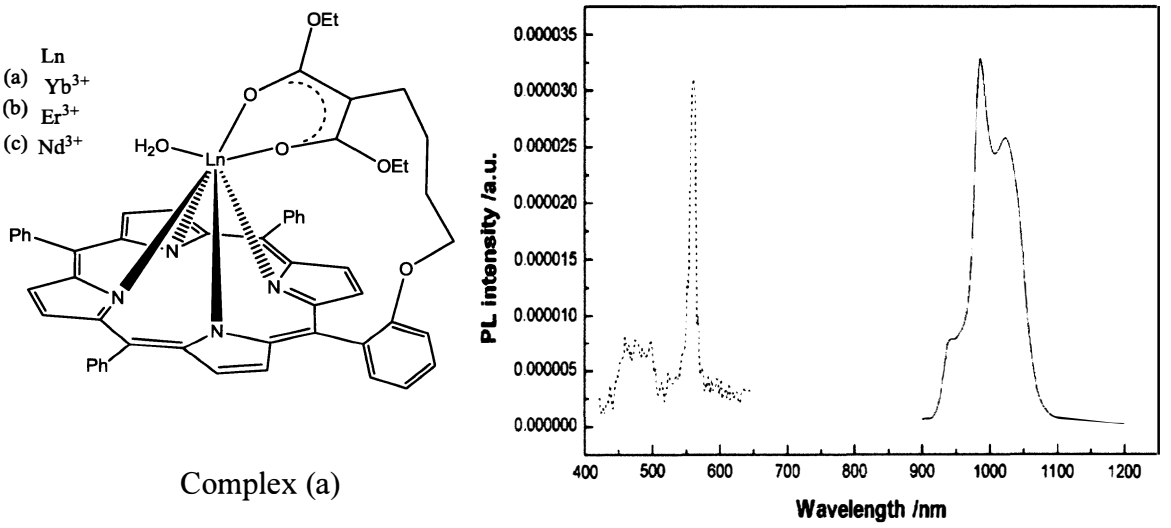

Complex (a)

Figure 1.12 NIR luminescence spectrum (—) and excitation spectrum (- - -), monitored at 980 nm, of complex (a) in $CHCl_3$. Reproduced with permission from ref 42. Copyright 2003 Royal Society of Chemistry.

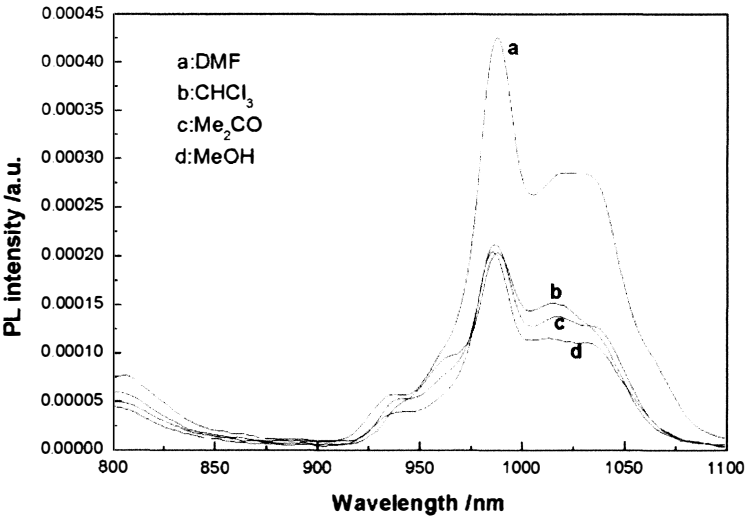

Figure 1.13 Photoluminescence of complex (a) in different solvents at room temperature. Reproduced with permission from ref 42. Copyright 2003 Royal Society of Chemistry.

In 2009, He research group synthesized several seven and eight coordinated ytterbium (III) tetraphenylporphyrinate complexes with diimines as ancillary ligands (Figure 1.14). They observed a Soret band at about 430 nm, and Q bands centered on 550 nm and 600 nm for porphyrinate ytterbium (III) complexesd-h. These results also agreed with the Gourterman's four-orbital model. They observed significant lower quantum efficiency (Ø = <0.005) for the Yb(III) complexes than the 5,10,15,20-tetraphenylporphyrin ligand (Ø = 0.11), indicating the efficiency of intersystem crossing energy transfer to its triplet state. The NIR emission of seven-coordinate Yb(III) complexes (d and h) was around 975 nm with three shoulders at 950 nm, 1000 nm, and 1025 nm, and eight-coordinate complexes (2-5) were emitted around 975 nm and 1005 nm with 946 nm shoulder peak (Figure 1.14).[43]

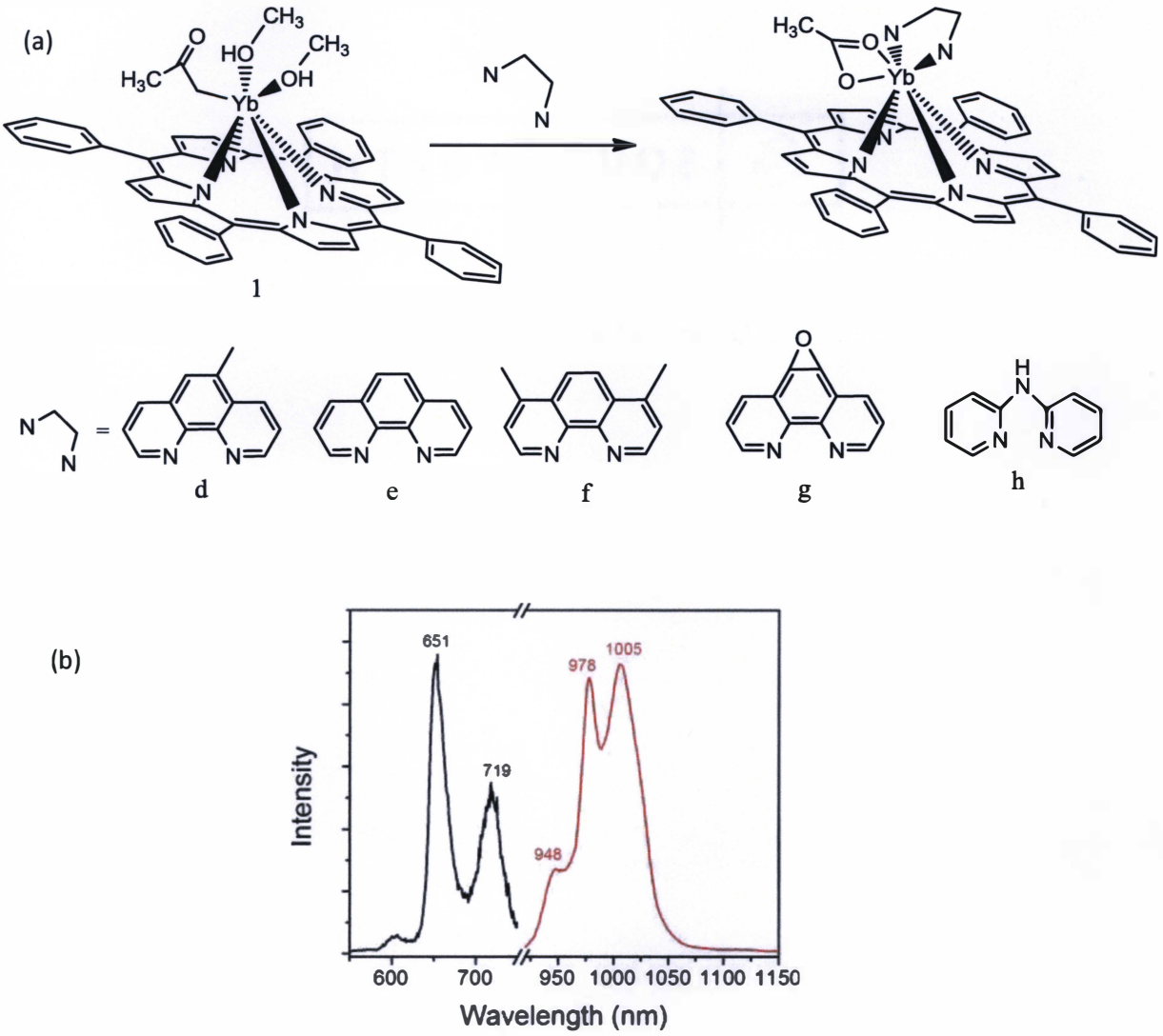

Figure 1.14 (a)Ytterbium (III) monoporphyrinate complexes (b)Visible (black) and NIR (red) emission of ytterbium complex e in toluene solution at room temperature (λ_{ex} =375 nm). Reproduced with permission from ref 43. Copyright 2003 Royal Society of Chemistry.

1.5.1.2 8-hydroxyquinoline based lanthanide complexes

8-Hydroxyquinoline (8-HOQ) and its halogenated derivatives can act as bidentate ligands. These ligands form metal complexes with lanthanide metals because of their excellent coordination properties. In 1936, Pirtea reported the first lanthanide

hydroxyquinoline complex. The hydroxyquinoline based ligands are used in the formation of metal complexes, not only because of their good coordination properties but also due to their of its useful photophysical properties. The triplet excited state of 8-hydroxyquinoline is located around 17100 $cm^{-1}$and increases the intramolecular energy transfer efficiency in metal complexes. The luminescence characteristics were investigated by H. Suzuki using different Er(III) hydroxyquinoline complexes.[44] They have synthesized a wide variety of hydroxyquinoline lanthanide complexes by using different binding chromophores. Antonio and co-workers have described the synthesis of the hydroxyquinoline based macrocyclic ligand using 8-hydroxyquinoline residue with Eu(III) and Er(III) lanthanide ions. The Eu(III) complex was exhibited an absorption around 268 nm and the photoluminescence emission of europium was displayed between 590 -700 nm (Figure 1.15).The Er(III) complex showed an emission at 1530 nm arising from $^4I_{13/2} \rightarrow {}^4I_{15/2}$ transitions. Both complexes Eu(III) and Er(III) displayed high stability with strong sensitization emission under UV radiation, even in aqueous solution or water-containing solvents. Moreover, the authors correlated the energy transfer ability from the sensitizer to the lanthanide ion with pH behavior of the antenna. This study revealed that the good solubility and sensitized emission in different solvents like organic and water are very important aspects of their technologic applications as NIR-emitting devices or luminescent probes.[39]

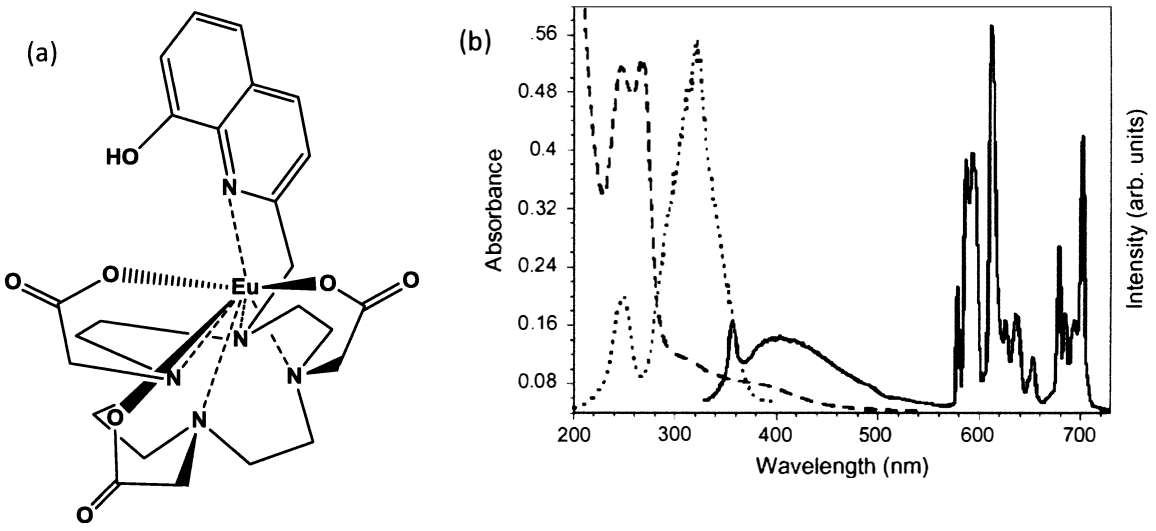

Figure 1.15 (a) 8-hydroxyquinoline Eu(III) complex, (b) Absorption (dashed line), excitation (.....) and emission (—) spectra for Eu(III)complex. Reproduced with permission from ref 42. Copyright 2009 Elsevier.

1.5.1.3β-Diketonate based lanthanide complexes

Among the lanthanide sensitization chromophores, β-diketonatesare the most popular and the most investigated compounds since the 19th century. In 1897, Urbain synthesized the first rare-earth β-diketonates by using lanthanum(III), Yttrium(III) and gadolinium(III) metal ions.[45] β-Diketonate rare-earth coordination complexes are used for different purposes, such as electroluminescence materials in organic light emitting diodes, catalysts in organic reactions, volatile reagents for chemical vapor deposition and as biological sensing materials. The substitute groups on β-diketonate can be substituted by the tertbutyl group to increase the solubility in organic solvents, by aromatic substituents to increase the light absorption and by perfluorinated alkyl groups to increase the Lewis acidity.[34]

β-Diketonate rare-earth complexes can be categorized into three main types: ternary rare-earth β-diketonates complexes, tris complexes, and tetrakis complexes. Ternary rare-earth complexes contain Lewis base adducts besides the β-diketonate ligand because it facilitates the expanding of the coordination sphere and increases the coordination number (typically eight or nine). The Lewis acidic lanthanide ions preferentially make complexes with Lewis bases having oxygen-donor or nitrogen-donor groups. 1,10-phonanthroline derivatives and 2.2'-bipyridine derivatives are mostly used as N-donor ligands. These types of β-diketonate complexes exhibit strong luminescence because of the better energy transfer in the rigid planar structure.[46,47,49]

In 2008, Bünzli and coworkers synthesized lanthanide complexes using a 1,3-diketonato ligand by incorporating both electron donor and acceptor groups into the ligand. The maximum absorption for synthesized HL ligand was around 339 nm and 442 nm. The lower energy band at 442 nm was assigned to an intra-ligand charge transfer. Also, they observed a characteristic line-like infrared emission for Yb(III), Nd(III), and Er(III) diketonate complexes due to f-f transition upon excitation in ligand absorption bands (Figure 1.16). The main advantage of the ligand HL is its lowest-energy absorption transition which extends into the visible range and allows excitation of lanthanide luminescence with wavelengths up to 550 nm. The overall luminescence efficiency of the Yb(III) complex, is 26 M^{-1} cm^{-1} at 428 nm (absorption maximum in the visible range), 5.2 M^{-1} cm^{-1} at 500 nm, and 0.4 M^{-1} cm^{-1} at 550 nm. According to the observed results, they concluded out that the push-pull 1,3-diketonato ligands are suitable for visible light excitation of NIR emitting lanthanide ions. This study has obtained long excitation and emission wavelengths with long conjugated system using β-diketonate ligand.[48]

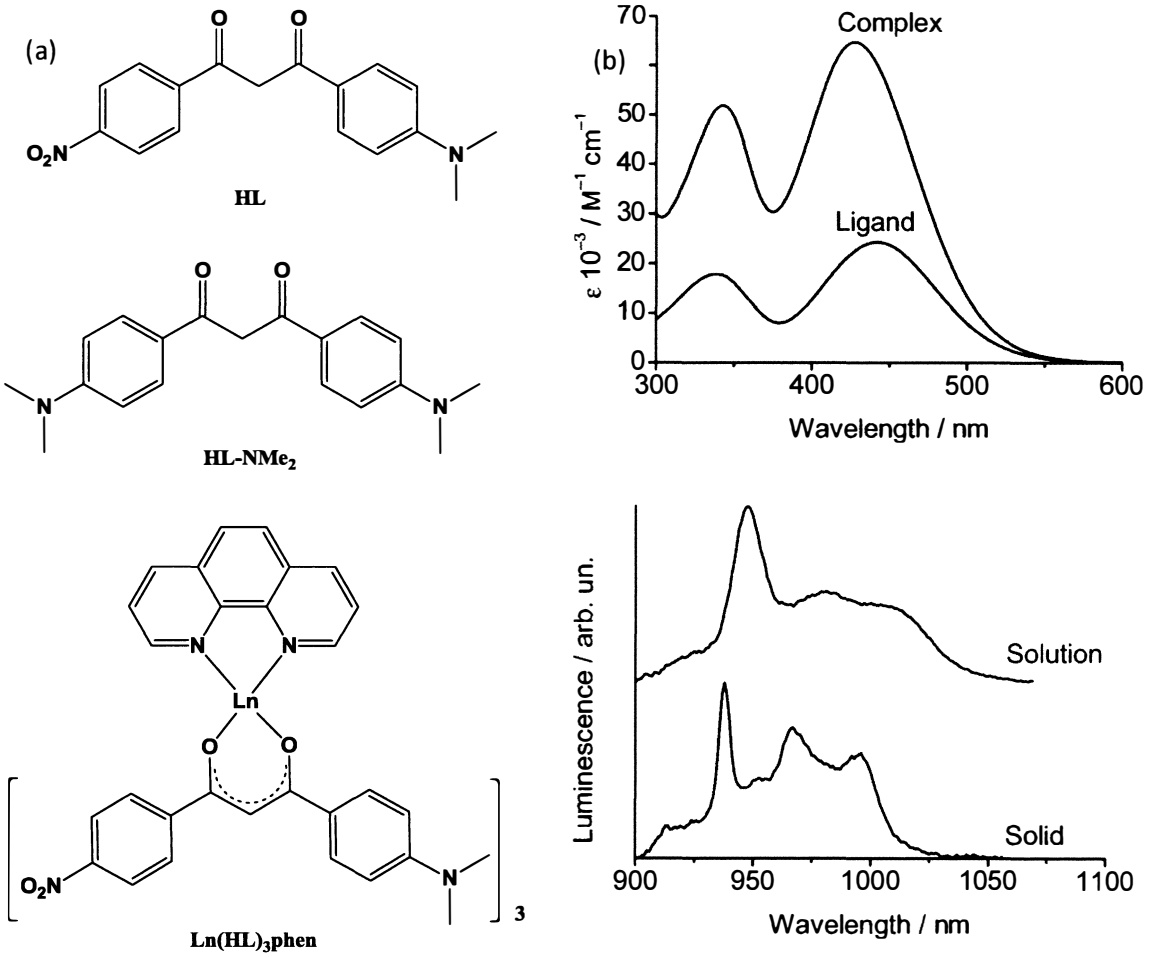

Figure 1.16 (a) Structures of 1,3-diketone ligands and lanthanide complex with HL ligand. (b) Absorption spectra of the ligand HL and the complex [Yb(HL)$_3$phen] in DMSO solution. Reproduced with permission from ref 48. Copyright 2008 John Wiley and Sons.

1.5.1.4 BODIPY based lanthanide complexes

The BODIPY dyes for the sensitization of lanthanide ions were only studied as antenna groups recently. The BODIPY dyes are used as chromophore because they have a high absorption coefficient, tunable spectral coverage, and chemical and photochemical resistance. Studies related to the NIR emission of BODIPY-lanthanide complexes are scarce because of the non-coordination ability of BODIPY core.[37] In 2006, Bunzil and co-

workers synthesized the first BODIPY lanthanide metal complex using terpyridine and BODIPY. Terpyridine was used as a ligand binding group and synthesized BODIPY-terpyridyl ligand and related complexes [Ln(L)-$(NO_3)_3$](L=4,4-difluoro-8-(2':2";6":2"'-terpyridin-4"-yl)-1,3,5,7-tetramethyl-2,6-diethyl-4-bora-3a,4a-diaza-s-indacene (Boditerpy) Ln = (Yb(III), Nd(III), Er(III), Gd(III), La(III)). They observed NIR bands in the spectral range of 1298-1428 nm, and 1030-1086nm for [Nd(L)$(NO_3)_3$] lanthanide complex. The NIR emission of Yb^{3+} complexes ([Yb(L)$(NO_3)_3$]) exhibited several peaks in the range 943 – 1075 cm^{-1} which corresponds to the $^2F_{5/2} \rightarrow {}^2F_{7/2}$ transition (Figure 1.17). The NIR emission efficiencies of Yb(III) and Nd(III) complexes were 0.31% and 0.016%, respectively. They also observed a very weak luminescence for the [Er(L)$(NO_3)_3$ complex under the same conditions. The authors reported that the quantum yield of the ligand decreased from 79% to 15-19% with the lanthanide complex formation. Moreover, authors revealed that the sensitization process is mainly achieved by perturbation of excited states of BODIPY core by lanthanide coordination, and it leads efficient energy transfer process to Ln(III) excited state from BODIPY triplet state.[49]

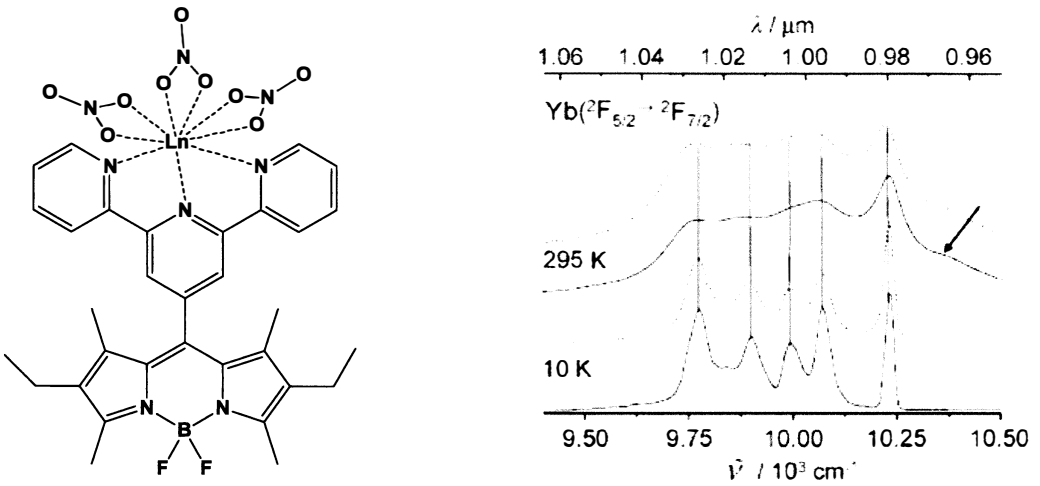

Figure 1.17 Emission spectra of the [Yb(L)$(NO_3)_3$] complex at 10 and 295 K (λ_{ex}=19 455 cm^{-1}); solid line: powdered sample, dotted line: single crystals. Reproduced with permission from ref 49. Copyright 2006 John Wiley and Sons.

In 2012, Bunzil and Ruy synthesized a benzoic acid functionalized BODIPY dye which formed terpyridine coordinated two lanthanide complexes which bear either hydrogen or bromine in the 2,6 positions (Figure 1.18).[51] The emission intensity of the lanthanide complex was decreased in the visible range due to the introduction of a Br atom to the BODIPY ligand. The NIR emission of the Yb^{3+} complex was observed at 978 nm and Er^{3+} complex at 1530 nm. They observed that the bromination enhanced the NIR emission intensity compared with the unbrominated complex. After bromination, the quantum yield of the ligands dropped from 31% to 21%. The authors' concluded that the BODIPY molecule could efficiently sensitize the lanthanide ions, under the long wavelengths excitation with large molar absorption coefficients (logε ~ 5.0-5.2). They also revealed the importance of conformation of the chromophores on the yield of intersystem crossing.[50]

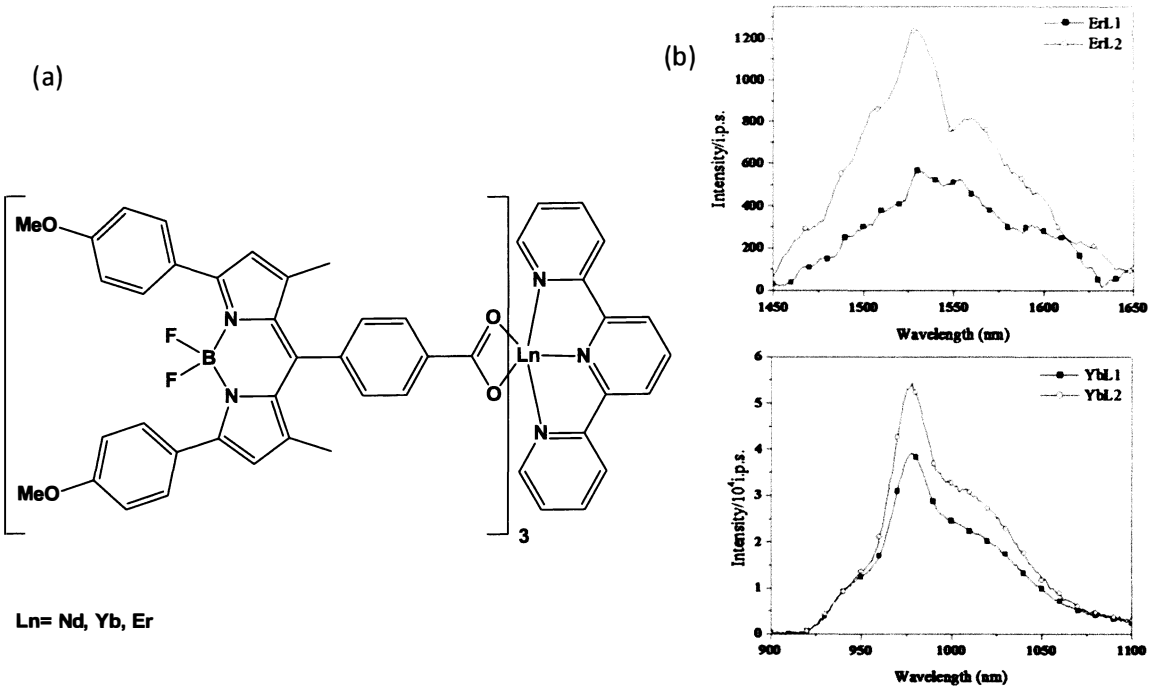

Figure 1.18 (a) $[Ln(L_i)_3(tpy)]$ lanthanide complex. (b) Metal-centered NIR emission of ErL_i and YbL_i with the concentration of 1×10^{-5} M in THF at room temperature λ_{ex} = 583 nm: L_i= hydrogen (L1) or bromine (L2) ligands. Reproduced with permission from ref 50. Copyright 2012 Royal Society of Chemistry.

In 2011, He and co-workers synthesized a BODIPY functionalized 8-hydroxyquinoline ligand for sensitization of lanthanide ions (Yb(III), Er(III), Nd(III)).[16] The ligand formed stable lanthanide complexes with Ln(III) ions with 1:3 metal to ligand molar ratio. The ligand exhibited a strong absorption at 506 nm and an emission at 510 nm in organic solvents with 0.45 quantum yields in dichloromethane and 0.005 in DMF. The lanthanide complexes Nd(III) and Er(III) have weak NIR emission at 1060 nm and 1382 nm, respectively. They observed a high emission for Yb(III) complex at 976 and 1003 nm (Figure 1.19). The authors also demonstrated that the BODIPY moieties are efficient visible light sensitizers for lanthanide NIR emitters.[16]

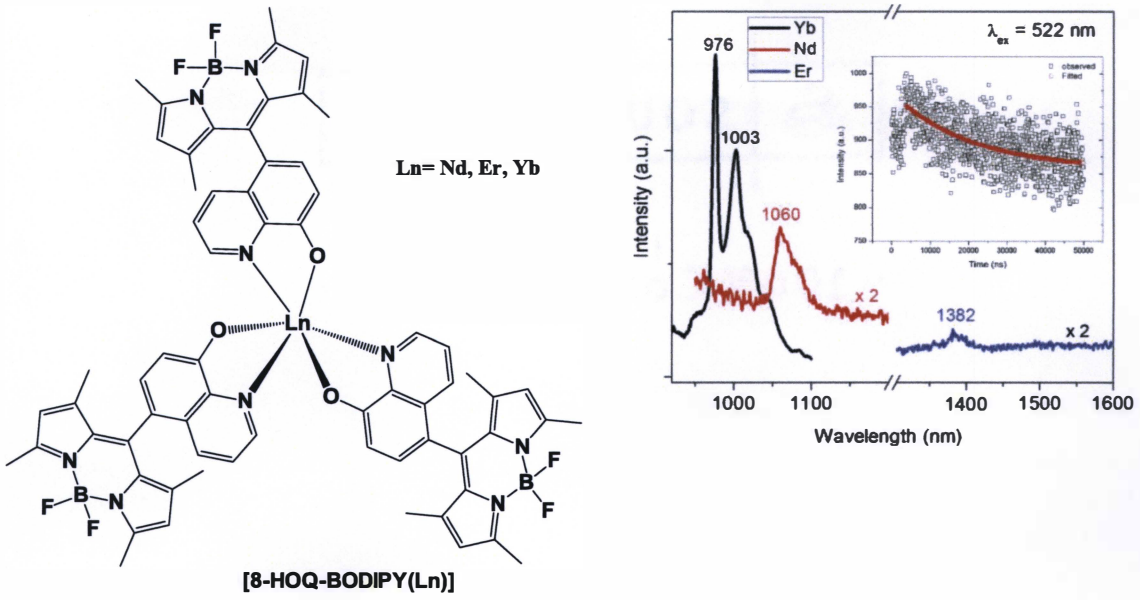

Figure 1.19 8-HOQ-BODIPY based lanthanide complex Emission spectra of the Yb^{3+}, $Nd^{3+}$and Er^{3+} complexes in CH_2Cl_2. The excitation wavelength was 522 nm. Reproduced with permission from ref 16. Copyright 2011 Royal Society of Chemistry.

In 2011, He et al modified 8-HOQ-BODIPY ligand to 8-HOQ-BODIPY-3I ligand and achieved efficient NIR emission with strong longer wavelength absorption.[52] This ligand sensitized the Yb(III) ion efficiently under excitation at 540 nm. This was the first Yb(III) complex that emits NIR emission at a longer wavelength. Also, they observed that the fluorescence quantum yield decreased to 0.00075 in DCM and to 0.0026 in ethanol due to the efficient intersystem crossing of energy from singlet excited state to the triplet state. The NIR emission of Yb(III) complex was observed at 975 nm and one broad peak centered at 1000 nm corresponding to the $^2F_{5/2} \rightarrow {}^2F_{7/12}$transition (Figure 1.20). The lifetime of the iodinated lanthanide complex (~95±17 μs) was much longer than the non-iodinated complex (19 μs) and the calculated emission efficiency was 4.75%.[51]

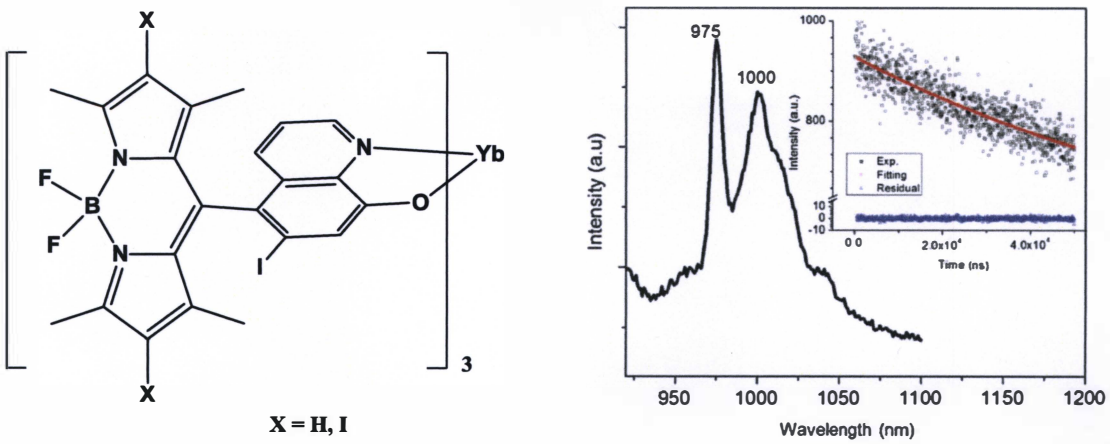

Figure 1.20 Emission of [Yb(8-HOQ–BODIPY–3I)$_3$] in CH_2Cl_2 at room temperature. The excitation wavelength is 543 nm. The inset is the decay curve monitored at 975 nm under excitation at 375 nm and its single exponential fitting. Reproduced with permission from ref 42. Copyright 2011 Royal Society of Chemistry.

1.6 Motivation

There has been an increasing demand for fluorescent materials because of their potential application in material diagnostic tests such as immunoassays. Most of the commercially available probes need UV or near-UV wavelength for excitation, which causes severe photobleaching of bio-substrates. Besides, the significant overlap of biological autofluorescence and the fluorescence from commercial optical probes dramatically decreases the detection sensitivity. Therefore, it is imperative to investigate novel fluorescent materials for visualization of biological substrates. The fluorescent dyes that have been synthesized so far, emitted in the NIR region under UV excitation. However, dyes with a π-conjugation should efficiently emit in the NIR region under long wavelength excitation and therefore can be used in widespread applications in non-invasive and *in vivo* fluorescence imaging. NIR probes will also eliminate background signals and increase detection sensitivity, since biological substrates do not exhibit NIR emission. In order to overcome these current problems, there is a need to design and synthesize lanthanide complexes that can be sensitized using the red light with strong emission in the NIR region. Following these previous studies, in this study, was focused to synthesize a ligand series which are exhibiting strong absorption at the longer wavelength with efficient NIR emission at 980 nm for ytterbium lanthanide complexes.

1.7 Objectives

- To synthesize ytterbium (III) complexes using BODIPY dyes with a large π-conjugation system.
- Modify the regular BODIPY dyes to enhance the absorption and emission wavelengths up to the deep red and NIR regions through Sonogashira coupling reaction at either 2 or 6 β positions of BODIPY dyes.
- Employ the other β position of BODIPY-bipyridine ligand by binding iodine group to enhance the ligand triplet state population.
- Attach 4-ethynylbenzoic acid and 1-ethynyl-4-isothiocyanatobenzene anchors by replacing the iodine group at β position to make a large conjugated system.
- Synthesize a series of novel Yb(III) complexes that can be sensitized by the new BODIPY ligands.
- Characterize the intermediates and final products via ^{1}H NMR spectroscopy.
- Record the UV-Vis, excitation and emission spectra of the ligands and their complexes.
- Measure the fluorescence quantum yield of ligands.

Chapter 2

EXPERIMENTAL

2.1 General

2.1.1 Materials

All reagents and solvents were obtained from commercial sources (Aldrich, Sigma, Acros Organic, and Fisher Scientific) and were used without further purification unless otherwise stated. Dichloromethane (DCM), chloroform, hexane, methanol and triethylamine were purchased from Fisher Chemical Scientific. The 2,3-dichloro-5,6-dicyano-1,4-benzoquinone (DDQ) was supplied by BIOSYNTH chemistry & biology. The N-iodosuccinamide (NIS), deuterated chloroform, tetrahydrofuran, copper (I) iodide, bis(triphenylphosphine)palladium(II)chloride ($Pd(PPh_3)_2Cl_2$), boron trifluoride diethyl etherate (BF_3OEt_2), 2,4-dimethylpyrrole, dry CH_2Cl_2, and K_2CO_3 were purchased from ACROS Organics. The ytterbium (III) hexafluoroacetylacetonatedihydrate (99.9%) was purchased from STREM Chemicals. The 5-bromo-5'-methyl-2,2'-N-bipyridine was synthesized according to a published procedure.[52] The 5-(trimethylsilyl)ethynyl-5'-methyl-2,2'-N-bipyridine was synthesized in collaboration with Dr. Radu Semeniuc, Eastern Illinois University. All, air and moisture sensitive reactions were conducted using either Schlenk techniques or in a MBRAun dry box under an inert atmosphere of dry nitrogen or argon. The nitrogen and argon gas were supplied by Geno Welding (Mattoon, IL). The 70-230 mesh silica gel was purchased from SILICYCLE Inc. The column chromatography was performed over 70-230 mesh silica gel.

2.1.2 Instrumentation

NMR spectra were obtained on a Bruker Avance II-NMR 400 MHz spectrometer. Chemical shifts (δ) were reported as ppm using the internal standard $CDCl_3$ 99.8% D, containing 0.03% (v/v) TMS. UV-VIS absorptions were measured on a Cary 100 Series UV-VIS Dual Beam Spectrometer over a range of 200 - 800 nm. The fluorescence spectra were collected on a spectrofluorometer FS5 from Edinburgh Instruments.

2.2 Synthesis

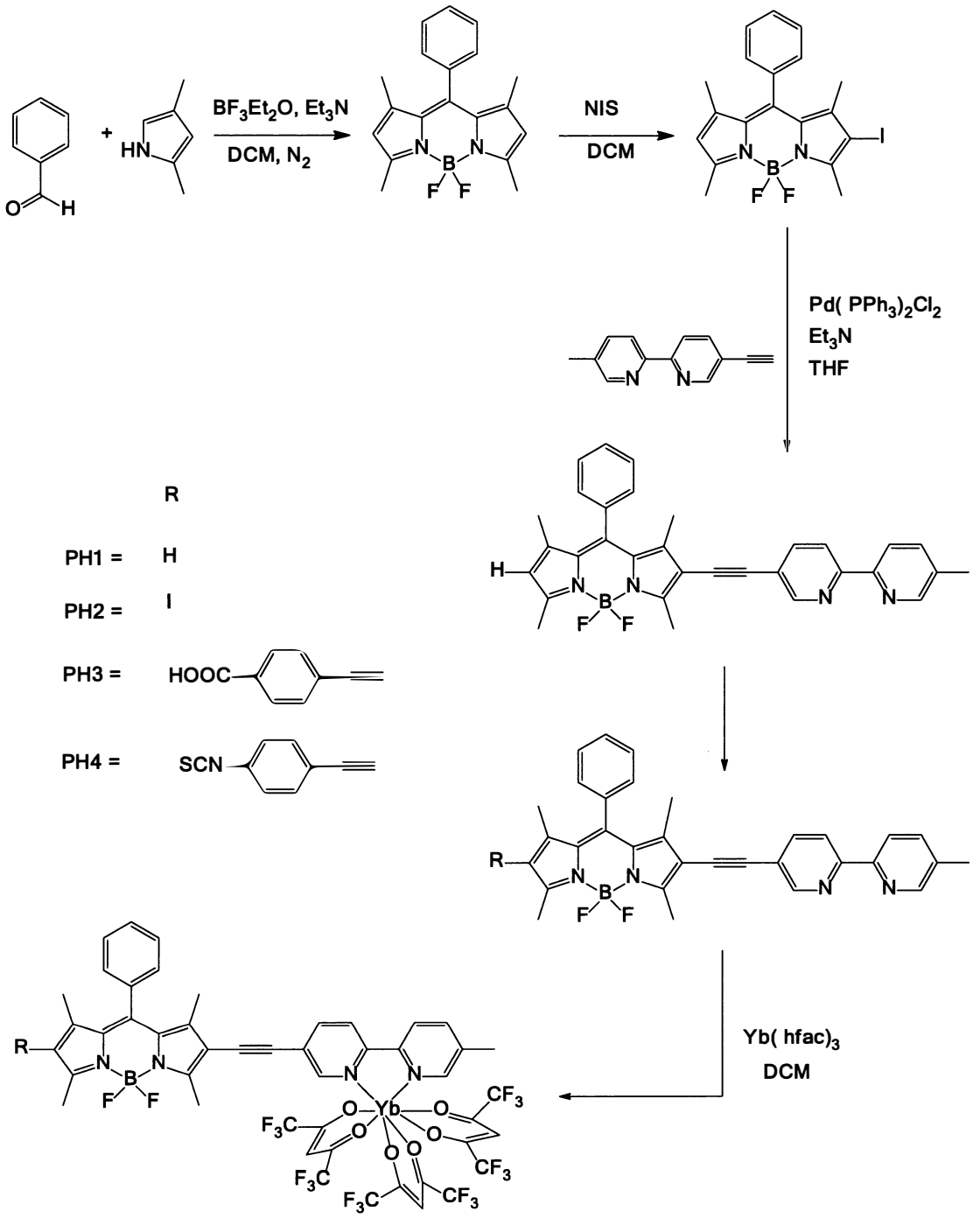

Figure 2.1 Synthetic overview of PH1, PH2, PH3, and PH4 ligand and four ytterbium metal complexes.

2.1.1 Synthesis of $C_{19}H_{19}BF_2N_2$ (PS 001)

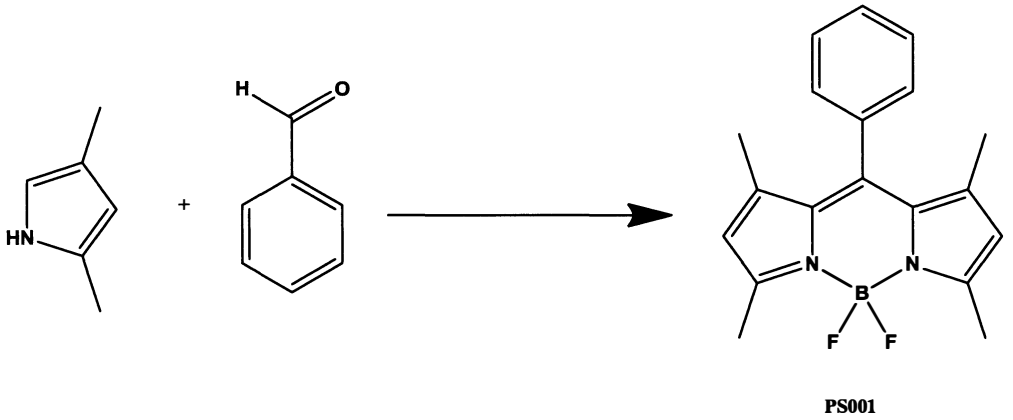

PS001

Figure 2.2 Synthesis of PS001

To a distilled dichloromethane (200.0 mL) solution of benzaldehyde (0.45 mL, 4.41 mmol) was added 2,4-dimethyl pyrrole (0.97 mL, 9.42 mmol) under nitrogen. A drop of $BF_3.Et_2O$ was added after 15 min and the reaction mixture was stirred magnetically at room temperature for overnight. To this solution 2,3-Dichloro-5,6-dicyano-1,4-benzoquinone (0.912 g, 4.01 mmol) was added over ten minutes while keeping the flask in an ice bath. The solution became dark purple immediately. After stirring for 2h, triethylamine (4.0 mL, 28.00 mmol) was added slowly and the solution was stirred for 30min. Then $BF_3.Et_2O$ (4.0 mL, 32.41 mmol) was added dropwise into the mixture and the solution became fluorescent immediately under a UV lamp, indicating the formation of the final product. The reaction mixture was magnetically stirred overnight, concentrated under reduced pressure and purified using column chromatography (silica gel, CH_2Cl_2: Hexane = 1:1, v/v) to give PS001 as an orange powder. Yield: 0.421 g, 29.46%. ^1H NMR (400 MHz, $CDCl_3$) δ 7.49 (m, J = 1.4 Hz, 2H, H^c, H^d), 7.29 (m, 2H, H^b), 5.98 (s, 2H, H^a), 2.56 (s, 6H, H^e), 1.37 (s, 6H, H^f).

2.2.2 Synthesis of $C_{19}H_{18}BF_2IN_2$ (PS002)

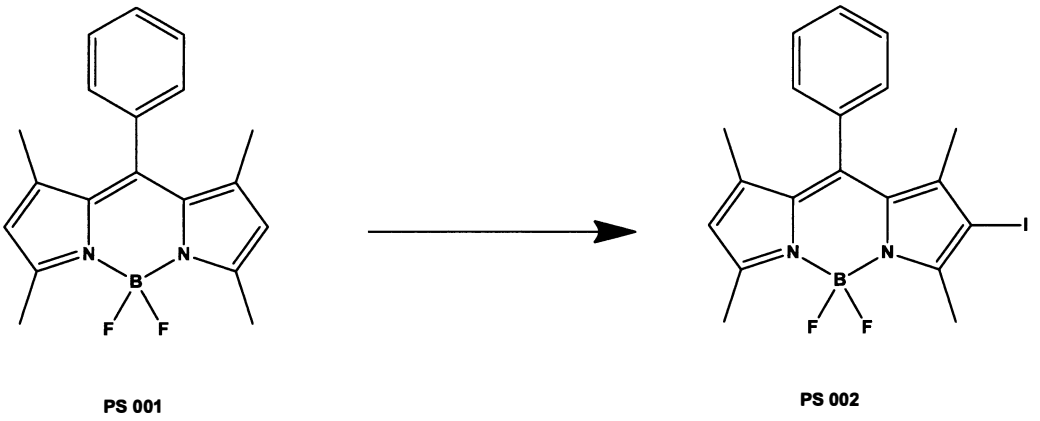

Figure 2.3 Synthesis of PS002

N-Iodosuccinimide (0.140 g, 0.62 mmol) in CH_2Cl_2 (30.0 mL) was added dropwise to a solution of PS001 (0.200 g, 0.62 mmol) in CH_2Cl_2 (100.0 mL) within 1h at 10-15°C. After the addition, the reaction mixture was magnetically stirred 5h at room temperature. The reaction mixture was concentrated under reduced pressure and the crude product was purified by column chromatography (silica gel, CH_2Cl_2: Hexane = 1:1, v/v) to give PS002 as a dark orange color powder. Yield: 0.185 g, 66.3%. ^{1}H NMR (400 MHz, $CDCl_3$) δ 7.53 (m, 3H, H^c, H^d), 7.30 (m, 2H, H^b), 6.07 (s, 1H, H^a), 2.66 (s, 3H, H^g), 2.59 (s, 3H, H^e), 1.40 (s, 6H, H^f, H^h).

2.2.3 Synthesis of $C_{13}H_{10}N_2$ (PS003)

First step

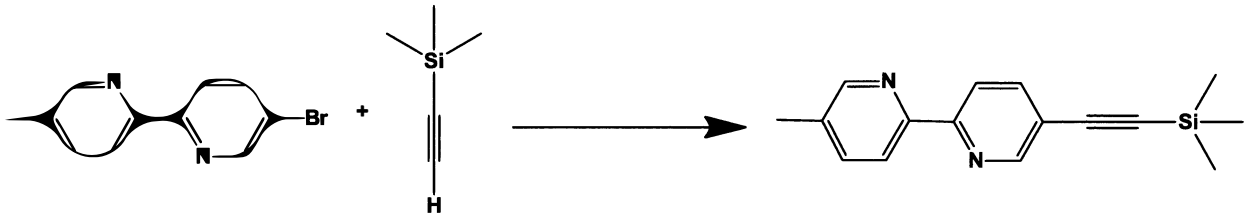

Figure 2.4 (a) Synthesis of PS003-step one

$PdCl_2(PPh_3)_2$ (0.422 g, 0.60 mmol), CuI (0.190 g, 0.99 mmol), and 5-bromo-5'-methyl-2.2'-bipyridine (1.000 g, 4.00 mmol) were dissolved in a dry THF (30.0 mL) and triethylamine (10.0 mL, 71.60 mmol) mixture under a nitrogen atmosphere. Ethynyltrimethylsylane (1.4 mL, 10.02 mmol) was added to the solution and the resulting mixture was stirred overnight at room temperature. The reaction mixture was filtered and the volatiles were removed under reduced pressure, to afford a black powder. The product was purified by flash chromatography (silica gel, CH_2Cl_2). Then Soxhlet extracted with hexane to give product as a pale brown color powder. Yield: 0.885 g, 82.8%.^{1}H NMR (400 MHz, $CDCl_3$) δ 8.72 (s, 1H), 8.48 (s, 1H), 8.32 (d, 2H), 7.85 (d, 1H), 7.78 (d, 1H), 2.48 (s, 9H).

Second step

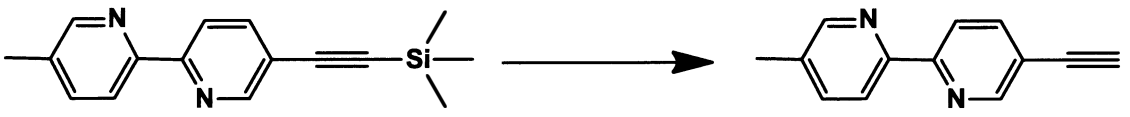

PS003

Figure 2.4 (b) Synthesis of PS003-step two

5-(Trimethylsilyl)ethynyl-2,2'-bipyridine (0.264 g, 0.99 mmol) and K_2CO_3 (0.250 g, 1.80 mmol) were dissolved in methanol (50.0 mL) and stirred for one hour at room temperature. The solution was decanted and the solvent was removed in vacuo to afford pale yellow color powder as a PS003. Yield: 0.182 g, 95 %. ^{1}H NMR (400 MHz, $CDCl_3$) δ 8.75 (s, 1H, H^d), 8.51 (s, 1H, H^c), 8.36 (d, J = 8.1 Hz, 1H, H^f), 8.30 (d, J = 8.1 Hz, 1H, H^a), 7.89 (d, J = 8.3 Hz, 1H, H^e), 7.87 (d, 8.3 Hz, 1H, H^b), 3.28 (s, 1H, H^g), 2.40 (s, 3H, H^h).

2.2.4 Synthesis of $C_{32}H_{27}BF_2N_4$ (ligand PH1)

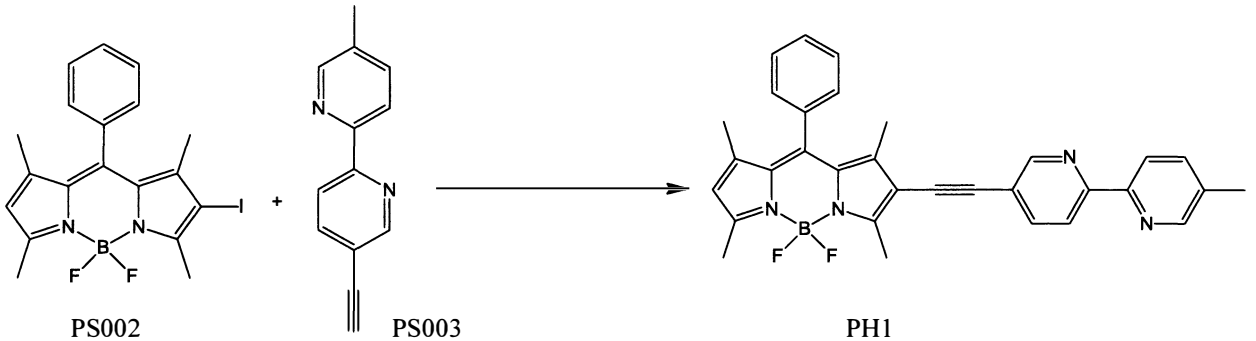

Figure 2.5 Synthesis of ligand PH1

Compound PS002 (0.107 g, 0.240 mmol), 5-ethynyl-5'-methyl-2,2'-N-bipyridine (0.046 g, 0.237 mmol), CuI (0.004 g, 0.024 mmol) and $PdCl_2(PPh_3)_2$ (0.016 g, 0.024 mmol) were dissolved in THF (30.0 mL) and Et_3N (10.0 mL) in a pressure tube under argon. The reaction mixture was stirred at 50°C for two days. Then the reaction mixture was concentrated under reduced pressure and the crude product was purified using column chromatography (silica gel, CH_2Cl_2:MeOH = 10:1,v/v) to give PH1 as a purple color solid. Yield: 0.127 g, 51.6%. ^{1}H NMR (400 MHz, $CDCl_3$) δ 8.70 (s, 1H, H^j), 8.51 (s, 1H, H^e), 8.32 (d, 1H, Hg), 8.31 (d, 1H,H^h), 7.84 (d, 1H, H^i), 7.63 (d, J = 8.3 Hz, 1H, H^f),

7.51 (m, 3H, H^c, H^d), 7.30 (m, 2H, H^b), 6.05 (s, 1H, H^a), 2.72 (s, 3H, H^l), 2.59 (s, 3H, H^o), 2.40 (s, 3H, H^m), 1.52 (s, 3H, H^n), 1.41 (s, 3H, H^k).

2.2.5 Synthesis of $C_{32}H_{26}BF_2IN_4$ (ligand PH2)

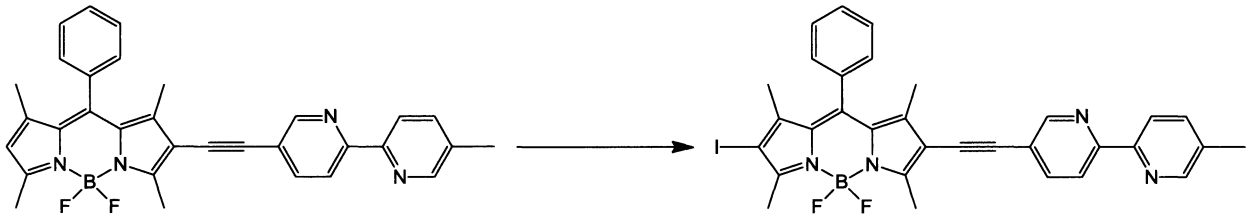

Figure 2.6 Synthesis of ligand PH2

Compound PH1 (0.185 g, 0.35mmol) was dissolved in CH_2Cl_2 (100.0 mL) and then N-iodosuccinimide (0.078 g, 0.35 mmol) in CH_2Cl_2 (40.0 mL) was added drop wise to the reaction flask at 10-15°C within 30 min. The reaction mixture was magnetically stirred over night at room temperature. Then the reaction mixture was concentrated under reduced pressure and the crude product was purified using column chromatography (silica gel, $CHCl_3$) to give PH2 as a dark purple color powder. Yield: 0.186 g, 82.85%. ^1H NMR (400 MHz, $CDCl_3$) δ (ppm) 8.71(s, 1H, H^j), 8.51(s, 1H, H^e), 8.37(d, 1H, H^g), 8.31(d, 1H, H^h), 7.84(d, 1H, H^i), 7.63(d, 1H, H^f), 7.54(m, 3H, H^c, H^d), 7.30(m, 2H, H^b), 2.73(s, 3H, H^l), 2.67(s, 3H, H^o), 2.40(s, 3H, H^m), 1.52(s, 3H, H^n), 1.42(s, 3H, H^k).

2.2.6 Synthesis of $C_{41}H_{31}BF_2N_4O_2$ (ligand PH3)

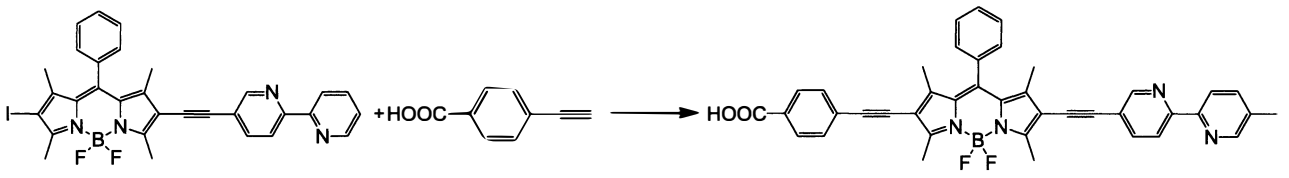

PH2 PH3

Figure 2.7 Synthesis of ligand PH3

4-Ethynylbenzoic acid (0.015 g, 0.1 mmol), compound PH2 (0.065g, 0.1 mmol), CuI (0.002 g, 0.01 mmol), $Pd_2(PPh_3)_2Cl_2$ (0.007 g, 0.01 mmol) were dissolved in THF (30.0 mL) and Et_3N (10.0 mL) in a pressure tube under argon. Reaction was magnetically stirred for 24 h at 50°C. Then the reaction mixture was concentrated under reduced pressure and the crude product was purified using column chromatography (silica gel, $CHCl_3$: MeOH = 10:2) to give PH3 as a red color solid. Yield: 0.025 g, 37.87%. ^{1}H NMR (400 MHz, $CDCl_3$) δ (ppm) 8.71 (s, 1H, H^j), 8.51(s, 1H, H^e), 8.36 (dd, 2H, H^q), 7.84 (d, 1H, H^g), 7.72 (d, 1H, H^h), 7.65 (d, 1H, H^i), 7.54 (m, 5H, H^c, H^d, H^p), 7.48 (d, 1H, H^f), 7.29 (m, 2H, H^b), 2.73 (s, 3H, H^l), 2.67 (s, 3H, H^o), 2.40 (s, 3H, H^m), 1.52 (s, 3H, H^n), 1.42 (s, 3H, H^k).

2.2.7 Synthesis of C_9H_5NS (PS004)

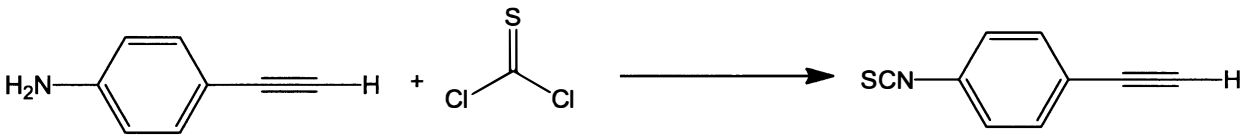

Figure 2.8 Synthesis of PS004

4-Ethynylbenzenamine (1.000 g, 8.53 mmol) and trimethylamine (5.0 mL, 35.82 mmol) in $CHCl_3$ (15.0 mL) were placed in a flask under an atmosphere of N_2. A solution of thiophosgene (3.0 mL, 19.30 mmol) in 20.0 mL $CHCl_3$ was added dropwise at room temperature within one hour. The mixture was heated under reflux for 2h, and then cooled to room temperature. The mixture was quenched by addition of 20.0 mL cold water and extracted with 300.0 mL (3×100.0 mL) $CHCl_3$. The organic layer was washed with H_2O (3×50.0 mL), dried over anhydrous Na_2SO_4 and concentrated to give a yellow residue. The crude product was purified using column chromatography (silica gel, Hexane: DCM = 3:1) to give PS004 as a pale yellow color solid. Yield: 0.87 g, 64%. ^1H NMR (400 MHz, $CDCl_3$) δ (ppm), 7.47 (d, 2H, H^c), 7.18 (d. 2H, H^b), 3.16 (s, 1H, H^a).

2.2.8 Synthesis of $C_{41}H_{30}BF_2N_5S$ (ligand PH4)

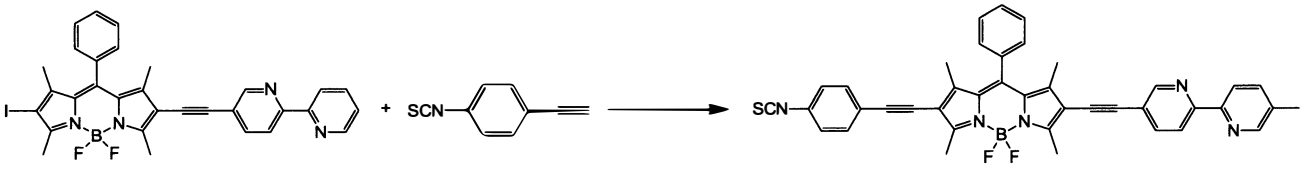

PH2 PH4

Figure 2.9 Synthesis of ligand PH4

1-Ethynyl-4-isothiocyanatobenzene (0.016 g, 0.100 mmol), ligand PH2 (0.064 g, 0.100 mmol), CuI (0.002 g, 0.010 mmol), $Pd_2(PPh_3)_2Cl_2$ (0.007 g, 0.005 mmol) were dissolved in THF (30 mL) and Et_3N (10 mL)in a pressure tube under argon. The reaction mixture was magnetically stirred for 24 h at 50°C. Then the reaction mixture was concentrated under reduced pressure and the crude product was purified using column chromatography (silica gel, $CHCl_3$: MeOH = 10:2) to give PH4 as a purple color solid. Yield: 27 mg, 40%. ^1H NMR (400 MHz, $CDCl_3$) δ 8.70 (s, 1H, H^m), 8.50 (s, 1H, H^j), 8.35 (dd, 2H, H^b), 7.84 (d, 1H, H^k), 7.70 (d, 1H, H^o), 7.63 (d, 1H, H^n), 7.54 (m, 5H, H^h, H^i, H^a),7.40 (d, 1H, H^l), 7.30 (m, 2H, H^g), 2.73 (s, 3H, H^f), 2.67 (s, 3H, H^c), 2.40 (s, 3H, H^e), 1.52 (s, 3H, H^d), 1.42 (s, 3H, H^p).

2.2.9 Synthesis of $C_{24}H_{27}BF_2N_2Si$ (PS005)

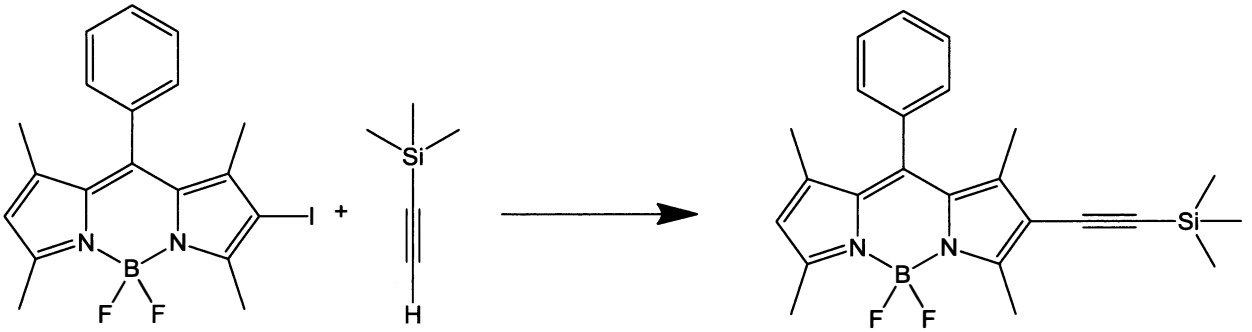

Figure 2.10 Synthesis of PS005

Compound PS002 (0.360g, 1.44 mmol), CuI (0.015 g, 0.08 mmol) and $PdCl_2(PPh_3)_2$ (0.056 g, 0.08mmol) were dissolved in THF (30 mL) and Et_3N (10 mL). Ethynyltrimethylsilane (0.22 mL, 1.60 mmol) was added under argon. The reaction mixture was stirred at 50°C for 24 h. Then the reaction mixture was concentrated under

reduced pressure and the crude product was purified using column chromatography (silica gel, CH_2Cl_2:hexane = 1:1,v/v) to give PS005 as a light orange color solid. Yield: 0.38 g, 65.3%. ^1H NMR (400 MHz, $CDCl_3$) δ 7.50 (m, 3H, H^i, H^h), 7.27 (m, 2H, H^j), 6.02 (s, 1H, H^a), 2.63 (s, 3H, H^c), 2.57 (s, 3H, H^b), 1.43 (s, 3H, H^e), 1.39 (s, 3H, H^d), 0.20 (s, 9H, H^k).

2.2.10 Synthesis of $C_{21}H_{19}BF_2N_2$ (PS006)

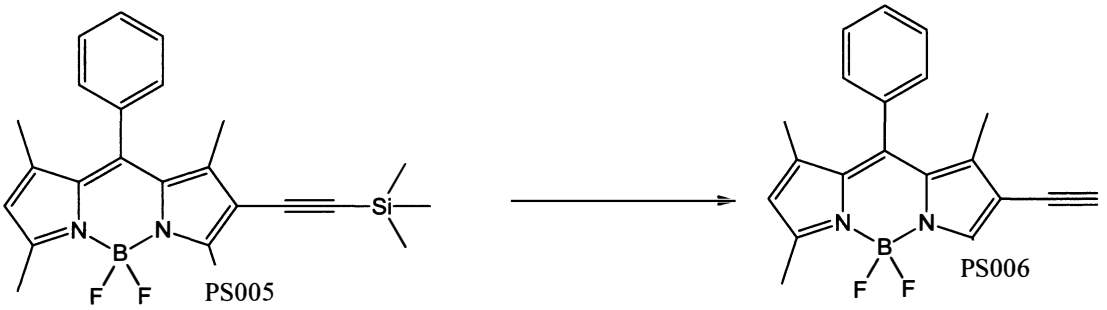

Figure 2.11 Synthesis of PS006

Compound PS005 (0.229 g, 0.56 mmol) and K_2CO_3 (0.133 g, 0.95 mmol) were combined in methanol (50.0 mL) and stirred for one hour at room temperature. The reaction was quenched by adding H_2O (40.0 mL) and product was extracted with CH_2Cl_2 (40.0 × 2 mL). The solvent was removed in vacuo and the crude product was purified using column chromatography (silica gel, CH_2Cl_2:hexane = 1:1) to give PS006 as an orange color solid. Yield: 0.124 g, 63.58%.^1H NMR (400 MHz, $CDCl_3$) δ 7.51 (m, 3H, H^i, H^h), 7.28 (m, 2H, H^j), 6.04 (s, 1H, H^a),3.28 (s, 1H, H^k), 2.64 (s, 3H, H^c), 2.58 (s, 3H, H^b), 1.44 (s, 3H, H^e), 1.39 (s, 3H, H^d).

2.2.11 Synthesis of ytterbium complexes

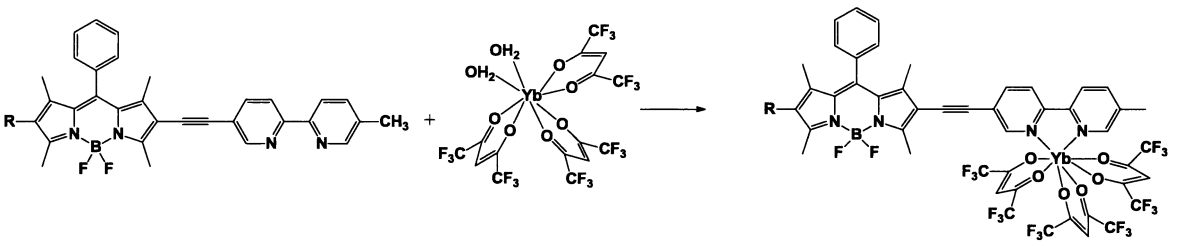

Figure 2.12 Synthesis of ytterbium metal complexes

All four ytterbium complexes were synthesized using a similar method. A typical procedure is described here using the ligand PH1. The PH1 ligand (0.052 g, 0.10 mmol) was dissolved in CH_2Cl_2 (50.0 mL), then $[Yb(hfhc)_3 \cdot (H_2O)_2]$ (0.079 g, 0.10 mmol) in CH_2Cl_2 (15.0 mL) was added to the ligand solution. The resulting mixture was magnetically stirred for 1 h at room temperature,and then concentrated under reduced pressure. The crude product was recrystallized using CH_2Cl_2 and hexane. Yields: PH1-Yb, 0.120 g 94.5%; PH2-Yb, 0.132 g 94.3%; PH3-Yb, 0.135 g 95.2%; PH4-Yb, 0.133 g 93%.

2.3 Measurements

2.3.1 UV-VIS Absorption Spectra in Solution

Electronic absorption spectra in the UV-Vis region were recorded on a Cary 100 Series UV-VIS Dual Beam Spectrometer using 1.0 cm glass cells at room temperature. The absorption spectra of ligands and complexes were obtained in CH_2Cl_2. The stock solution concentration of the samples was 2.0×10^{-4} M in CH_2Cl_2, and 50 μL of each was added to 2.5 mL of CH_2Cl_2in a 1.0 cm glass cuvette. The spectra were recorded from 200-800 nm. The final concentration of each dye was 3.9×10^{-5} M (Table 2.1).

Table 2.1 Concentration of dye solutions used for UV-Vis absorbance measurement.

Compound	Used mass for stock solution (mg)	Conc. of stock solution (mol/L)	Vol. of stock used in cuvette (µL)	Vol. of diluted solution (CH_2Cl_2) used in cuvette (mL)	Conc. Of diluted solution (mol/L)
PH1	2.12	2×10^{-4}	50	2.5	3.9×10^{-5}
PH2	2.62	2×10^{-4}	50	2.5	3.9×10^{-5}
PH3	2.64	2×10^{-4}	50	2.5	3.9×10^{-5}
PH4	2.69	2×10^{-4}	50	2.5	3.9×10^{-5}
PH1-Yb	2.57	2×10^{-4}	50	2.5	3.9×10^{-5}
PH2-Yb	2.81	2×10^{-4}	50	2.5	3.9×10^{-5}
PH3-Yb	2.83	2×10^{-4}	50	2.5	3.9×10^{-5}
PH4-Yb	2.86	2×10^{-4}	50	2.5	3.9×10^{-5}

2.3.1 Fluorescence measurements

Visible emission and excitation spectra of ligands and complexes were acquired using steady-state excitation on a spectrofluorometer with a Xenon arc lamp as a light source. The same stock solutions (Table 2.1) were used for the fluorescence measurements and each of the solution was diluted in 2.5 mL of CH_2Cl_2 to obtain 1.6×10^{-6} M final concentration. The samples were excited at 375nm on FS5 spectroflourometer to obtain emission spectra of the ligands and complexes in UV-Vis region.

2.3.1 Quantum measurements

Visible emission spectra were acquired using steady-state excitation and absorbance spectra of the same samples were obtained using UV-Vis spectrophotometer. Quantum yield in the visible region was calculated using the following equation:

$$\emptyset_X = \emptyset_{ST}\left[\frac{Grad_X}{Grad_{ST}}\right]\left[\frac{n_X}{n_{ST}}\right]$$

where $\emptyset_X$ is the fluorescence quantum yield of compound, $\emptyset_{ST}$ is the standard fluorescence quantum yield ($\emptyset_X$= 0.95, λ_{ex} = 480 nm), $Grad_X$ is the gradient from the plot of the intergraded fluorescence intensity *vs* absorbance of ligands and complexes with different concentrations, $Grad_{ST}$ is the gradient from the intergraded fluorescence intensity *vs* absorbance of Rhodamine 6G standard in ethanol, η_X and η_{ST} are refractive index of the compound and standard dissolved solvents, respectively. (η_{DCM} = 1.4241, η_{EtOH} = 1.3614)

Ex: Quantum yield measurements for PH1 ligand

Table 2.2 Concentration of PH1 ligand used for quantum yield measurement. (Stock solution concentration 2×10^{-4} M in CH_2Cl_2)

Vol. of stock used in cuvette (µL)	Vol. of diluted solution (DCM) used in cuvette (mL)	Conc. Of diluted solution (mol/L)
5	2.5	$3.99\text{x } 10^{-7}$
10	2.5	$7.98\text{x } 10^{-7}$
15	2.5	$1.19\text{x } 10^{-6}$
25	2.5	$1.99\text{x } 10^{-6}$
35	2.5	$2.79\text{x } 10^{-6}$

First step: UV-Vis absorption spectra of PH1 ligand were obtained using different concentrations as shown in table 2.2.

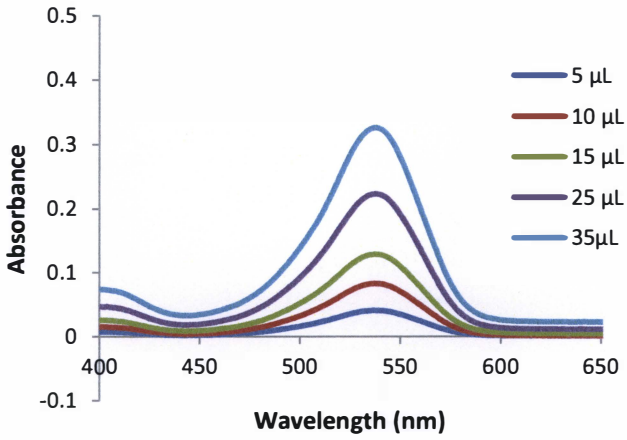

Figure 2.13 UV-Vis absorbance of PH1 ligand in CH_2Cl_2.

Second step: The fluorescence spectra of PH1 ligand were obtained using same concentration (monitored at 480 nm).

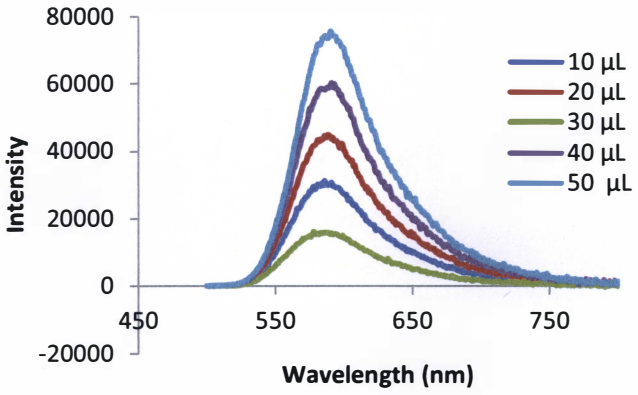

Figure 2.14 UV-Vis fluorescence spectra of PH1 ligand in CH_2Cl_2 λ_{ex}= 480 nm.

Third step: Quantum yield was calculated using the slope from the plot of the intergraded fluorescence intensity *vs* absorbance of PH1 ligands at 480 nm in $CH_2Cl_2$and slope from the intergraded fluorescence intensity *vs* absorbance of rhodamine 6G standard at 480 nm in ethanol.

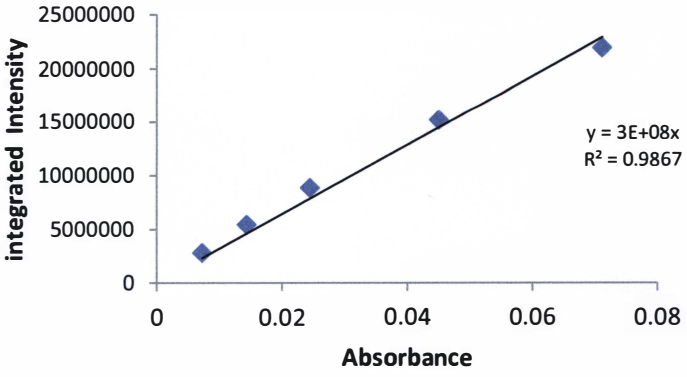

Figure 2.15 Plot of Fluorescence intensity *vs* absorbance of PH1 ligand in CH_2Cl_2 at 480 nm.

Quantum yield measurements for PH2 ligand

Table 2.3 Concentration of PH2 ligand used for quantum yield measurement. (Stock solution concentration 2×10^{-4} M in CH_2Cl_2)

Vol. of stock used in cuvette (µL)	Vol. of diluted solution (DCM) used in cuvette (mL)	Conc. Of diluted solution (mol/L)
10	2.5	$7.97x10^{-7}$
20	2.5	$1.59x10^{-6}$
30	2.5	$2.39x10^{-6}$
40	2.5	$3.18x10^{-6}$
50	2.5	$3.98x10^{-6}$

First step: UV-Vis absorption spectra of PH2 ligand were obtained using different concentrations as shown in table 2.2.

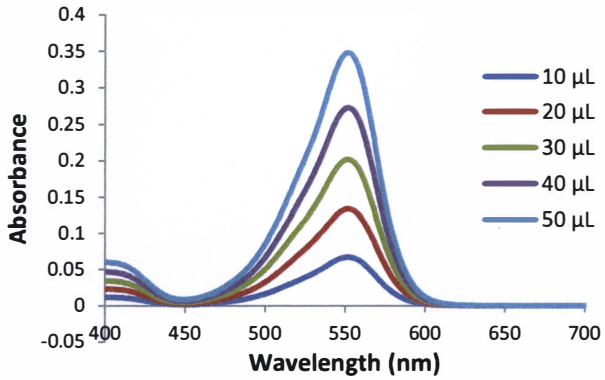

Figure 2.16 UV-Vis absorbance of PH2 ligand in CH_2Cl_2.

Second step: The fluorescence spectra of PH2 ligand were obtained using same concentration (monitored at 480 nm).

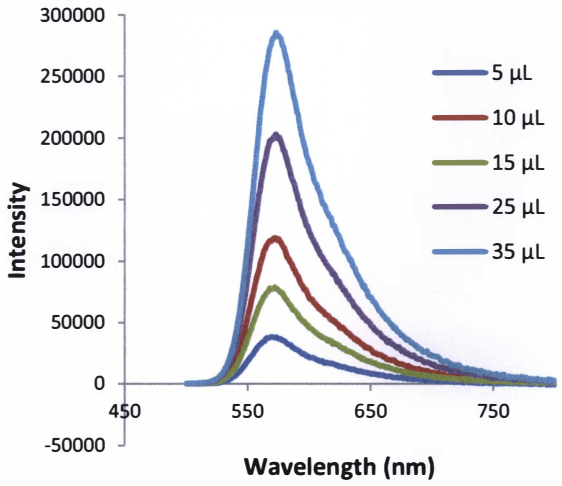

Figure 2.17 UV-Vis fluorescence spectra of PH2 ligand in CH_2Cl_2 λ_{ex}= 480 nm.

Third step: Quantum yield was calculated using the slope from the plot of the intergraded fluorescence intensity *vs* absorbance of PH2 ligands at 480 nmin $CH_2Cl_2$and slope from the intergraded fluorescence intensity *vs* absorbance of rhodamine 6G standard at 480 nm in ethanol.

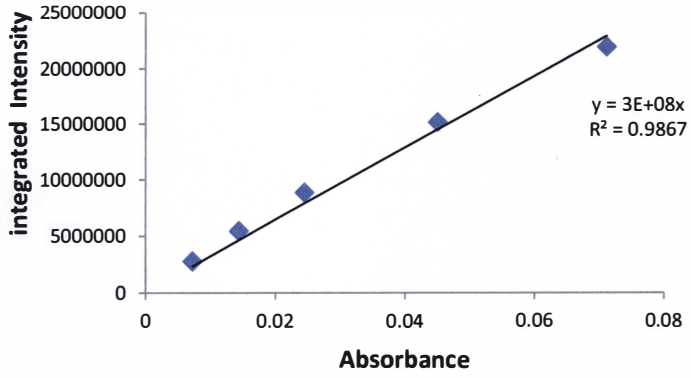

Figure 2.18 Plot of Fluorescence intensity *vs* absorbance of PH2 ligand in CH_2Cl_2 at 480 nm.

2.3.2 Lifetime measurement in the Vis region

A pulse diode laser (EPL-375, Edinburgh Instruments, Inc) with excitation wavelength at 375nm was used as the light source and life times were obtained by exponential fitting of decay curves. Decay curves of the sample in the visible region were acquired using a time-correlated single photon counting (TCSPC) technique. The life times were calculated by exponential tail fitting of the data for visible emission. The concentration of the ligands and complexes were 1.6×10^{-6} M.

2.3.3 Lifetime measurement in the NIR region

The ytterbium complexes were sent out to Dr. May Stanley (South Dakota University) to obtain lifetime measurements in NIR region. NIR decay curves were acquired using an optical parametric oscillator (OPTEK Opelette) as an excitation source. NIR emission was detected using a 0.3 m flat field monochromator (JobinYvon TRIAX 320) equipped with a NIR-sensitive photomultiplier tube (Hamamatsu R2658P). The intrinsic quantum yield ($\emptyset_{Yb}^{Yb}$) of ytterbium complexes were calculated using lifetimes in NIR region using following equation.

$$\emptyset_{Yb}^{Yb} = \frac{\tau_{obs}}{\tau_{rad}} = \frac{\tau_{obs}}{2300\ \mu s}$$

τ_{obs} = Observed lifetime of ytterbium complex

τ_{rad} = Radiative lifetime of Yb^{3+} (2300 μs)

2.3.4 Spectroscopic titration

The spectroscopic titration curves in the visible and NIR region were obtained by titrating PH1, PH2, PH3 and PH4 ligands solutions (1×10^{-6} M) in $CH_2Cl_2$with $[Yb(hfac)_3\cdot(H_2O)_2]$ (4×10^{-5} M) solution separately. The visible region emission spectra were obtained using steady state excitation at 375 nm. NIR emission spectra were acquired at 980 nm emission wavelength and excited at their own maximum wavelengths (PH1-Yb; 542 nm, PH2-Yb; 562 nm, PH3-Yb; 570 nm, PH4-Yb; 551 nm).

2.3.5 Crystallography

Single crystals of PS001 were obtained by slow evaporation of CH_2Cl_2-hexane solution and PH2-Ybwasobtained by vapor diffusion of same solution at room temperature. The crystals were wrapped with paraton-N oil and mounted on glass fibers. The diffraction measurements were made on Bruker APEXII CCD detector at 100 K. The structure was refined on F^2 using the SHELXS software package. Relevant crystal data and structure refinement details for PS001 and PH2-Yb are listed in (Table 2.1).

Table 2.4 Crystal data and structure refinement details for PS001 and PH2-Yb

	PS001	**PH2-Yb**
Empirical formula	$C_{19}H_{19}BF_2N_2$	$C_{48}H_{31}BCl_2F_{20}IN_4O_6Yb$
Formula weight	324.17	1521.42
T/K	100	100
Crystal system	Orthorhombic	Monoclinic
Space group	Pbca	$P2_1/C$
Cell dimensions		
a/Å	13.1431(6)	12.6619 (5)
b/Å	12.7129 (5)	18.7236 (8)
c/Å	20.5093 (8)	22.661 (1)
α	90°	90°
β	90°	91.456° (2)
γ	90°	90°
Volume/$Å^3$	3426.8 (2)	5370.7 (4)
Z	8	4
μ(Cu-Kα)/mm^{-1}	0.73	9.76
No.of reflection/restraints	3051/0/222	9827/78/755
No.of parameters		
R_{int}	0.108	0.150
Final R indices	R_1= 0.066	R_1= 0.052
	wR2= 0.186	wR_2= 0.132
Goodness-of-fit on F^2	0.99	1.02
Refl.collected/independent	42493,3051	81326,9827

CHAPTER 3

RESULTS AND DISCUSSION

3.1 Synthesizing and purification

The synthetic strategy for preparing metal complexes of BODIPY-bipyridine ligands followed the steps shown in Figure 2.1. 2,4-Dimethylpyrrole and benzaldehyde were reacted in distilled dichloromethane at room temperature, followed by addition of 2,3-dichloro-5,6-dicyano-1,4-benzoquinone (DDQ) for oxidation and $BF_3 \cdot OEt_2$ for coordination in the presence of Et_3N. The reaction mixture was filtered through silica gel to remove the impurities from the reaction mixture. Then, it was easy to purify the reaction mixture using column chromatography. The prepared 5-ethynyl-5'-methyl-2,2'-N-bipyridine was used as a binding group to synthesize lanthanide metal complexes because the BODIPY core does not have the capability to form metal complexes. To synthesize the BODIPY-bipyridine ligand, we first introduced an iodine atom to the BODIPY core at either C2 or C6 position of the BODIPY core using N-iodosuccinimide (NIS) in CH_2Cl_2at room temperature. This reaction condition afforded two products: the mono and di-iodinated BODIPY. The similar polarities of these compounds made their purification difficult. CH_2Cl_2:hexane (1:1) was found to be the best solvent system. However, it was difficult to separate the two bands as pure products. BODIPY-bipyridine (PH1 ligand) was synthesized by Sonogashira cross-coupling reaction using iodinated-BODIPY and 5-ethynyl-5'-methyl-2,2'-N-bipyridine under argon condition. A purple color solid was obtained as the final product after purification of the reaction mixture via column chromatography. To make the extended conjugated system, BODIPY-bipyridine

(PH1) was further iodinated (C2 or C6 positions) with NIS in CH_2Cl_2 solution at room temperature. The synthesized iodinated BODIPY-bipyridine (PH2) was modified using 4-ethynylbenzoic acid (PH3) and 1-ethynyl-4-isothiocyanatobenzene (PH4) under the Sonogashira cross-coupling reaction conditions. The final products were purified using column chromatography after several solvent systems were tested to obtain a clear band separation.

Four ytterbium (III) complexes were synthesized using the ligands PH1, PH2, PH3 and PH4 with ytterbium hexafluoroacetyl-acetonatedihydrate [$Yb(hfac)_3 \cdot (H_2O)_2$] in CH_2Cl_2 at room temperature. This reaction was straightforward, and the mixture was purified by using recrystallization. First, methanol was tried as a recrystallization solvent, but the disappearance of emission at NIR region was observed. After that, hexane was used as a solvent and a clear emission spectrum in the NIR region was observed. According to the observations, methanol could trigger the decomposition of these ytterbium complexes.

3.2 Characterization

All compounds were characterized by ^{1}H NMR spectroscopy; in addition, the structure of the PH2 ytterbium complex was confirmed by X-ray diffraction studies.

3.2.1 NMR spectroscopy

3.2.1.a. ^{1}H NMR of Compound $C_{19}H_{19}BF_2N_2$ (PS001)

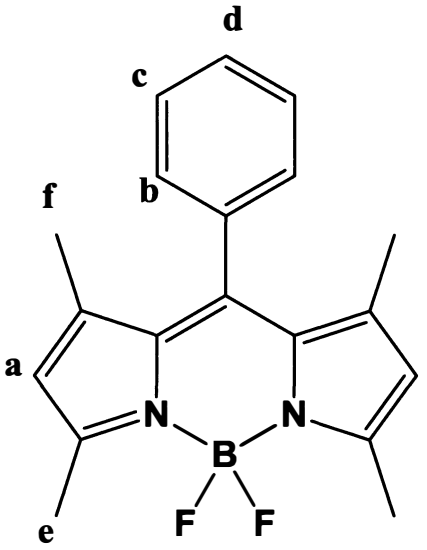

^{1}H NMR (400 MHz, $CDCl_3$) δ 7.49 (m, J = 1.4 Hz, 2H, H^c, H^d), 7.29 (m, 2H,H^b), 5.98 (s, 2H, H^a), 2.56 (s, 6H, H^e), 1.37 (s, 6H, H^f)

The ^{1}H NMR spectrum for PS001 is illustrated in the appendix (A.1). Five major peaks were observed in the spectrum. The most deshielded three aromatic protons, labeled as *c* and *d*, produced a multiplet at 7.49 ppm. The two aromatic protons, labeled as *b*, appeared as a doublet at 7.29 ppm. The two protons on C2 and C6 positions of pyrrole, labeled as *a*, produced a singlet at 5.98 ppm. The methyl groups bound to the pyrrole adjacent to the nitrogen atoms, labeled as *e*, appeared as a singlet at 2.56 ppm. The other two methyl groups on the BODIPY core, labeled as *f*, produced a singlet at 1.37 ppm.

3.2.1.b. ^1H NMR of Compound $C_{19}H_{18}BF_2IN_2$ (PS002)

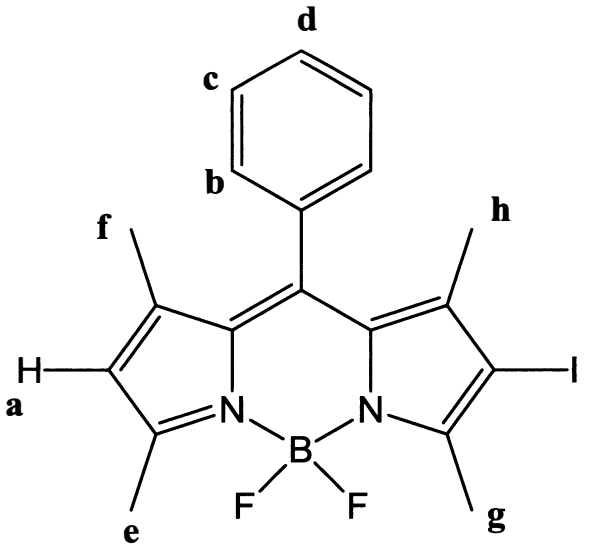

^{1}H NMR (400 MHz, $CDCl_3$) δ 7.53 (m, 3H, H^c, H^d), 7.30 (m, 2H, H^b), 6.07 (s, 1H, H^a), 2.66 (s, 3H, H^g), 2.59 (s, 3H, H^e), 1.40 (s, 6H, H^f, H^h).

The ^{1}H NMR spectrum for PS002 is illustrated in the appendix (A.2). Six major peaks were observed in the spectrum. The most deshielded three aromatic protons, labeled as *c* and *d*, produced a multiplet at 7.53 ppm. The two aromatic protons, labeled as *b*, appeared as a doublet at 7.30 ppm. The one proton on β positions of pyrrole, labeled as *a*, produced a singlet at 6.07 ppm. The methyl group bound to the pyrrole adjacent to the nitrogen atom and iodine atom, labeled as *g*, appeared as a singlet at 2.66 ppm. The methyl group bound to the pyrrole adjacent to the nitrogen, labeled as *e*, produced a singlet at 2.59 ppm. The other two methyl groups on the BODIPY core, labeled as *f* and *h*, produced a singlet at 1.40 ppm.

3.2.1.c. ^1H NMR of Compound $C_{13}H_{10}N_2$ (PS003)

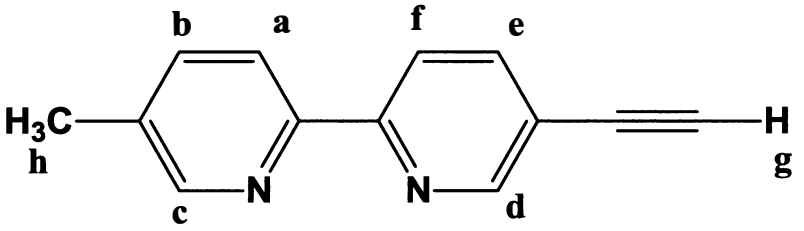

^1H NMR (400 MHz, $CDCl_3$) δ 8.75 (s, 1H, H^d), 8.51 (s, 1H, H^c), 8.36 (d, J = 8.1 Hz, 1H, H^f), 8.30 (d, J = 8.1 Hz, 1H, H^a), 7.89 (d, J = 8.3 Hz, 1H, H^e), 7.87 (d, 8.3 Hz, 1H, H^b), 3.28 (s, 1H, H^g), 2.40 (s, 3H, H^h).

The ^1H NMR spectrum for PS003 is illustrated in the appendix (A.3). Eight major peaks were observed in the spectrum. The protons on pyridine ring adjacent to the nitrogen atoms, labeled as *d* and *c*, produced two singlets at 8.75 ppm and 8.51 ppm respectively. The two protons, labeled as *f* and *a*, appeared as two doublets at 8.36 ppm and 8.30 ppm. The two protons, labeled as *e* and *b*, produced two doublets at 7.89 ppm and 7.65 ppm, respectively. The methyl group bound to the pyridine ring, labeled as *h*, appeared as a singlet at 2.40 ppm. The proton on alkyne group, labeled as *g*, appeared as a singlet at 3.28 ppm.

3.2.1.d. ^1H NMR of Compound $C_{32}H_{27}BF_2N_4$ (PH1)

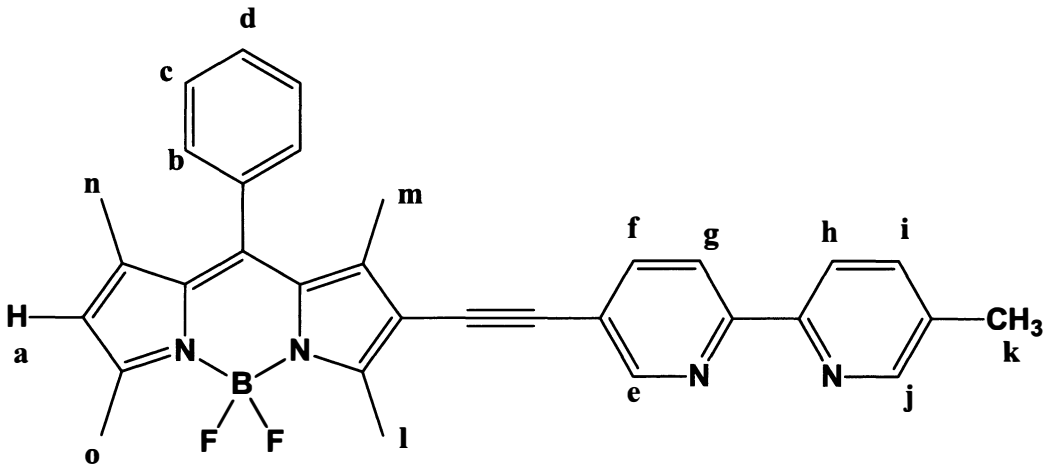

^1H NMR (400 MHz, $CDCl_3$) δ 8.70 (s, 1H, H^j), 8.51 (s, 1H, H^e), 8.32 (d, 1H, Hg), 8.31 (d, 1H, H^h), 7.84 (d, 1H, H^i), 7.63 (d, J = 8.3 Hz, 1H, H^f), 7.51 (m, 3H, H^c, H^d), 7.30 (m, 2H, H^b), 6.05 (s, 1H, H^a), 2.72 (s, 3H, H^l), 2.59 (s, 3H, H^o), 2.40 (s, 3H, H^m), 1.52 (s, 3H, H^n), 1.41 (s, 3H, H^k).

The ^1H NMR spectrum for PH1 is illustrated in the appendix (A.4). Fourteen major peaks were observed in the spectrum. The protons on pyridine ring adjacent to the nitrogen atoms, labeled as *j* and *e*, produced two singlets at 8.70 ppm and 8.51 ppm respectively. The proton, labeled as *g* appeared as a doublet at 8.32 ppm. The proton, labeled as *h*, produced a doublet at 8.31 ppm. The two protons, labeled as *i* and *f,* produced doublets at 7.84 ppm and 7.63 ppm, respectively. The two protons *c* and *d* which are bound to the aromatic ring of the BODIPY core produced a multiplet at 7.51 ppm. The two aromatic protons *b*, which is close to the BODIPY core, appeared as a multiplet at 7.30 ppm. The proton *a* on β position of pyrrole produced a singlet at 6.05 ppm. The methyl groups bound to the pyrrole ring, labeled as *l*, *o*, *m*, and *n*, appeared as singlet peaks at 2.72,

2.59, 2.40, and 1.52 ppm, respectively. The methyl group on pyridine group protons, labeled as *k*, produced a singlet at 1.41 ppm.

3.2.1.e. ^1H NMR of Compound $C_{32}H_{26}BF_2IN_4$ (PH2)

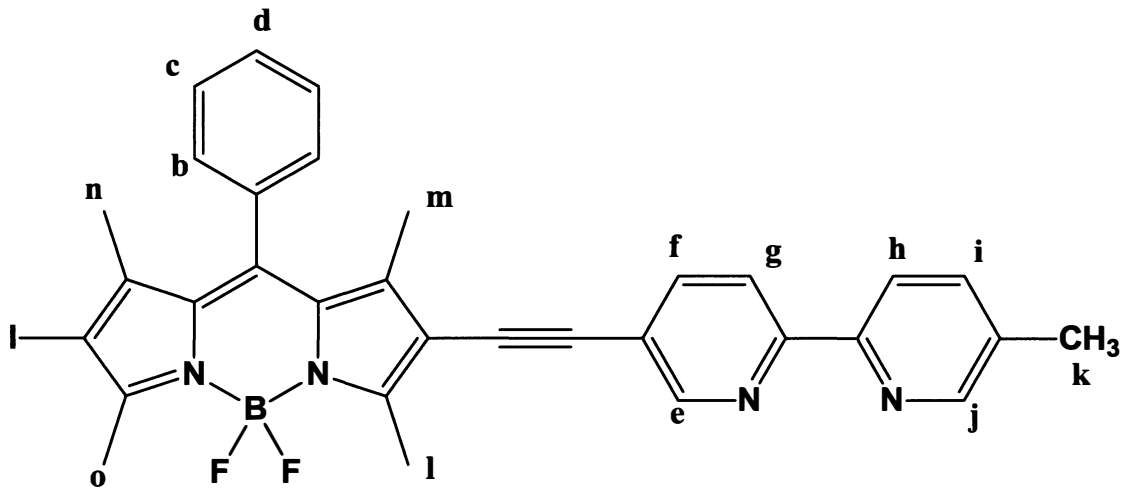

^1H NMR (400 MHz, $CDCl_3$) δ (ppm) 8.71(s, 1H, H^j), 8.51(s, 1H, H^e), 8.37(d, 1H, H^g), 8.31(d, 1H, H^h), 7.84(d, 1H, H^i), 7.63(d, 1H, H^f), 7.54(m, 3H, H^c, H^d), 7.30(m, 2H, H^b), 2.73(s, 3H, H^l), 2.67(s, 3H, H^o), 2.40(s, 3H, H^m), 1.52(s, 3H, H^n), 1.42(s, 3H, H^k).

The ^1H NMR spectrum for PH2 is illustrated in the appendix (A.5). Thirteen major peaks were observed in the spectrum. The protons on pyridine ring adjacent to the nitrogen atoms, labeled as *j* and *e*, produced two singlets at 8.71 ppm and 8.51 ppm, respectively. The two protons, labeled as *g* and *h*, appeared as two doublets at 8.37 ppm and 8.31 ppm. The two protons, labeled as *i* and *f*, produced doublets at 7.84 ppm and 7.63 ppm, respectively. The two protons *c* and *d* which are bound to the aromatic ring produced a multiplet at 7.54 ppm. The two protons labeled as *b* on the aromatic ring appeared as a multiplet at 7.30 ppm. The peak at 6.05ppm related to the β position of PH1 disappeared in the PH2 NMR spectrum by the iodine atom. The methyl groups bound to the pyrrole

ring, labeled as *l*, *o*, *m*, and *n*, appeared as singlet peaks at 2.73, 2.67, 2.40, and 1.52 ppm, respectively. The methyl group on pyridine group protons, labeled as *l*, produced a singlet at 1.42 ppm.

3.2.1.f. ^{1}H NMR of Compound $C_{41}H_{31}BF_2N_4O_2$ (PH3)

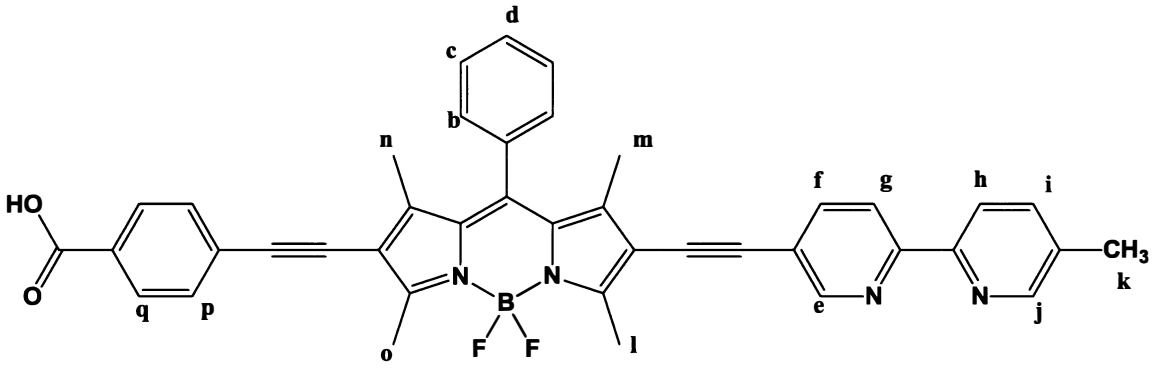

^{1}H NMR (400 MHz, $CDCl_3$) δ (ppm) 8.71 (s, 1H, H^j), 8.51(s, 1H, H^e), 8.36 (dd, 2H, H^q), 7.84 (d, 1H, H^g), 7.72 (d, 1H, H^h), 7.65 (d, 1H, H^i), 7.54 (m, 5H, H^c, H^d, H^p), 7.48 (d, 1H, H^f), 7.29 (m, 2H, H^b), 2.73 (s, 3H, H^l), 2.67 (s, 3H, H^o), 2.40 (s, 3H, H^m), 1.52 (s, 3H, H^n), 1.42 (s, 3H, H^k).

The ^{1}H NMR spectrum for PH3 is illustrated in the appendix (A.6). Fourteen major peaks were observed in the spectrum. The protons on the pyridine ring adjacent to the nitrogen atoms, labeled as *j* and *e*, produced a singlet at 8.71 ppm and 8.51 ppm respectively. The protons on the aromatic ring adjacent to the benzoic acid group, labeled as *q*, appeared as a double doublet at 8.36 ppm. The two protons labeled as *g* and *h*, produced doublets at 7.84 ppm and 7.72 ppm, respectively. The proton on bipyridine close to the methyl group, labeled as *i* produced a doublet at 7.65 ppm. The aromatic protons *c*, *d*, and *p* have overlapped together and appeared as a multiplet at 7.54 ppm. The proton on bipyridine

labeled as *f* appeared as a doublet at 7.48 ppm. The two aromatic protons *b* produced a multiplet at 7.29 ppm. The methyl groups bound to the pyrrole ring, labeled as *f*, *c*, *e*, and *d*, appeared as singlet peaks at 2.73, 2.67, 2.40, and 1.52 ppm, respectively. The methyl group on pyridine group protons, labeled as *k*, produced a singlet at 1.42 ppm.

3.2.1.g. ^{1}H NMR of Compound C_9H_5NS (PS004)

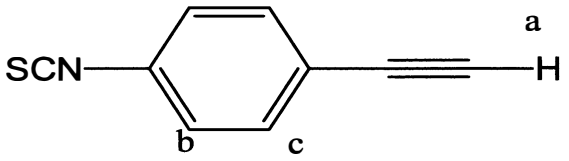

^{1}H NMR (400 MHz, $CDCl_3$) δ (ppm), 7.47 (d, 2H, H^c), 7.18 (d. 2H, H^b), 3.16 (s, 1H, H^a).

The ^{1}H NMR spectrum for PS004 is illustrated in the appendix (A.7). Three major peaks were observed in the spectrum. The protons on the aromatic ring adjacent to the alkyne group, labeled as *c*, produced a doublet at 7.47 ppm, and the protons on the aromatic ring adjacent to the thiocyanide group, labeled as *b*, produced a doublet at 7.18 ppm. The proton on the alkyne group, labeled as a, appeared as a singlet at 3.16 ppm.

3.2.1.h. ^{1}H NMR of Compound $C_{41}H_{30}BF_2N_5S$ (PH4)

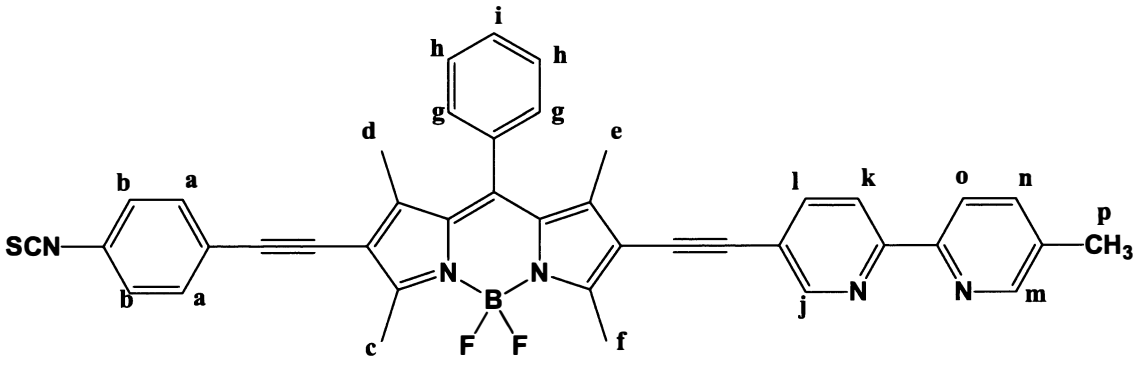

^{1}H NMR (400 MHz, $CDCl_3$) δ 8.70 (s, 1H, H^m), 8.50 (s, 1H, H^j), 8.35 (dd, 2H, H^b), 7.84 (d, 1H, H^k), 7.70 (d, 1H, H^o), 7.63 (d, 1H, H^n), 7.54 (m, 5H, H^h, H^i, H^a),7.40 (d, 1H, H^l), 7.30 (m, 2H, H^g), 2.73 (s, 3H, H^f), 2.67 (s, 3H, H^c), 2.40 (s, 3H, H^e), 1.52 (s, 3H, H^d), 1.42 (s, 3H, H^p).

The ^{1}H NMR spectrum for PH4 is illustrated in the appendix (A.8). Fourteen major peaks were observed in the spectrum. The protons on the pyridine ring adjacent to the nitrogen atoms, labeled as *j* and *m*, produced a singlet at 8.70 ppm and 8.50 ppm respectively. The two protons, labeled as *k* and *l*, produced doublets at 8.40 ppm and 8.27 ppm, respectively. The two protons *a* and *b* on the aromatic ring, produced a multiplet at 7.47 ppm. The protons on the *meso* position aromatic ring, labeled as *h* and *i*, appeared as a multiplet at 7.27 ppm. The methyl groups bound to the pyrrole ring, labeled as *f*, *c*, *e*, and *d*, appeared as singlet peaks at 2.73, 2.67, 2.40, and 1.52 ppm, respectively. The methyl group on the pyridine group protons, labeled as *p*, produced a singlet at 1.42 ppm.

3.2.1.i. ^{1}H NMR of Compound $C_{21}H_{19}BF_2N_2$ (PS005)

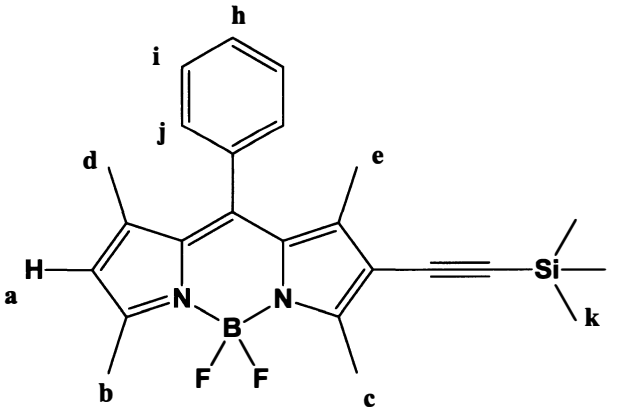

^{1}H NMR (400 MHz, $CDCl_3$) δ 7.50 (m, 3H, H^i, H^h), 7.27 (m, 2H, H^j), 6.02 (s, 1H, H^a), 2.63 (s, 3H, H^c), 2.57 (s, 3H, H^b), 1.43 (s, 3H, H^e), 1.39 (s, 3H, H^d), 0.20 (s, 9H, H^k).

The ^{1}H NMR spectrum for PS005 is illustrated in the appendix (A.9). Seven major peaks were observed in the spectrum. The protons on aromatic ring I and *h* appeared as a multiplet at 7.50 ppm, and the proton *j*, produced a doublet at 7.27 ppm. The proton on the β position of BODIPY core, labeled as *a*, produced a singlet at 6.02 ppm. The methyl group protons on the BODIPY core, labeled as c, *b*, *e*, and *d*, appeared as singlets at 2.63, 2.57, 1.43, and 1.39 ppm, respectively. The methyl protons on the silane group, labeled as *k*, produced a singlet at 0.20 ppm.

3.2.1.j. ^{1}H NMR of Compound $C_{21}H_{19}BF_2N_2$ (PS006)

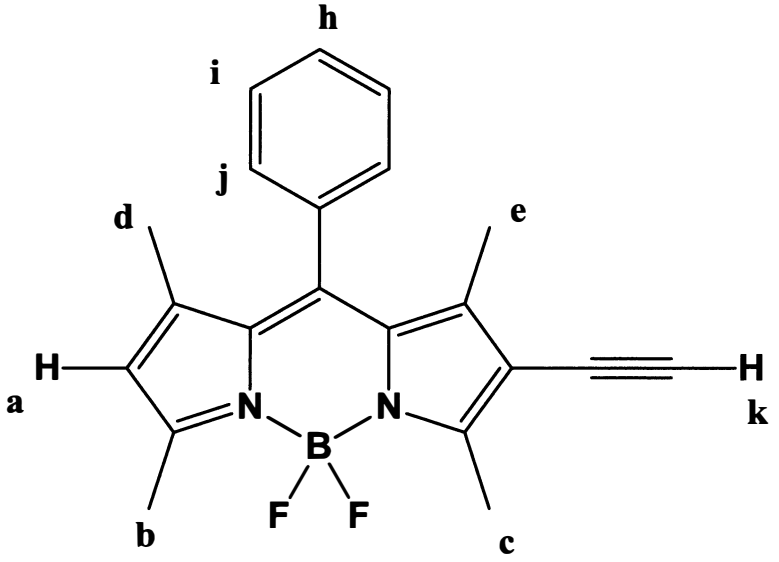

^{1}H NMR (400 MHz, $CDCl_3$) δ 7.51 (m, 3H, H^i, H^h), 7.28 (m, 2H, H^j), 6.04 (s, 1H, H^a), 3.28 (s, 1H, H^k), 2.64 (s, 3H, H^c), 2.58 (s, 3H, H^b), 1.44 (s, 3H, H^e), 1.39 (s, 3H, H^d).

The ^{1}H NMR spectrum for PS005 is illustrated in the appendix (A.9). Eight major peaks were observed in the spectrum. The protons on the aromatic ring *i* and *h* appeared as a multiplet at 7.51 ppm, and the protons labeled as *j* produced a doublet at 7.28ppm. The proton on the β position of BODIPY core, labeled as *a*, produced a singlet at 6.04 ppm.

The product formation was confirmed by the proton *k* on alkyne group, which appeared as a singlet at 3.28 ppm. The methyl group protons on the BODIPY core, labeled as *c*, *b*, *e*, and *d*, appeared as singlets at 2.64, 2.58, 1.44, and 1.39 ppm, respectively.

3.2.2 X-Ray Crystallography

The structures of the PS001 precursor and PH2-Yb complex were ascertained by single crystal X-ray diffraction analysis. For PS001, single crystals were obtained by slow evaporation of a dichloromethane and hexane, and for the PH2-Yb complex, single crystals were obtained by vapor diffusion method using the same solvent system. Perspective views of PS001 and PH2-Yb are shown in Fig 3.1 while selected bond angles and bond lengths are summarized in Table 3.1. According to the crystal data for PS001 the crystal system is orthorhombic, and for the complex PH2-Yb the crystal system is monoclinic. The space groups are Pbca and $P2_1/c$ for PS001 and PH2-Yb complex, respectively. The single crystal structure of PS001 revealed that the phenyl group is almost perpendicular to the BODIPY core, as shown by the torsion angle between the two planes of the BODIPY core and benzene unit is 84.15° (Figure 3.2). The PH2-Yb crystal structure revealed that the Yb(III) ion is eight-coordinated by two N atoms from the bipyridine and six O atoms from the coordinated trifluoroacetic acid. The boron atom of the BODIPY core is in a tetrahedral geometry with bond angles averaging 109.05°. According to the torsion angle between BODIPY core and bipyridine group, the two units are tilted by 21.19°.

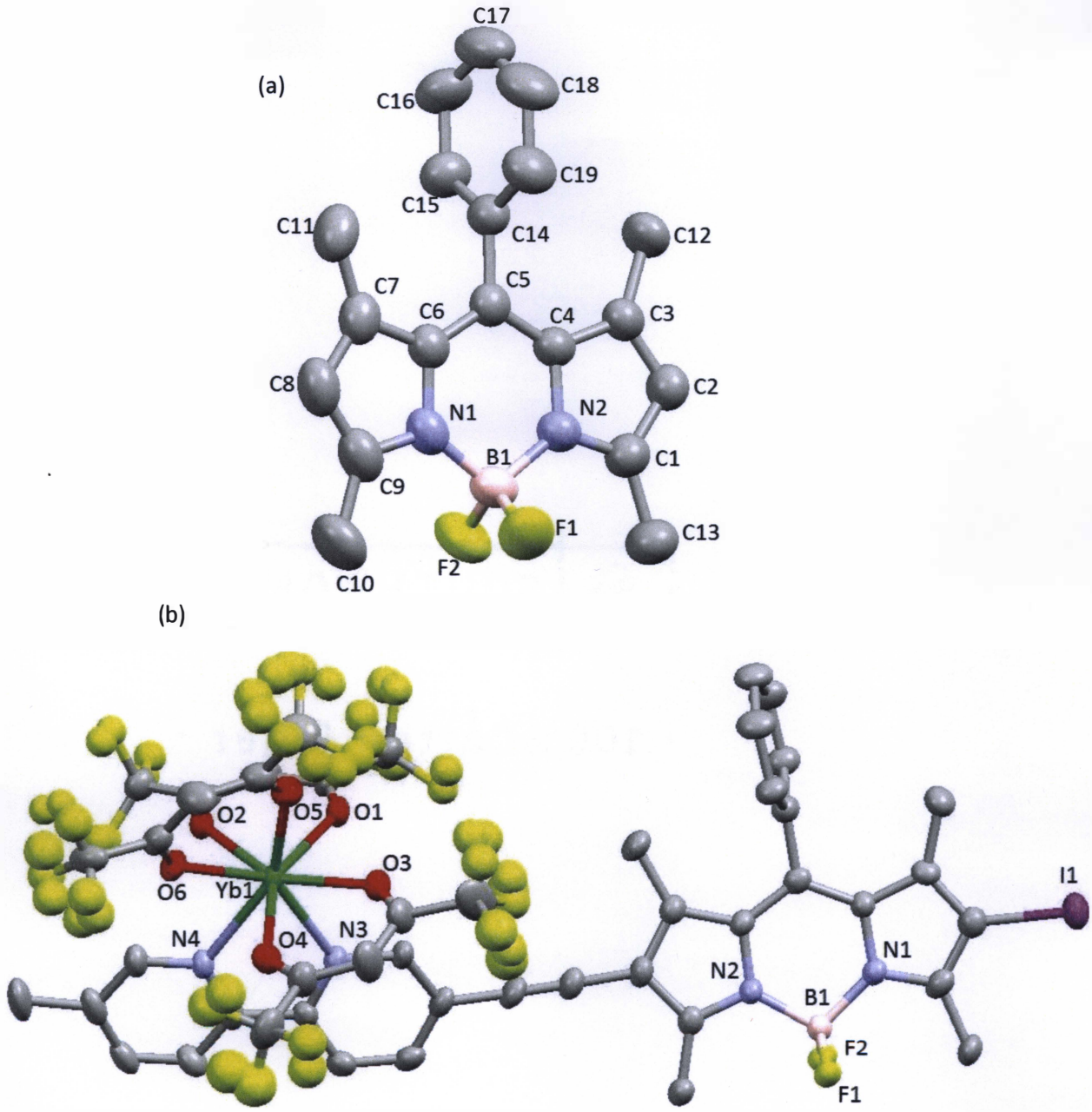

Figure 3.1 ORTEP diagrams of a single-crystal structures of (a) PS001 and (b) PH2-Yb with 50% thermal ellipsoid probability. The H atoms were omitted for clarity. F atoms on each CF_3 unit are disordered.

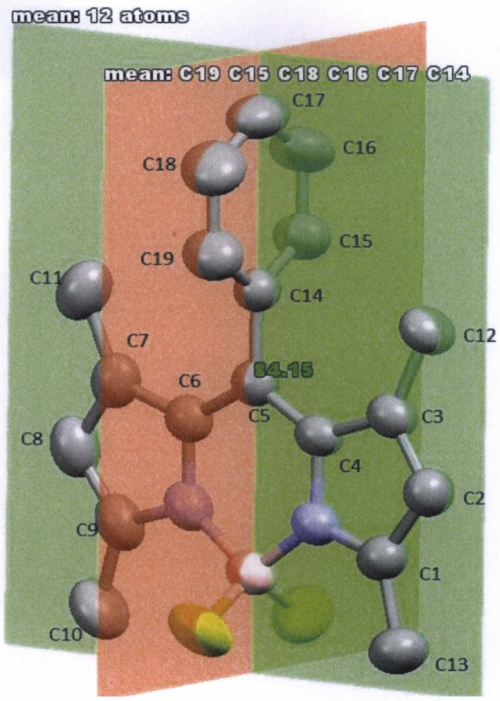

Figure 3.2 Torsion Angle between the two planes of the BODIPY core and phenyl ring

Table 3.1 Selected bond lengths and bond angles of PS001 and PH2-Yb(hfac)$_3$

Bond	Bond length (Å)
N4-Yb1	2.474(5)
N3-Yb1	2.468(5)
C4-I1	2.089(7)
N2-B1	1.566(9)
N1-B1	1.564(9)
B1-F1	1.390(8)
B1-F2	1.387(8)

Bond	Bond angle (°)
N4-Yb1- N3	65.3(2)
N3- B1- F2	110.7(5)
N2- B1- F1	110.1(5)
N2- B1- N1	106.1(5)
F1- B1- F2	109.3(5)

3.3 Photophysical Properties

3.3.1 UV-Vis Absorption

The absorption spectra of ligands and complexes in CH_2Cl_2 are shown in Figure 3.3, and the results are summarized in Table 3.2. The data illustrates that the characteristic pattern of the four different ligands and their complexes. The absorption coefficient and absorption wavelengths rely significantly on the substituent of BODIPY core. The ligands have strong absorptions from 537 to 573 nm; their complexes have similar absorption wavelengths between 535 -571 nm. As shown in Table 3.2, the ligands PH1-PH4 exhibit longer wavelength absorptions at 537, 552, 573 and 553 nm, respectively. This data illustrates that the bathochromic shift of ligands varies with the higher conjugation of the system. The PS001 produced a maximum absorption peak at 498 nm. Its absorption coefficient was 7.34×10^4 $M^{-1}cm^{-1}$. Upon iodination (PS002), the absorption shifted by 16 nm, with an absorption coefficient of 7.31×10^4 $M^{-1}cm^{-1}$. Once the 5-ethynyl-5'-methyl-2,2'-N-bipiridinwas attached to the C2 or C6 position of BODIPY core, the absorption was shifted by 37 nm to the longer wavelength and the absorption coefficient dropped down to 7.43×10^3 $M^{-1}cm^{-1}$. After synthesizing the π-conjugated molecule by employing the C2 or C6 position of BODIPY core with 4-ethynylbenzoic acid (PH3), the absorption peak red-shifted by 72 nm. Compared with the PH3 ligand, 1-ethynyl-4-isothiocyanatobenzene BODIPY ligand (PH4) exhibited a low red shift under the same conditions. The respective moderate and good electron withdrawing ability of –COOH and –NCS groups may have influenced the absorption and emission properties of the new derivatized ligands. The extended conjugation reduces the energy gap between HOMO and LUMO energy level, thus broadens the absorption and emission wavelength

to longer wavelength region. The bipyridine group significantly quenches the fluorescence of BODIPY core due to the internal charge transfer process between the donor bipyridine unit and the BODIPY core. The ligands and their complexes exhibited variable fluorescence intensities at a similar concentration. However, the PH3 ligand has lower absorption intensity than PH4, even though they both have quite similar π-conjugation systems. The most probable reason is the lower solubility of the PH3 ligand in the CH_2Cl_2 solvent. The PH3-Yb complex has higher absorption intensity than the PH3 ligand, and the other complexes have a more or less similar intensity to the ligands. Also, one shoulder peak was observed at 623 nm in PH3 ligand absorption spectrum and this peak was disappeared with MeOH. The PH3 ligands have some possibility to make acid-acid hydrogen bonding dimer and acid-pyridine hydrogen bonding polymer intramolecular interactions (Figure 3.4).This hypothesis was confirmed by titrating the PH3 ligand with MeOH. Interestingly, two sharp absorption peaks were observed in UV spectrum at 573 nm and 625 nm (without MeOH), and the absorption peak at 625 nm disappeared as a result of MeOH addition (Figure 3.5). Also, the emission intensity at UV-Vis region was increased with the MeOH (Figure 3.6). The MeOH molecules can interact with –COOH groups instead of the nitrogen lone pairs. As a consequence of these interactions, the PH3 ligand becomes free molecules in the solution and gave one absorption peak corresponding to the PH3 ligand. Also, the fluorescence emission peak intensity was increased with the MeOH.

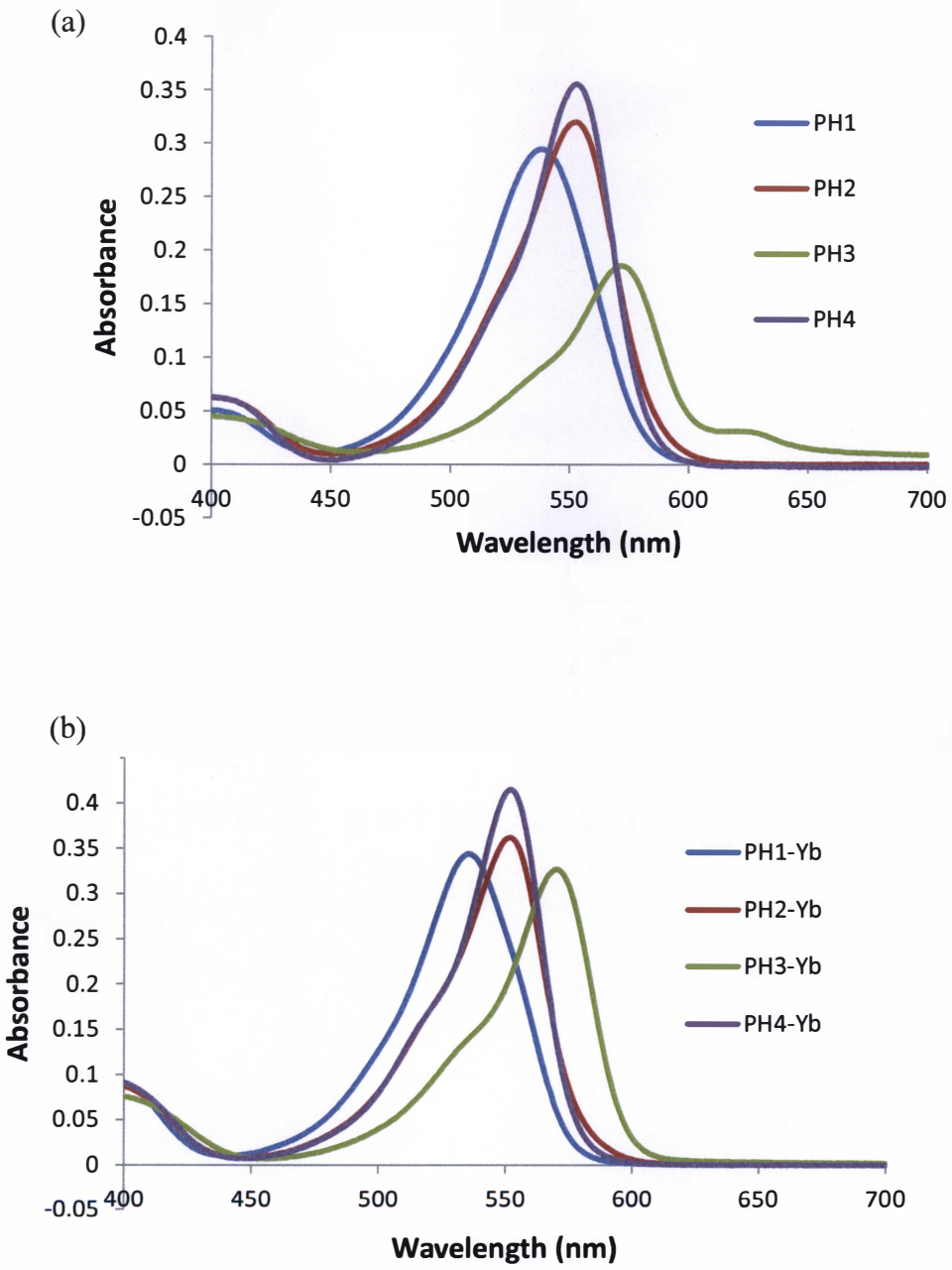

Figure 3.3. (a) Experimental UV-Vis absorption spectra of PH1, PH2, PH3, and PH4 ligand in CH_2Cl_2 (3.9×10^{-5} M), (b) Experimental UV-Vis absorption spectra of PH1-Yb, PH2-Yb, PH3-Yb, and PH4-Yb ligand in CH_2Cl_2 (3.9×10^{-5} M)

Table 3.2 Absorptivity and maximum absorption wavelengths of PH1, PH2, PH3 and PH4 ligands and their complexes in CH_2Cl_2.

Compound	Absorbance	ε ($M^{-1}cm^{-1}$)	λ_{max} (nm)
PS001	2.891	7.34×10^4	498
PS002	2.207	7.31×10^4	516
PH1	0.290	7.43×10^3	535
PH2	0.314	8.05×10^3	549
PH3	0.185	4.74×10^3	570
PH4	0.353	9.04×10^3	551
PH1-Yb	0.339	8.69×10^3	533
PH2-Yb	0.371	9.51×10^3	545
PH3-Yb	0.325	8.33×10^3	569
PH4-Yb	0.410	10.51×10^3	550

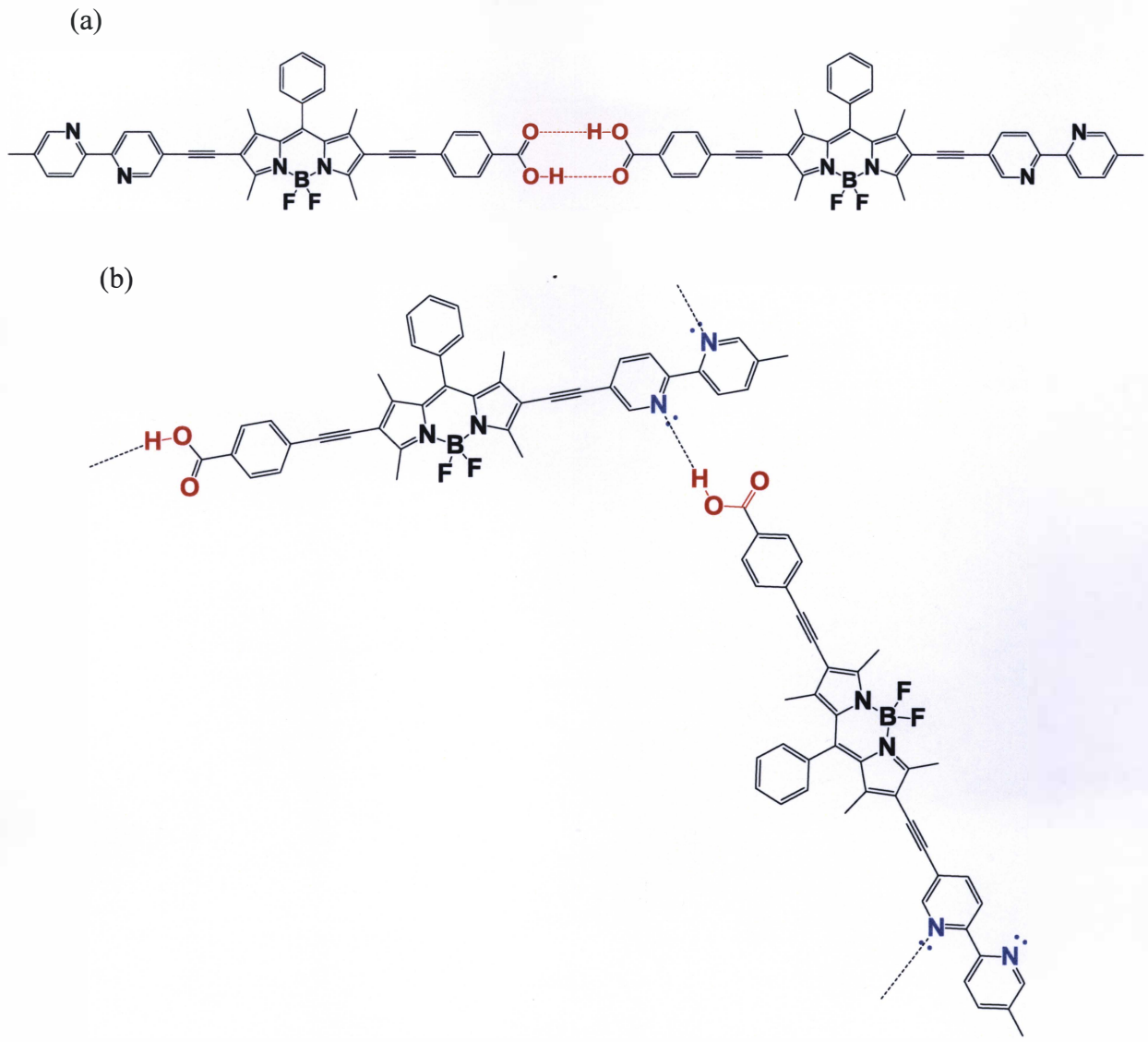

Figure 3.4 (a) Acid–acid hydrogen-bonding dimer (b) Acid–pyridine hydrogen-bonding polymer

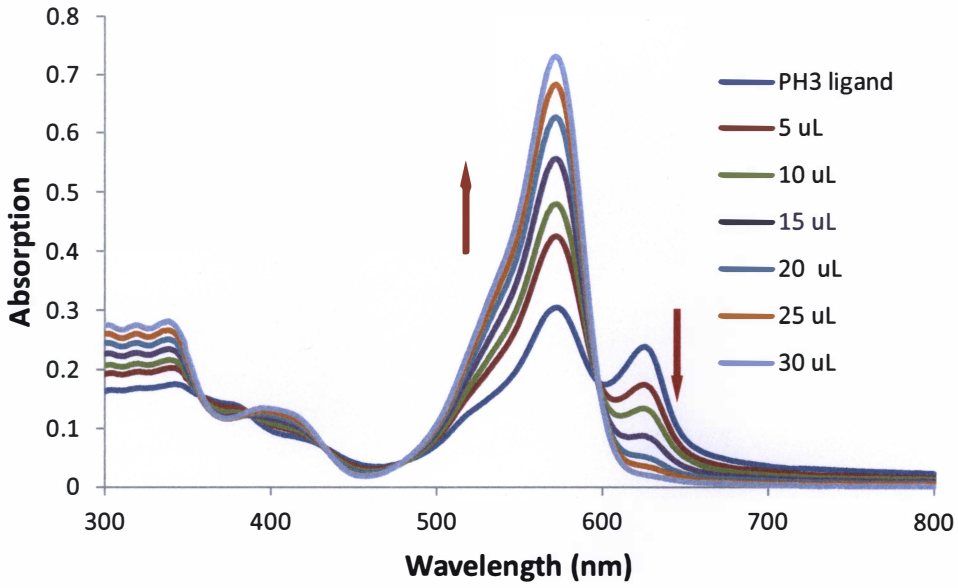

Figure 3.5 UV-Vis spectral changes of the PH3 ligand in dry CH_2Cl_2upon addition of different amounts of MeOH.

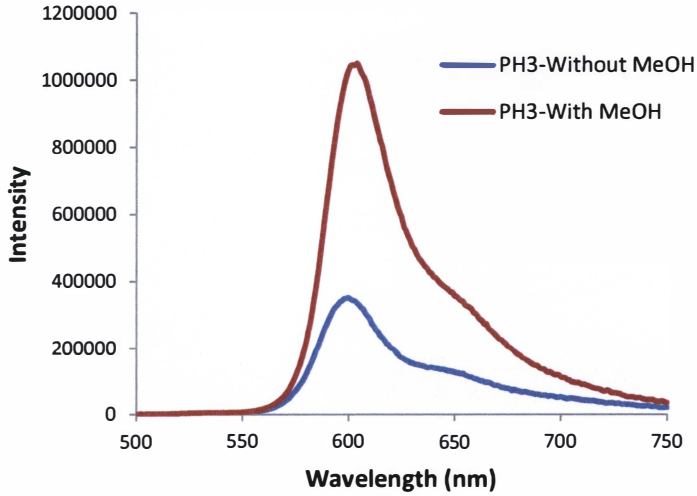

Figure 3.6 Emission spectra of the PH3 ligand before adding MeOH and after adding MeOH.

3.3.2 Fluorescence Spectroscopy

The emission and excitation spectra for PH1-PH4 ligands and their complexes in the visible region are shown in Figure 3.7 and Figure 3.8, respectively, and the spectral data is summarized in Table 3.3 and Table 3.4. The maximum absorption and excitation wavelengths of ligands and complexes were similar to each other. The emission wavelength of the PH1 ligand was at 542 nm, and has the lowest emission wavelength compared with the other compounds. PH3 ligand and its complex have longer emission wavelength around 597 nm and 592 nm. Also, emission wavelength was increased from PH1 to PH4, whereas PH3 ligand and its complex exhibited the longest emission wavelength in the visible region. The emission intensity decreased from PH1 to PH2 ligand by 35%. Heavy atoms like iodine facilitate the triplet state of ligand and, it quenches the initial fluorescence of the ligand in the visible region. Extension of the π-conjugation system in BODIPY precursor from bipyridine, 4-ethynylbenzoic acid and 1-ethynyl-4-isothiocyanatobenzene caused a significant redshift in their absorption and emission (Figure 3.9). The emission wavelengths of BODIPY bipyridine derivatives appear in the range of 500 – 600 nm, which was related to the BODIPY molecule emission wavelengths. It can be concluded that the energy transfer occurs from the BODIPY chromophore to the Yb(III) ion. According to the data, PH1 has lowest excitation wavelength at 533 nm, and PH3 ligand has highest excitation wavelength at 571 nm. This observation illustrates the fact that the extended conjugated system compounds absorb at lower energy for excitation than the non-conjugated compounds. The PH2 and PH4 ligands exhibited mostly similar excitation wavelengths 552 nm and 551 nm in the visible region. The normalized excitation spectrum of ytterbium complexes

at 980 nm illustrates the best excitation wavelengths for maximum emission at NIR region (Figure 3.10).

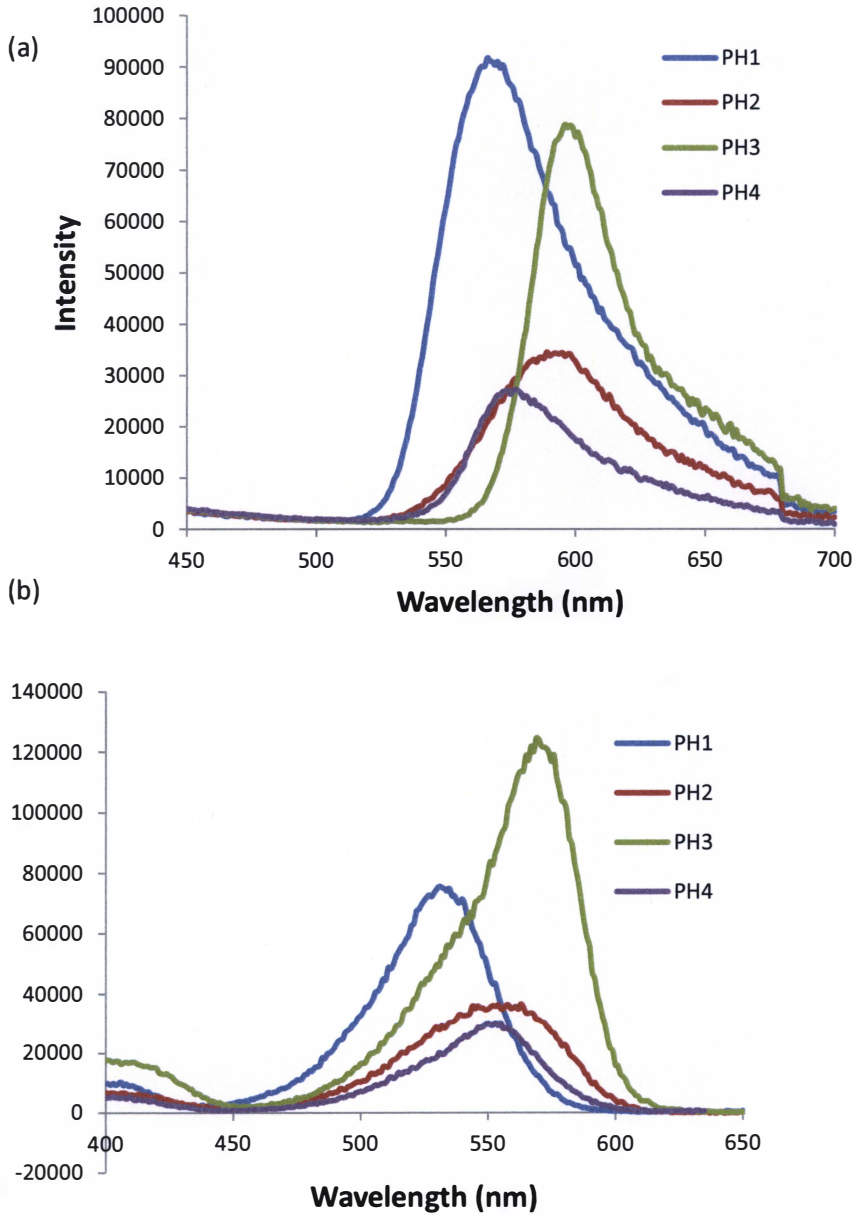

Figure 3.7 (a) Emission and (b) excitation spectra of PH1, PH2, PH3, and PH4 ligands in CH_2Cl_2 (1.6×10^{-6} M). The excitation wavelength was 375 nm. The emission wavelengths for PH1: 570 nm, PH2:552 nm, PH3: 571 nm and PH4: 551 nm

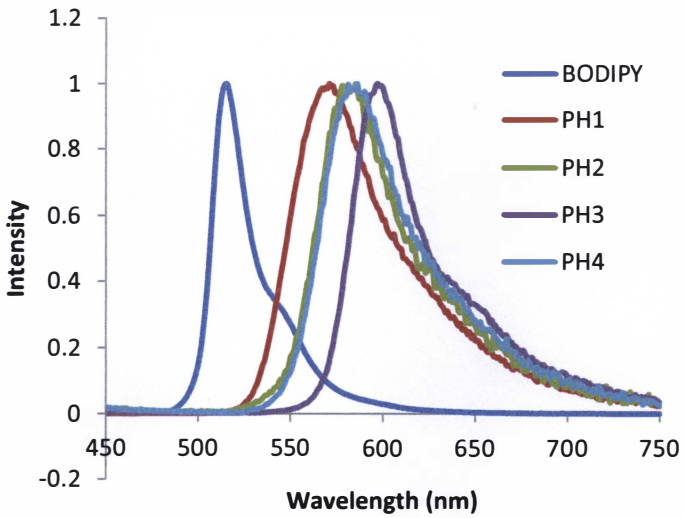

Figure 3.8 Normalized emission spectra of BODIPY precursor, PH1, PH2, PH3, and PH4 ligands in CH_2Cl_2at room temperature.

(a)

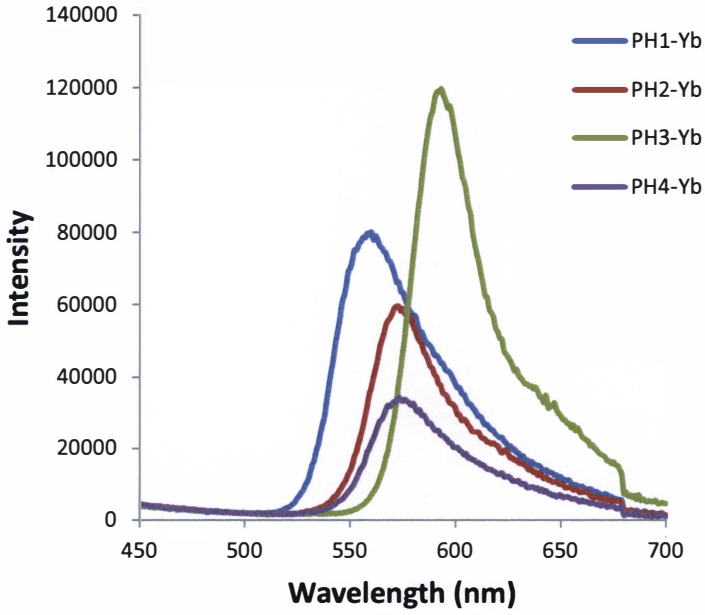

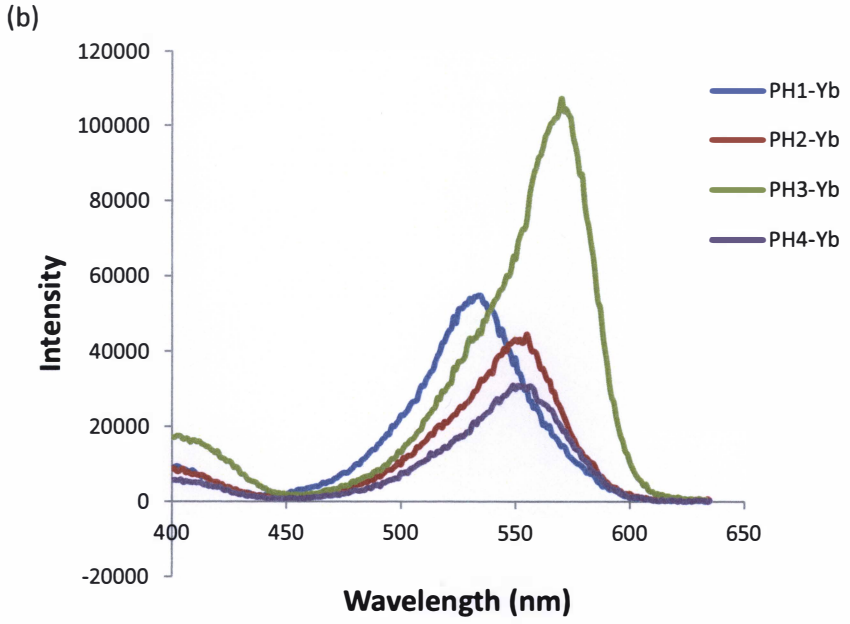

Figure 3.9 (a) Emission and (b) excitation spectra of PH1-Yb, PH2-Yb, PH3-Yb, and PH4-Yb complexes in CH_2Cl_2 (1.6×10^{-6} M). The excitation wavelength was 375 nm. The emission wavelengths for PH1: 558 nm, PH2:574 nm, PH3: 592 nm and PH4: 574 nm.

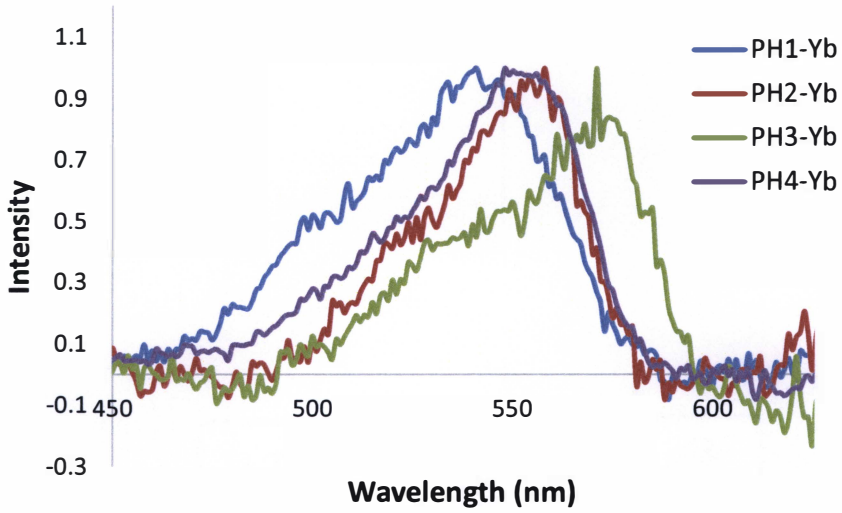

Figure 3.10 Normalized excitation spectra of ytterbium complexes at 980 nm in CH_2Cl_2 at room temperature.

Formation of lanthanide complexes was confirmed by the emission in the NIR region. The NIR emission spectra of ligands are shown in Figure 3.11. The NIR emission of lanthanide ions is usually achieved by energy transfer from the ligand to the excited state of the lanthanide (III) ion. The PH1-Yb complex has the lowest NIR emission intensity while the PH4-Yb and PH2-Yb complexes have the highest NIR emission intensity in a similar level. The observed NIR emission pattern was PH4≈PH2 > PH3 > PH1. This observation suggests that the heavy atom effect of PH2 ligand is much stronger to sensitize the lanthanide ion than PH1 ligand. Also, 1-ethynyl-4-isothiocyanatobenzene electron withdrawing group in PH4 ligand can affect the sensitization process than the 4-ethynylbenzoic acid group in PH3 ligand. All Yb(III) complexes exhibited three peaks, centered at 975, 1001, and 1027 nm respectively. The intensity at 1001 nm is stronger than the intensities at 980 and 1027 nm. They can be assigned to the transition between $^2F_{5/2}$ ground state and $^2F_{7/12}$ excited state of Yb(III) in BODIPY-bipyridine complex.

The lifetime of ligands and complexes in visible and NIR regions are summarized in Table 3.6. The visible region lifetimes were determined by excitation at 375 nm. The PH1 ligand has a long lifetime (3.67 ns) and PH2 ligand exhibited the lowest excited state lifetime of 2.68 ns, which indicates the heavy atom effect. Ytterbium complexes have more or less similar life times to the ligands. The lifetimes of complexes in the NIR region were similar to each other (10.9 μs - 11.1 μs). According to the quantum yield efficiencies, PH1 ligand exhibited the highest quantum yield than other ligands (Table 3.3). PH2 ligand has a slightly lower fluorescence quantum yield because of the heavy atom effect.

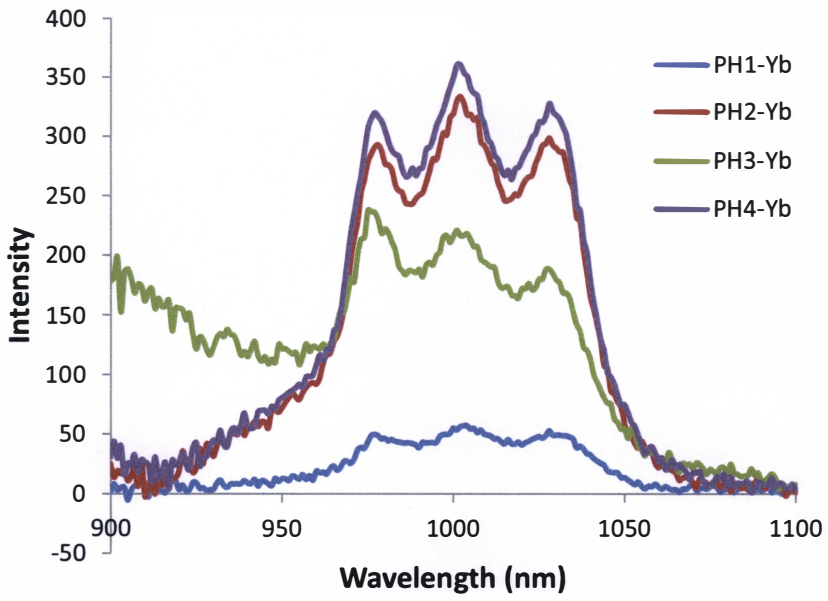

Figure 3.11 NIR emission spectra of complexes in CH_2Cl_2 (1.6×10^{-6} M) PH1-Yb λ_{ex} = 530 nm, PH2-Yb λ_{ex} = 550 nm, PH3-Yb λ_{ex} = 570 nm, Ph4-Yb λ_{ex} = 555 nm.

Table 3.3 Photophysical properties (fluorescence) of ligands and BODIPY precursor, Fluorescence quantum yields of ligands were calculated by using rhodamine-6G excited at 480 nm in EtOH as the reference quantum yield efficiency (Ø = 0.95)

Ligands	λ_{ex} (nm)	λ_{em}(nm)	τ (ns) (Visible region)	Quantum yield Ø in DCM
PS001	502	515	3.52	0.57±0.10
PH1	533	570	3.67	0.468±0.02
PH2	552	580	2.68	0.209±0.01
PH3	571	597	3.41	0.318±0.04
PH4	551	583	2.96	0.113±0.01

Table 3.4 Photophysical properties (fluorescence) of complexes

Complexes	λ_{ex} (nm) (λ_{em} = 980 nm)	λ_{em}(nm) (Vis) (λ_{ex} = 375 nm)	λ_{em}(nm) (NIR)	τ (ns) (Visible region)	τ (μs) (NIR region)	$\emptyset_{Yb}^{Yb}$
PH1-Yb	542	558	977, 1001, 1028	3.74	11.0	0.0048
PH2-Yb	562	574	978, 1002, 1029	2.73	11.1	0.0048
PH3-Yb	570	592	975, 1001, 1025	3.37	11.0	0.0048
PH4-Yb	551	574	975, 1001, 1027	2.97	10.9	0.0047

The ligand to metal ratio was investigated using spectrophotometric titration for all the ligands under the same conditions (Equation3.1). As an example, the titration of the PH1 ligand with $[Yb(hfac)_3 \cdot (H_2O)_2]$ produces a gradual increase in the emission intensity in both UV-vis region and NIR region (Figure 3.12), and at saturation, the intensity is around 1:1 ratio between the ligand and Yb^{3+} ion. Also, the λ_{em} of PH1 ligand UV-Vis spectrum was gradually blue shifted (575 nm to 562 nm) with the complex formation. This pattern clearly was observed for all the ligands except for PH3 ligand in this study. One isosbestic point was observed for PH1 (579 nm), PH2 (625 nm) and PH4 (637 nm) ligands in UV-Vis spectra. The UV-Vis and NIR spectra of PH3 ligand were exhibited increasing of emission intensity at 595 nm and 1001 nm in UV-Vis region and NIR region (Figure 3.13). These observations are significantly different from the studies that

have been done so far. Theoretically, UV-Vis emission should decrease with the NIR emission increase, due to the energy transfer process from the ligand to the ytterbium ion. However, in this study both UV-Vis and NIR emission increased for all four ligands. The bipyridine ligand binding group can quench the BODIPY fluorescence by donating electron to the BODIPY fluorophore using intersystem charge transfer process. Therefore, the BODIPY- bipyridine ligand emission intensity is comparatively lower than the actual fluorescence intensity. However, the electron donating process is gradually inhibited by the ytterbium complex formation, and fluorescence intensity is simultaneously increased with the Yb(III) complex formation.

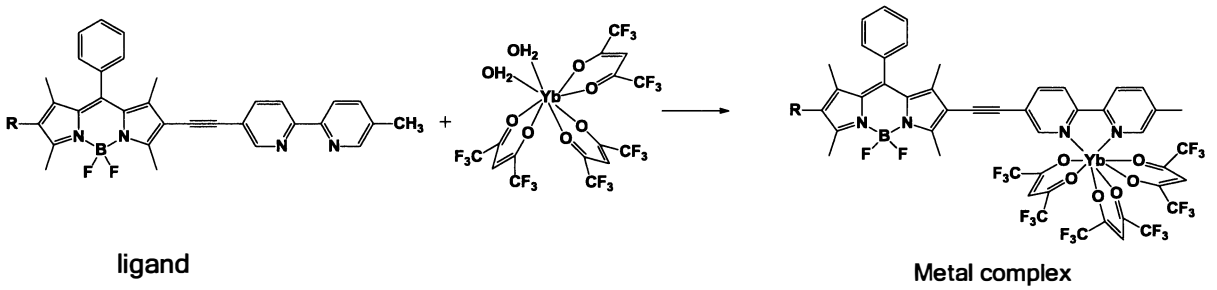

Equation 3.1 Metal complex formation using ligand and $[Yb(hfac)_3 \cdot (H_2O)_2]$

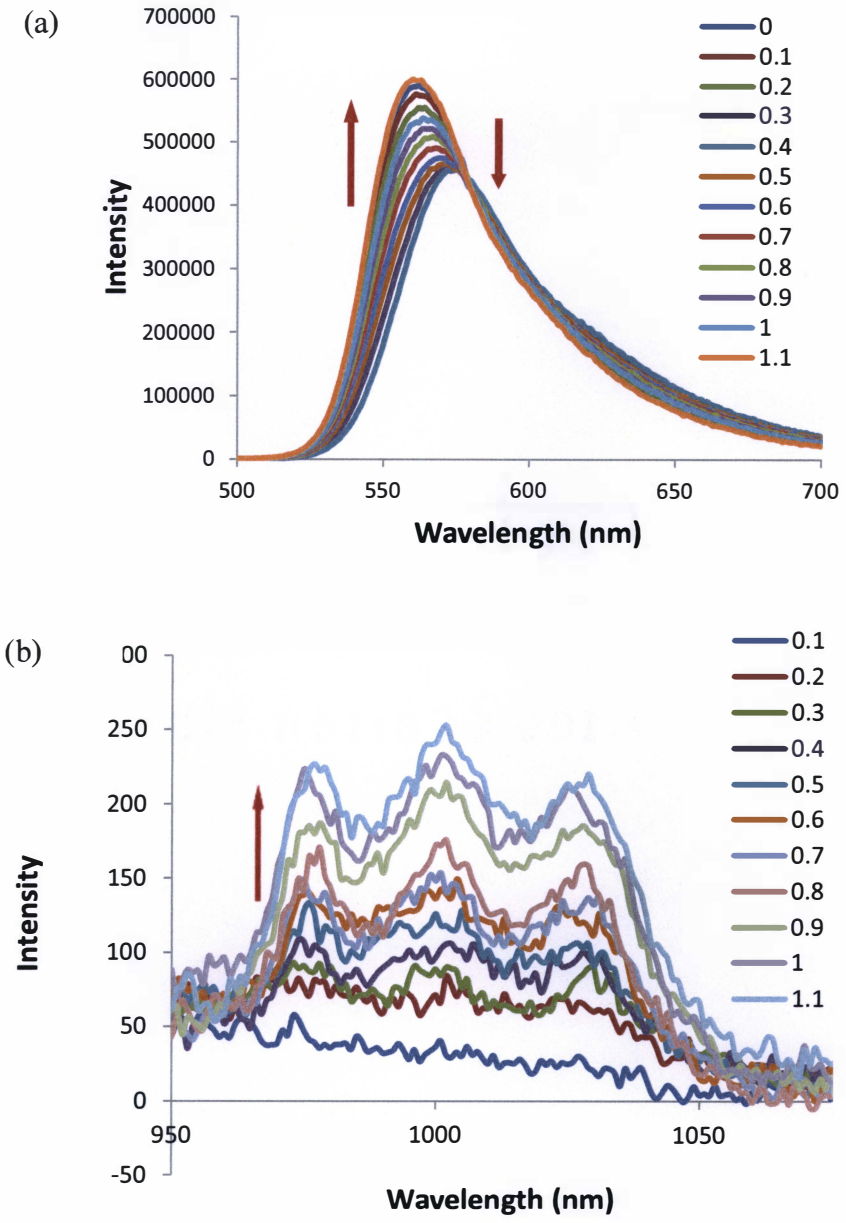

Figure 3.12 (a) UV-Vis emission and (b) NIR emission spectral changes of PH1 ligand upon addition of different amount of $[Yb(hfac)_3 \cdot (H_2O)_2]$in CH_2Cl_2 at room temperature. The concentration of PH1 ligand is 1.6×10^{-6} M. The excitation wavelength was 540 nm.

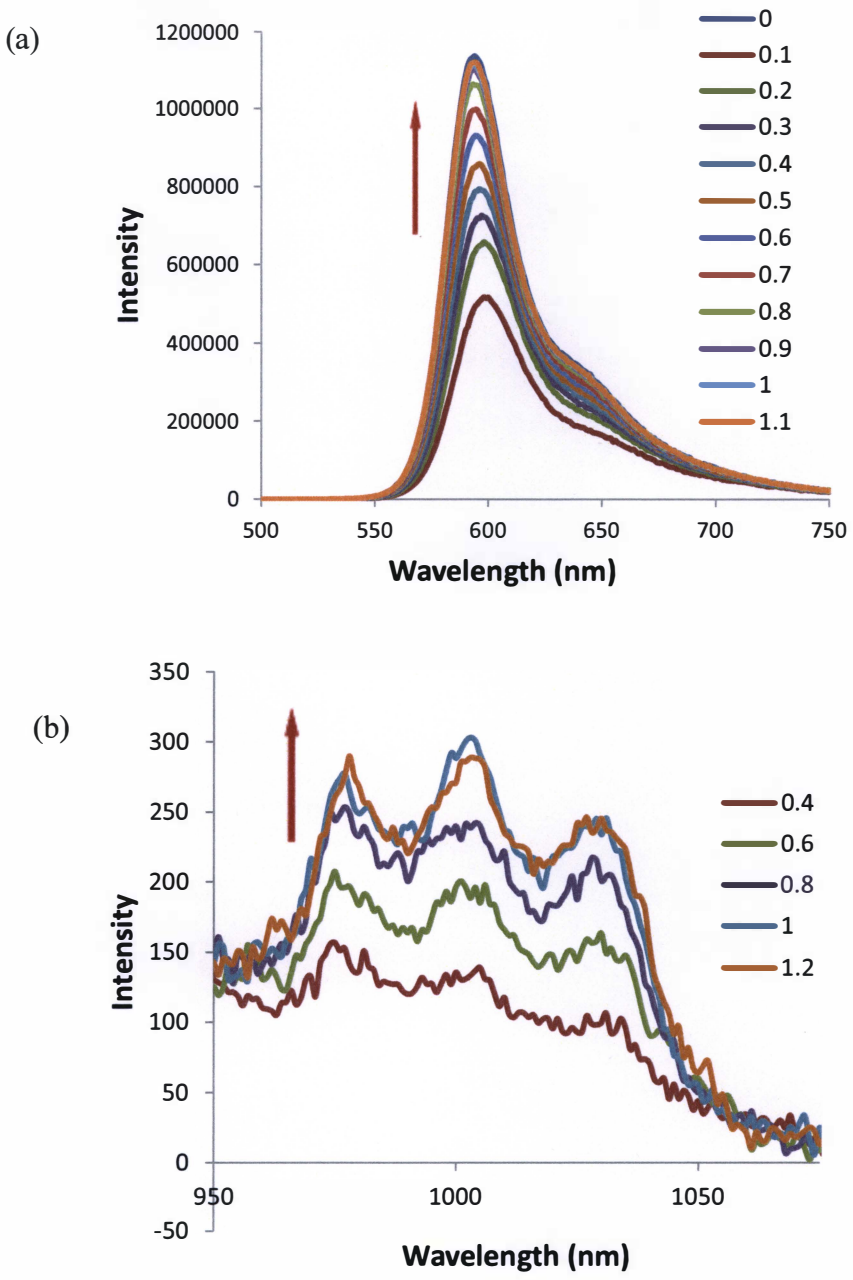

Figure 3.13 (a) UV-Vis emission and (b) NIR emission spectral changes of PH3 ligand upon addition of different amount of $[Yb(hfac)_3 \cdot (H_2O)_2]$ in CH_2Cl_2 at room temperature. The concentration of PH3 ligand is 1.6×10^{-6} M. The excitation wavelength was 570 nm.

CHAPTER 4

CONCLUSION

Currently, medical diagnosis probes have several drawbacks for improvement. One of those is the poor sensitivity of the diagnosis. The application of fluorescent probes inside living cells or biological tissues is a much more complicated process. The biological substrate fluorescence and diagnostic probes fluorescence are significantly overlapped, and it decreases the detection sensitivity.[2] The fluorescence in the ultraviolet region and short wavelength of visible light (<500 nm) causes some issues with the biological applications rather than long wavelength probes because it causes biological degradation of tissues and reduces the detection sensitivity of the measurements by overlapping with the autofluorescence of biological substrates. Therefore, these probes should have some features to give a proper outcome in the biological sensing and imaging diagnosis process. One method for overcoming this problem is to shift the emission from the visible region to the near-infrared region. The NIR region does not only reduce the biological degradation but also increase the detection sensitivity. In addition, NIR light facilitates the *in vivo* tests due to the ability of deep penetration (up to 1-2 cm in depth) of NIR light.[15] One strategy for shifting the absorbance towards these longer wavelength regions involves the extending conjugation of the sensitizer using attaching groups. BODIPY molecules are especially responsive to this method.

The BODIPY scaffold was used as the main skeleton because of its excellent chemical and photophysical properties and high tunable spectral coverage capability. Furthermore, the absorbance and emission spectra are highly influenced by the substituents added to

the BODIPY core. BODIPY dyes are photostable compared to many current dyes, and also their excited state lifetimes are relatively longer than other dyes. The primary goal of this research was to enhance the detection sensitivity by modifying the BODIPY molecule to make long absorption and emission wavelengths. In this study, we attempted to address each of these challenges by synthesizing novel BODIPY dyes with different substituents. Each of the designed dyes contained 5-ethynyl-5'-methyl-2,2'-N-bipyridine group at C2 position of BODIPY core. The desired red-shifted absorbance was obtained by changing the C6position of BODIPY core using hydrogen (PH1), iodine (PH2), 4-ethynylbenzoic acid (PH3) and 1-ethynyl-4-isothiocyanatobenzene (PH4) groups. Finally, a series of novel ytterbium (III) complexes were synthesized by using these ligands.

After column chromatography purification, different yield parentages were obtained for further studies. The first synthetic step produced low and inconsistent yields. Several reaction conditions were attempted, including replacing TFA from boron trifluoride diethyl etherate as a catalyst, placing the reaction mixture in ice during the oxidative process with DDQ and use gravity filtration through silica gel to remove impurities. However, the yields remained around 29%. The iodination reaction was successful with high yields above 75% after column chromatography purification. The Sonogashira reactions were also successful but resulted in comparatively low yields below 40% after purification.

The absorption spectra, emission spectra, and decay curves of synthesized compounds were obtained in CH_2Cl_2 at room temperature. The absorption spectra of ligands and complexes were very similar, and maximum absorption wavelengths increased from 537

nm to 573 nm in the ligands and 535 nm to 571 nm in their complexes. The absorption wavelengths were bathochromically shifted with the π-conjugated system of ligands. PH3 ligand has the longest absorption wavelength compare with the other ligands. The Yb(III) complexes exhibited three peaks centered at 975 nm, 1001 nm, and 1027 nm, respectively. The lifetimes (NIR region) of the Yb(III) complexes (10.9 – 11.1 μs) were mostly similar, which gave the emission yield 0.09%. The PH1 has the highest fluorescence quantum yield efficiency (Ø = 0.478) and the PH4 ligand has the lowest quantum yield efficiency compared with the other two ligands. PH2 also has low quantum yield than PH1 ligand because of the heavy atom iodine significantly quenches its fluorescence. This data illustrated that the NIR emission efficiency decreases in the order PH4 ≈ PH2 > PH3> PH1. The spectrophotometric titration data confirmed the 1:1 ratio of ligand:[$Yb(hfac)_3 \cdot (H_2O)_2$] metal complex. The intensities of both visible and NIR spectra intensity were increased with the Yb(III) concentration, indicating the low efficiency of sensitization by BODIPY-bipyridine ligands. The sensitization process can be inhibited by intermolecular charge transfer process between bipyridine unit and BODIPY core because bipyridine group can facilitate the back charge transfer process. Therefore, this main disadvantage of bipyridine ligand binding group is significantly affected by the sensitization process. However, further improvement of the ligand design has to be implemented to increase the energy-transfer efficiency in NIR region. Future work include the investigation of highly efficient energy transfer ligand using 1,10-phenanthroline ligand binding group by replacing bipyridine ligand.

REFERENCES

1. Buenzli, J.-C. G. *Luminescent Lanthanide Probes as Diagnostic and Therapeutic Tools*; Dekker: 2004.
2. Wu, J.; Wang, G.; Jin, D.; Yuan, J.; Guan, Y.; Piper, J., Luminescent Europium Nanoparticles with a Wide Excitation Range from UV tto Visible Light for Biolabeling and Time-Gated Luminescence Bioimaging. *Chem Commun* **2008**, 365-367.
3. Comby, S.; Bünzli, J.-C. G., Lanthanide Near-Infrared Luminescence in Molecular Probes and Devices. *Handbook on the Physics and Chemistry of Rare Earths* **2007,** *37*, 217-470.
4. He, H., Near-Infrared Emitting Lanthanide Complexes of Porphyrin and BODIPY Dyes. *Coord Chem Rev* **2014,** *273*, 87-99.
5. Pershagen, E.; Borbas, K. E., Designing Reactivity-Based Responsive Lanthanide Probes for Multicolor Detection in Biological Systems. *Coord Chem Rev* **2014,** *273*, 30-46.
6. Lakowicz, J. R., Fluorescence Anisotropy. in *Principles of Fluorescence Spectroscopy*, Springer: 1999; Pp 291-319.
7. Udenfriend, S., Development of the Spectrophotofluorometer and its Commercialization. *Protien Sci* **1995,** *4*, 542-551.
8. Pringsheim, P., Fluorescence And Phosphorescence. **1949,** pp 54-62.
9. Mcgown, L. B.; Nithipatikom, K., Molecular Fluorescence And Phosphorescence. **2000,** pp 154-168.

10. Albani, J. R., Fluorescence Quenching. *Principles And Applications Of Fluores Spectr* **2007**, 139-159.

11. Wilkinson, M. H.; Schut, F., Digital Image Analysis of Microbes: Imaging, Morphometry, Fluorometry and Motility Techniques and Applications. *John Wiley & Sons:* **1998**.

12. Mason, W. T., Fluorescent and Luminescent Probes for Biological Activity: A Practical Guide To Technology For Quantitative Real-Time Analysis. *Academic Press:* **1999,** pp 75-82

13. Demchenko, A. P., Introduction to Fluorescence Sensing. *Springer Science & Business Media*: **2008,** pp 94-108.

14. Lakowicz, J. R., Topics in Fluorescence Spectroscopy: *Probe Design And Chemical Sensing. Springer Science & Business Media:* 1994; Vol. 4.

15. Zhang, J., Design and Development of Bodipy-Based Fluorescent Probes for Sensing and Imaging of Cyanide, Zn (II) Ions, Lysosomal Ph and Cancer Cells. Masters' dissertation, Michigon Technological University, **2015,** pp 8- 54

16. Zhong, Y.; Si, L.; He, H.; Sykes, A. G., BODIPY Chromophores as Efficient Green Light Sensitizers for Lanthanide-Induced Near-Infrared Emission. *Dalt Trans* **2011,** *40*, 11389-11395.

17. Loudet, A.; Burgess, K., BODIPY Dyes And Their Derivatives: Syntheses And Spectroscopic Properties. *Chem Rev* **2007,** *107*, 4891-4932.

18. Tram, K.; Yan, H.; Jenkins, H. A.; Vassiliev, S.; Bruce, D., The Synthesis and Crystal Structure of Unsubstituted 4, 4-Difluoro-4-Bora-3a, 4a-Diaza-S-Indacene (BODIPY). *Dyes and Pigm* **2009,** *82*, 392-395.

19. Yogo, T.; Urano, Y.; Ishitsuka, Y.; Maniwa, F.; Nagano, T., Highly Efficient and Photostable Photosensitizer Based on BODIPY Chromophore. *Jour of the Amer Chemical Soc* **2005,** *127*, 12162-12163.

20. Lim, S. H.; Thivierge, C.; Nowak-Sliwinska, P.; Han, J.; Van Den Bergh, H.; Wagnieres, G.; Burgess, K.; Lee, H. B., In Vitro And In Vivo Photocytotoxicity Of Boron Dipyrromethene Derivatives for Photodynamic Therapy. *Jour of Med Chem* **2010,** *53*, 2865-2874.

21. Adarsh, N.; Avirah, R. R.; Ramaiah, D., Tuning Photosensitized Singlet Oxygen Generation Efficiency of Novel Aza-BODIPY Dyes. *Org Lett***2010,** *12*, 5720-5723.

22. Sonogashira, K.; Tohda, Y.; Hagihara, N., A Convenient Synthesis of Acetylenes: Catalytic Substitutions of Acetylenic Hydrogen with Bromoalkenes, Iodoarenes and Bromopyridines. *Tetra Lett* **1975,** *16*, 4467-4470.

23. Liang, Y.; Xie, Y.-X.; Li, J.-H., Modified Palladium-Catalyzed Sonogashira Cross-Coupling Reactions Under Copper-, Amine-, And Solvent-Free Conditions. *The Jour of Org Chem* **2006,** *71*, 379-381.

24. Chinchilla, R.; Nájera, C., The Sonogashira Reaction: a Booming Methodology in Synthetic Organic Chemistry. *Chem Rev* **2007,** *107*, 874-922.

25. Hänninen, P.; Härmä, H., *Lanthanide Luminescence: Photophysical, Analytical and Biological Aspects*. *Springer Science & Business Media*: **2011,** Vol. 7.

26. Heffern, M. C.; Matosziuk, L. M.; Meade, T. J., Lanthanide Probes for Bioresponsive Imaging. *Chem Rev* **2013,** *114*, 4496-4539.

27. Vogler, A.; Kunkely, H., Excited State Properties of Lanthanide Complexes: Beyond Ff States. *Inorg Chim Acta* **2006,** *359*, 4130-4138.

28. Bünzli, J.-C. G.; Piguet, C., Taking Advantage of Luminescent Lanthanide Ions. *Chem Soci Rev* **2005,** *34*, 1048-1077.

29. Thibon, A.; Pierre, V. C., Principles of Responsive Lanthanide-Based Luminescent Probes for Cellular Imaging. *Analy and Bioanaly Chem* **2009,** *394*, 107-120.

30. Weissman, S., Intramolecular Energy Transfer the Fluorescence of Complexes of Europium. *The Jour of Chem Phys* **1942,** *10*, 214-217.

31. Grabowski, Z. R.; Rotkiewicz, K.; Rettig, W., Structural Changes Accompanying Intramolecular Electron Transfer: Focus on Twisted Intramolecular Charge-Transfer States and Structures. *Chem Rev* **2003,** *103*, 3899-4032.

32. Hemmilä, I.; Laitala, V., Progress In Lanthanides As Luminescent Probes. *Jour of Fluores* **2005,** *15*, 529-542.

33. Varlan, M., Selective Activation of Terbium (III) And Europium (III) Luminescence with Triarylboron-Functionnalized Carboxylate Ligands. And Luminescent 8-Hydroxyquinoline Dipicolylamine Complexes as Sensors for Zinc (II), Masters' dissertation, Queen's University, **2012,** pp 9-20.

34. Lunstroot, K.; Driesen, K.; Nockemann, P.; Van Hecke, K.; Van Meervelt, L.; Görller-Walrand, C.; Binnemans, K.; Bellayer, S.; Viau, L.; Le Bideau, J., Lanthanide-Doped Luminescent Ionogels. *Dalt Trans* **2009,** 298-306.

35. Lenaerts, P.; Ryckebosch, E.; Driesen, K.; Van Deun, R.; Nockemann, P.; Görller-Walrand, C.; Binnemans, K., Study of The Luminescence of Tris (2-Thenoyltrifluoroacetonato) Lanthanide (III) Complexes Covalently Linked to 1, 10-Phenanthroline-Functionalized Hybrid Sol–Gel Glasses. *Journal of Luminescence* **2005,** *114*, 77-84.

36. Zhang, Y.; Shi, J.; Zheng, Y.; Yu, M.; Liu, G., Lanthanide Porphyrin Complexes: Synthesis And Properties. *Synth and Reacti in Inorg, Metal-Org, and Nano-Metal Chem* **2009,** *39*, 605-608.

37. Ning, Y.; Ke, X.-S.; Hu, J.-Y.; Liu, Y.-W.; Ma, F.; Sun, H.-L.; Zhang, J.-L., Bioinspired Orientation of B-Substituents on Porphyrin Antenna Ligands Switches Ytterbium (III) NIR Emission with Thermosensitivity. *Inorg Chem* **2017**.

38. Shavaleev, N. M.; Scopelliti, R.; Gumy, F.; BüNzli, J.-C. G., Surprisingly Bright Near-Infrared Luminescence and Short Radiative Lifetimes Of Ytterbium in Hetero-Binuclear Yb− Na Chelates. *Inorg Chem* **2009,** *48*, 7937-7946.

39. Rizzo, F.; Meinardi, F.; Tubino, R.; Pagliarin, R.; Dellepiane, G.; Papagni, A., Synthesis of 8-Hydroxyquinoline Functionalised DO3A Ligand and Eu (III) and Er (III) Complexes: Luminescence Properties. *Synth Metals* **2009,** *159*, 356-360.

40. Song, S. N.; Li, D. M.; Wu, J. F.; Zhuang, C. F.; Ding, H.; Song, W. B.; Cui, L. F.; Cao, G. Z.; Liu, G. F., Syntheses and Characterization of Molybdenum/Zinc Porphyrin Dimers Bridged by Aromatic Linkers. *Euro Jour of Inorg Chem* **2007**, 1844-1853.

41. Wong, W.-K.; Hou, A.; Guo, J.; He, H.; Zhang, L.; Wong, W.-Y.; Li, K.-F.; Cheah, K.-W.; Xue, F.; Mak, T. C., Synthesis, Structure and Near-Infrared Luminescence of Neutral 3d–4f Bi-Metallic Monoporphyrinate Complexes. *Jour of the Chem Soci, Dalt Trans* **2001,** 3092-3098.

42. He, H.-S.; Zhao, Z.-X.; Wong, W.-K.; Li, K.-F.; Meng, J.-X.; Cheah, K.-W., Synthesis, Characterization and Near-Infrared Photoluminescent Studies of Diethyl Malonate Appended Mono-Porphyrinate Lanthanide Complexes. *Dalt Trans* **2003,** 980-986.

43. He, H.; Sykes, A. G.; May, P. S.; He, G., Structure And Photophysics of Near-Infrared Emissive Ytterbium (III) Monoporphyrinate Acetate Complexes Having Neutral Bidentate Ligands. *Dalt Trans* **2009,** 7454-7461.

44. Gschneidner, K. A.; Bünzli, J.-C. G.; Pecharsky, V. K., Handbook on the Physics and Chemistry of Rare Earths*: Opti Spectro*. Elsevier: **2011**; Vol. 37.

45. Gschneider, K.; Eyring, L.; Roth, T., Handbook on The Physics and Chemistry of Rare Earths, Vol. 1: Metals. *Jour of The Electrochemical Society* **1979,** *126*, 464C-464C.

46. Martín-Ramos, P.; Silva, M. R.; Coya, C.; Zaldo, C.; Álvarez, Á. L.; Álvarez-García, S.; Beja, A. M. M.; Martín-Gil, J., Novel Erbium (III) Fluorinated B-Diketonate Complexes With N, N-Donors for Optoelectronics: from Synthesis to Solution-Processed Devices. *Jour of Mater Chemi C* **2013,** *1*, 2725-2734.

47. Xin, H.; Li, F. Y.; Shi, M.; Bian, Z. Q.; Huang, C. H., Efficient Electroluminescence from a New Terbium Complex. *Jour of the Amer Chem Soc* **2003,** *125*, 7166-7167.

48. Shavaleev, N. M.; Scopelliti, R.; Gumy, F.; Bünzli, J. C. G., Visible-Light Excitation of Infrared Lanthanide Luminescence via Intra-Ligand Charge-Transfer State In 1, 3-Diketonates Containing Push-Pull Chromophores. *Euro Jour of Inorg Chem* **2008,** 1523-1529.

49. Ziessel, R. F.; Ulrich, G.; Charbonnière, L.; Imbert, D.; Scopelliti, R.; Bünzli, J. C. G., NIR Lanthanide Luminescence by Energy Transfer from Appended Terpyridine–Boradiazaindacene Dyes. *Chem a Euro Jour* **2006,** *12*, 5060-5067.

50. Ryu, J. H.; Eom, Y. K.; Bünzli, J.-C. G.; Kim, H. K., Ln (III)-Cored Complexes Based on Boron Dipyrromethene (Bodipy) Ligands for NIR Emission. *New Jour of Chem* **2012,** *36*, 723-731.

51. He, H.; Si, L.; Zhong, Y.; Dubey, M., Iodized BODIPY as a Long Wavelength Light Sensitizer for the Near-Infrared Emission of Ytterbium (III) Ion. *Chem Commun* **2012,** *48*, 1886-1888.

52. Kong, J.-F.; Wang, J.-R.; Yuan, L.-H.; Lu, X.-X.; Li, W.-P., Synthesis of Redox-Active Macrocyclic Diimine Ligands as Flexible Building Blocks. *Asian Jour of Chem* **2013,** *25*, 3301.

APPENDIX

Experimental details of crystal data collection: PS001

Data collection	
Diffractometer	Bruker APEXII CCD
Absorption correction	Multi-scan
No. of measured, independent and observed [$I > 2\sigma(I)$] reflections	42493, 3051, 1844
R_{int}	0.108
$(\sin \theta/\lambda)_{max}$ ($Å^{-1}$)	0.602
Refinement	
$R[F^2 > 2\sigma(F^2)]$, $wR(F^2)$, S	0.066, 0.186, 0.99
No.of reflections	3051
No.of parameters	222
H-atom treatment	H-atom parameters constrained
$\Delta\rho_{max}$, $\Delta\rho_{min}$ (e $Å^{-3}$)	0.19, −0.36

Computer programs: *SHELXL2014/7* (Sheldrick, 2014).

Experimental details of crystal data collection: PH2-Yb

Data collection	
Diffractometer	Bruker APEXII CCD
Absorption correction	Multi-scan
T_{min}, T_{max}	0.482, 0.753
No. of measured, independent and observed [$I > 2\sigma(I)$] reflections	81326, 9827, 6952
R_{int}	0.150
$(\sin \theta/\lambda)_{max}$ (Å^{-1})	0.602
Refinement	
$R[F^2 > 2\sigma(F^2)]$, $wR(F^2)$, S	0.052, 0.132, 1.02
No. of reflections	9827
No. of parameters	755
No. of restraints	78
H-atom treatment	H-atom parameters constrained $w = 1/[\sigma^2(F_o^2) + (0.0441P)^2 + 16.4545P]$ where $P = (F_o^2 + 2F_c^2)/3$
$\Delta\rho_{max}$, $\Delta\rho_{min}$ (e Å^{-3})	1.19, −0.94

NMR data

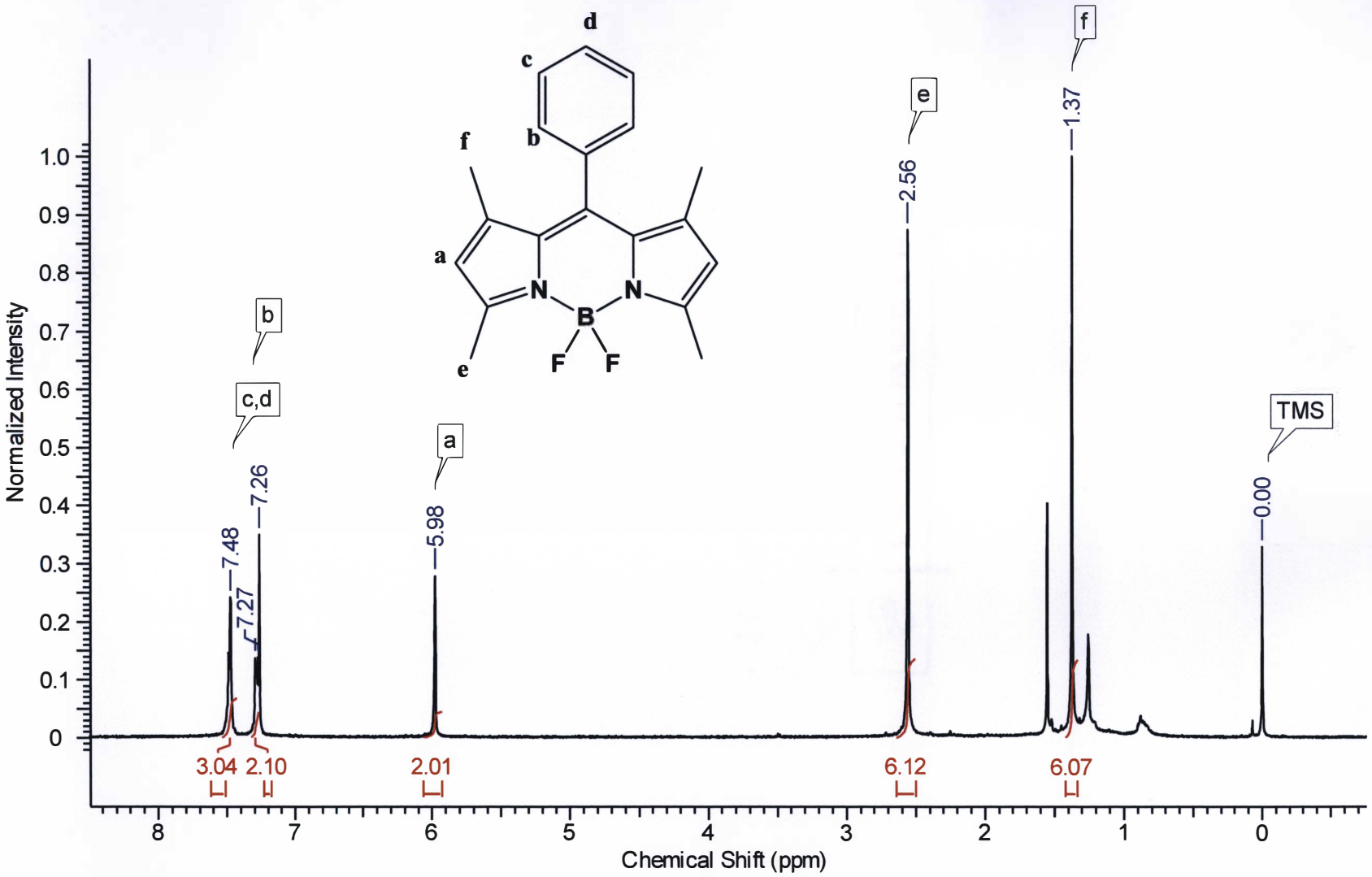

Figure A.1 The 1H NMR spectrum of PS001

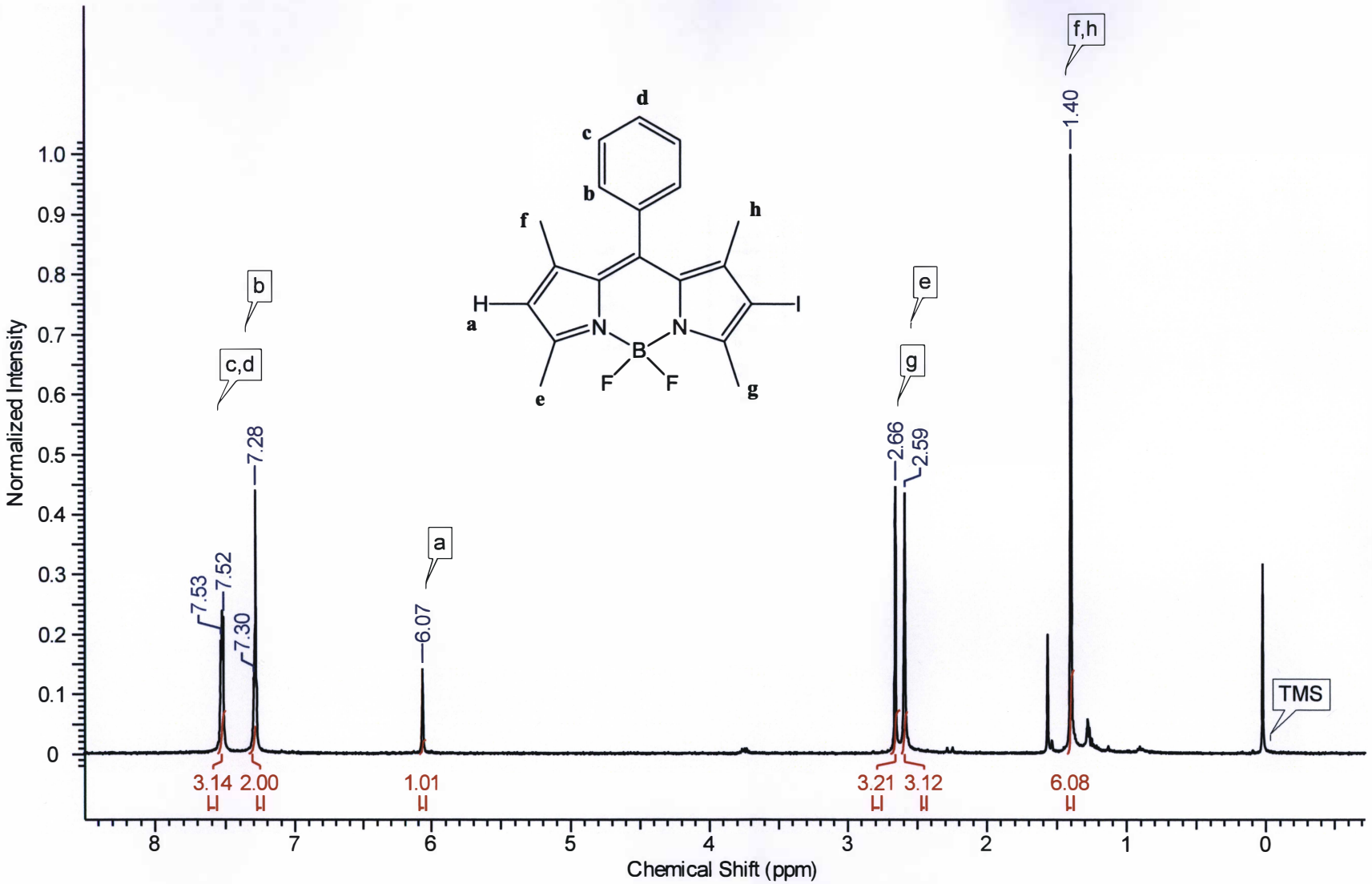

Figure A.2 The 1H NMR spectrum of PS002

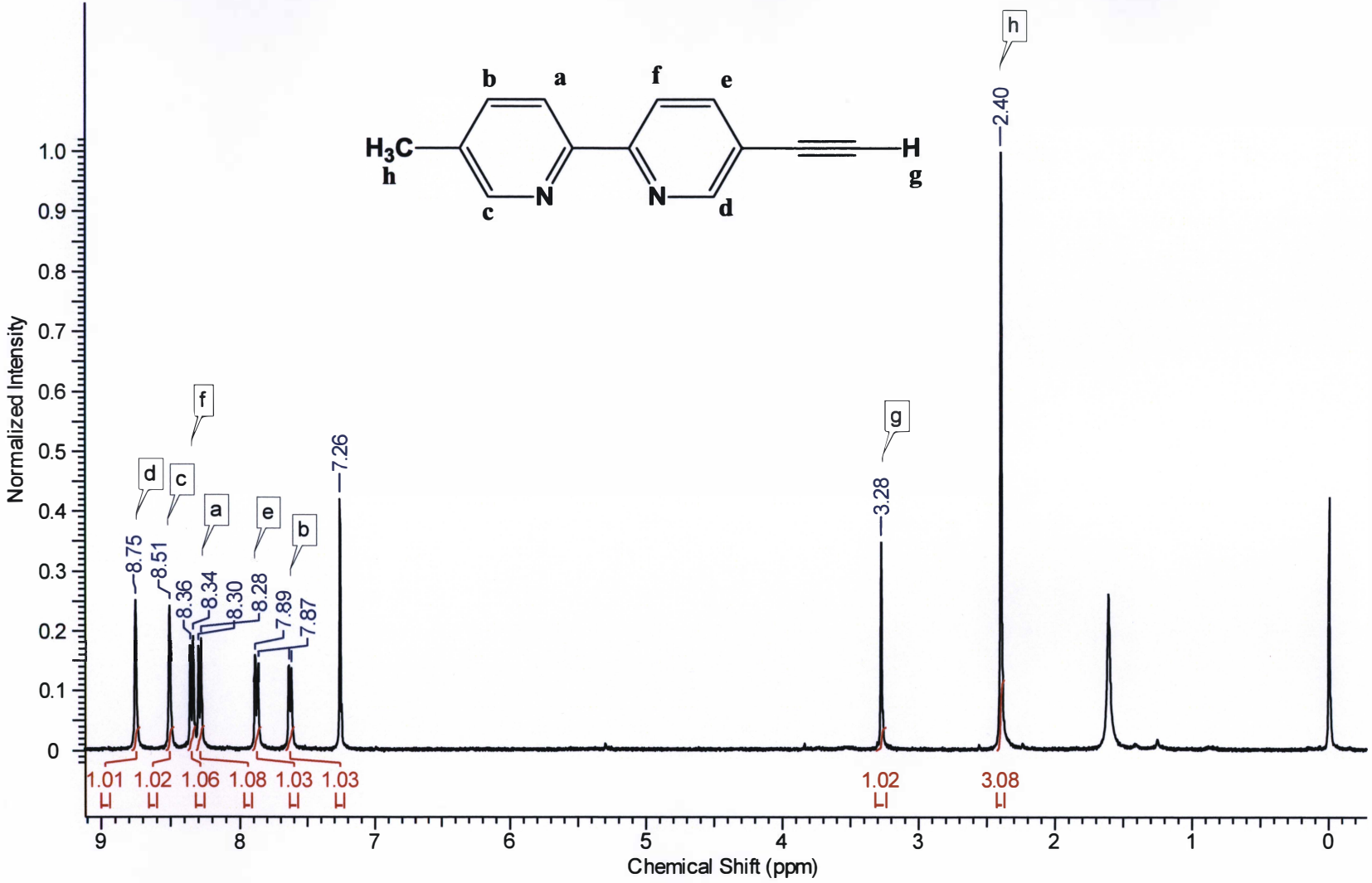

Figure A.3 The 1H NMR spectrum of PS003

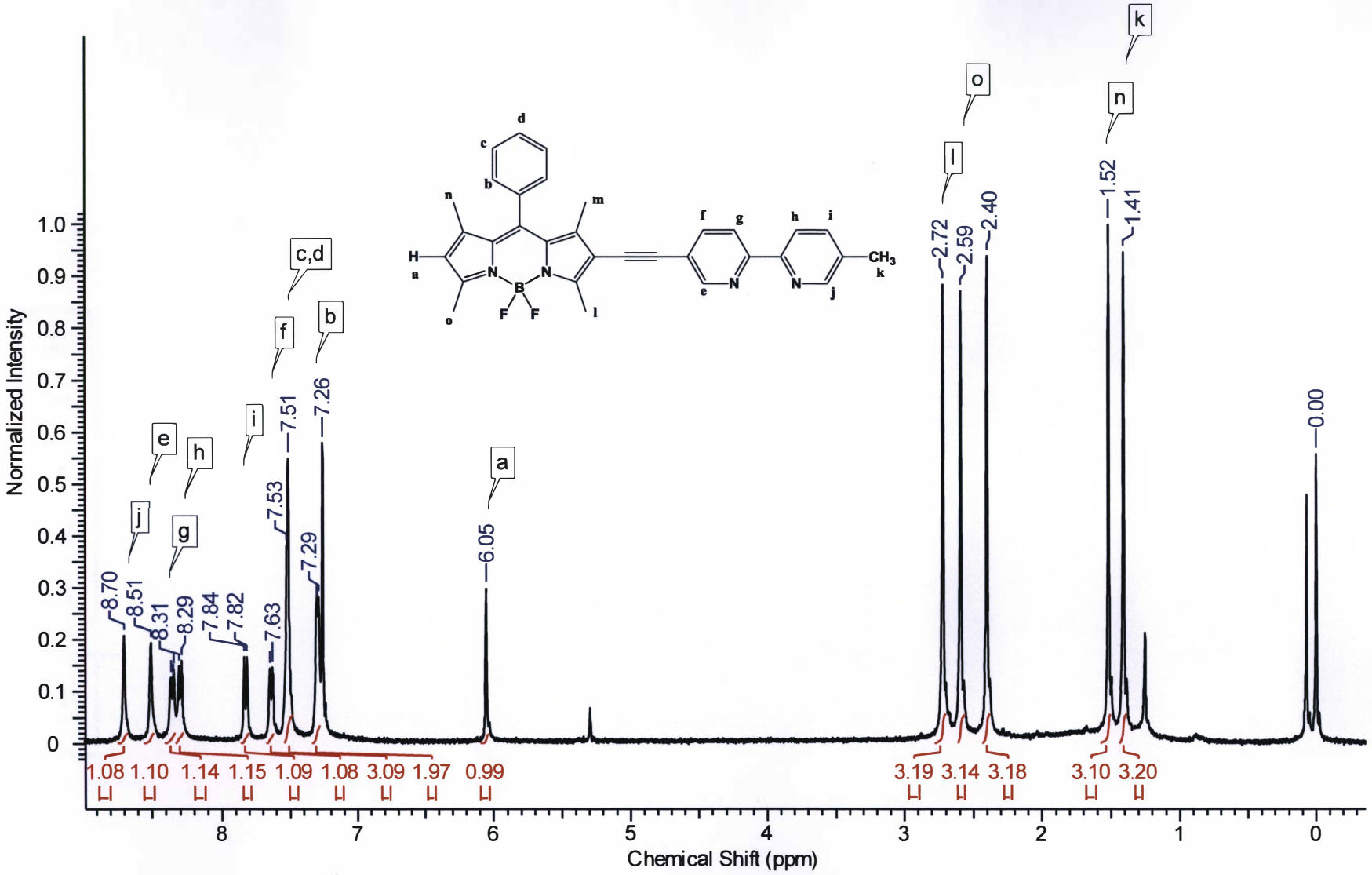

Figure A.4 The 1H NMR spectrum of PH1

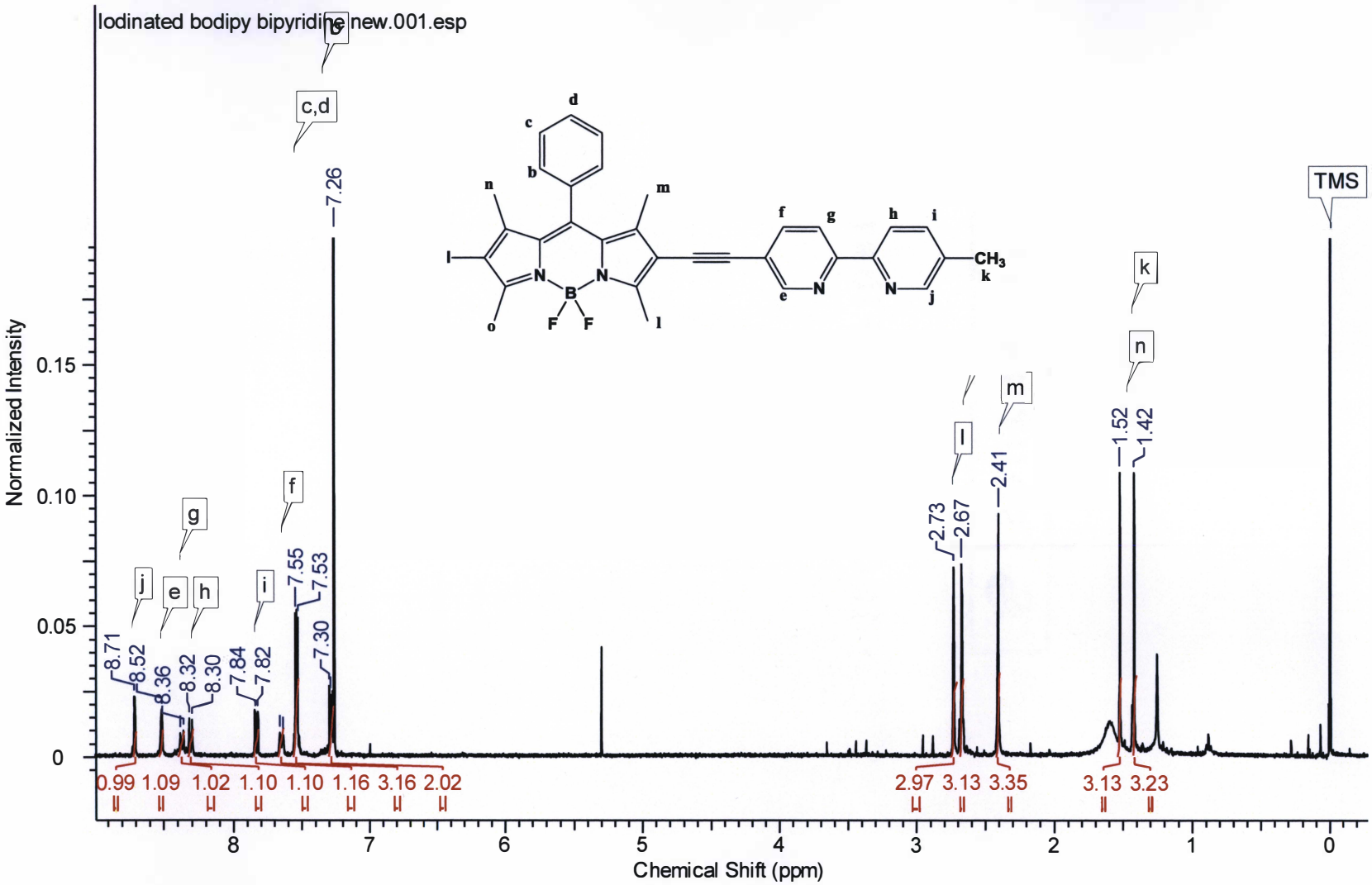

Figure A.5 The 1H NMR spectrum of PH2

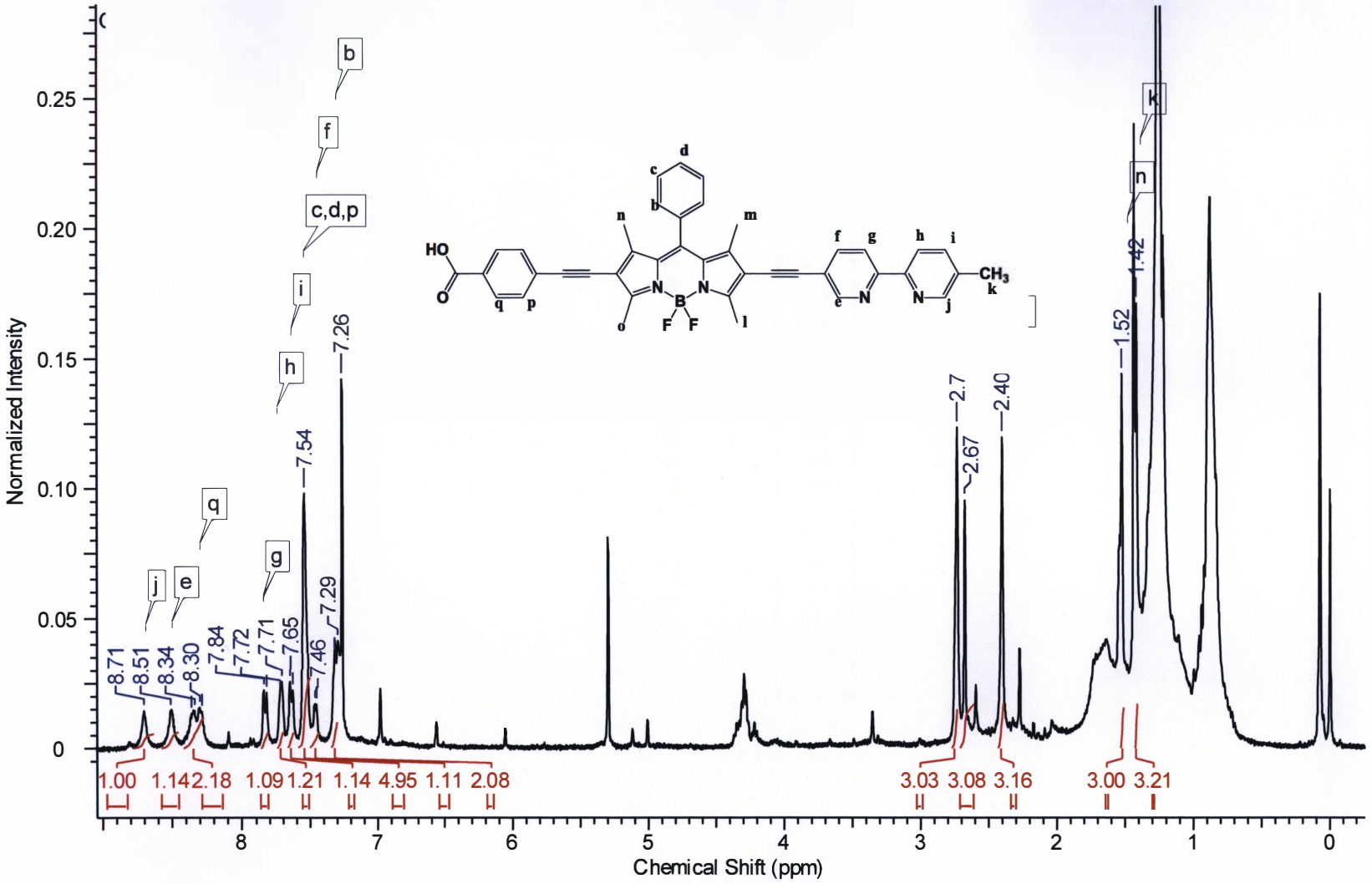

Figure A.6 The 1H NMR spectrum of PH3

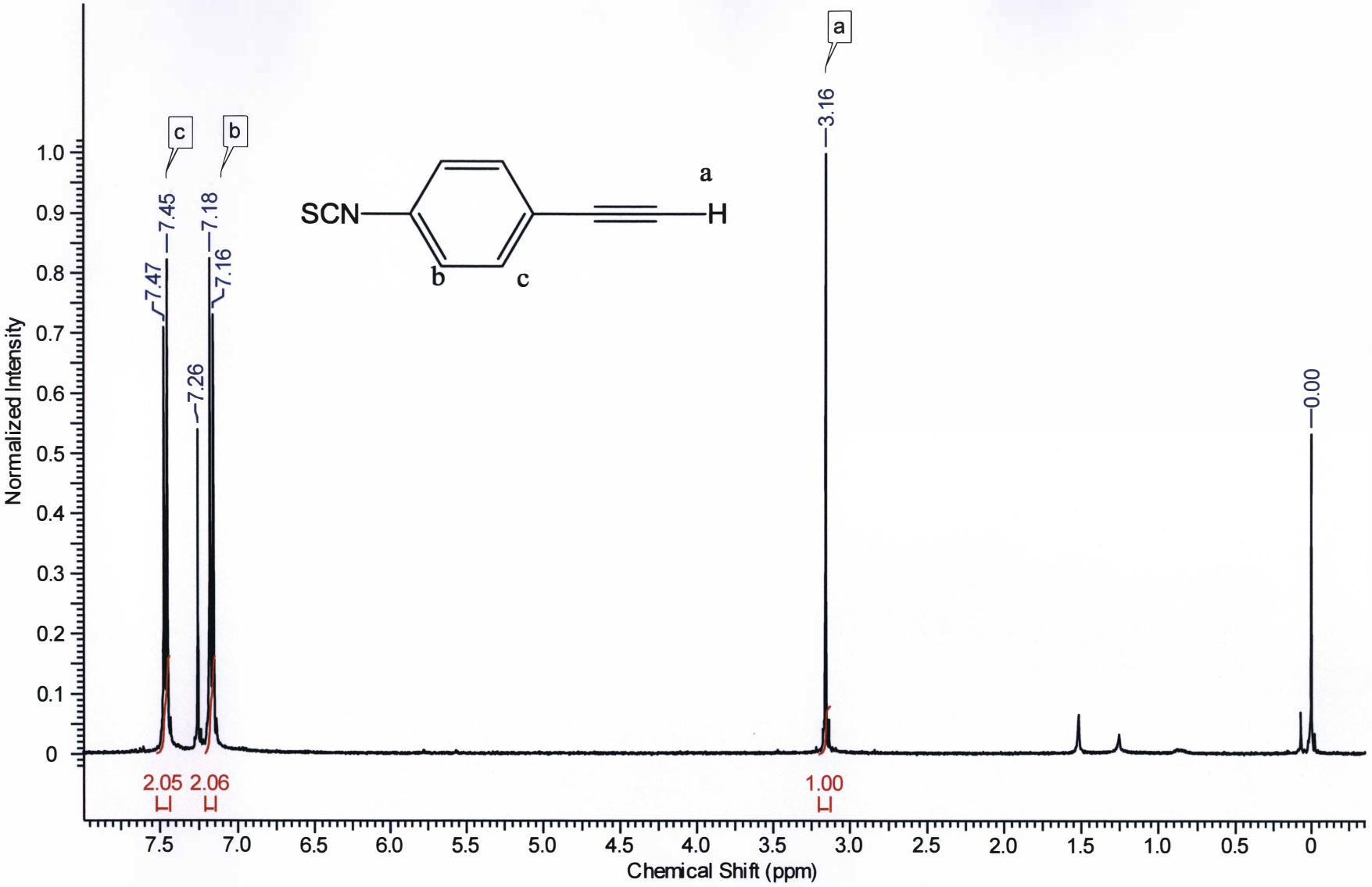

Figure A.7 The 1H NMR spectrum of PS004

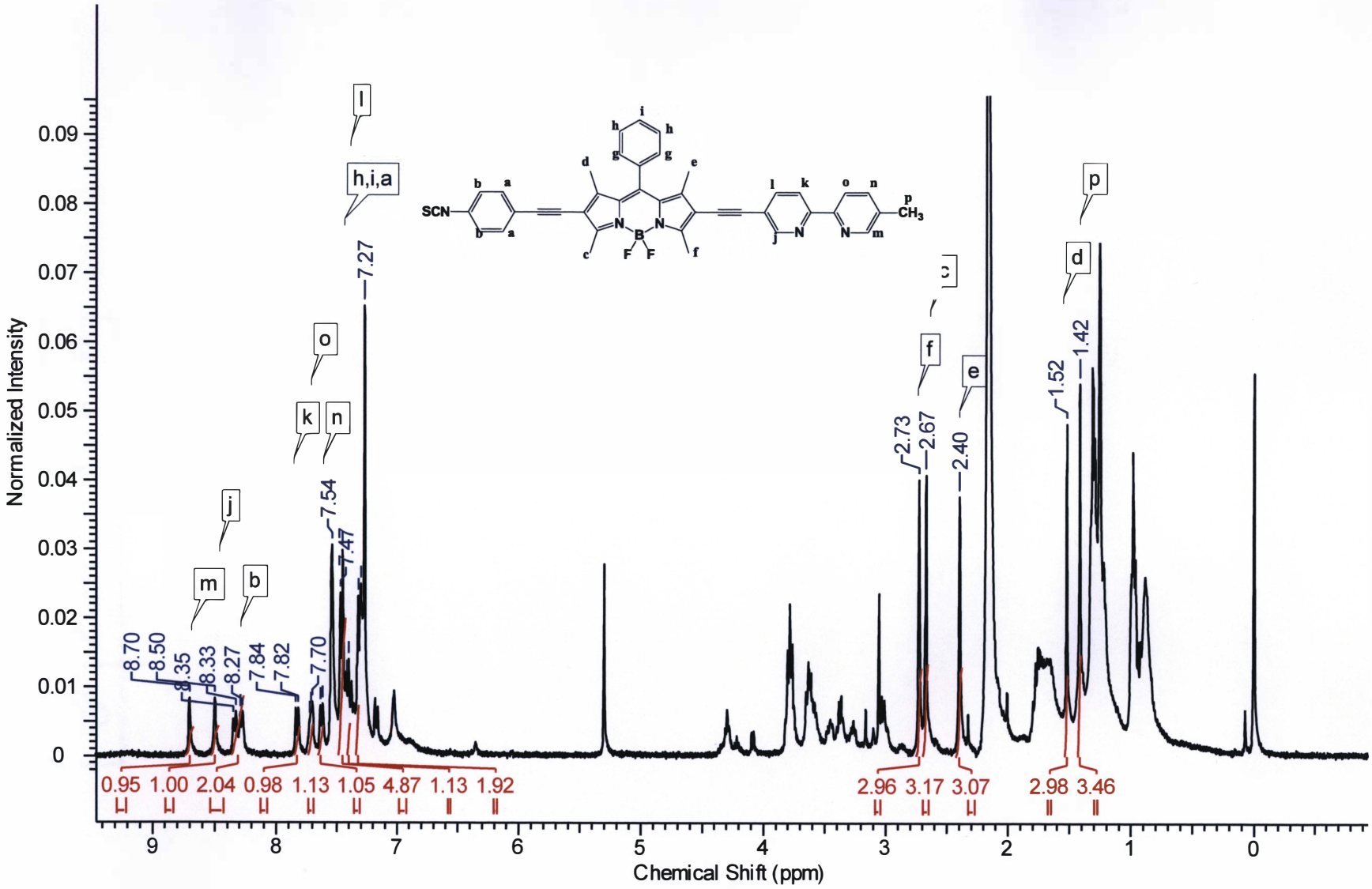

Figure A.8 The 1H NMR spectrum of PH4

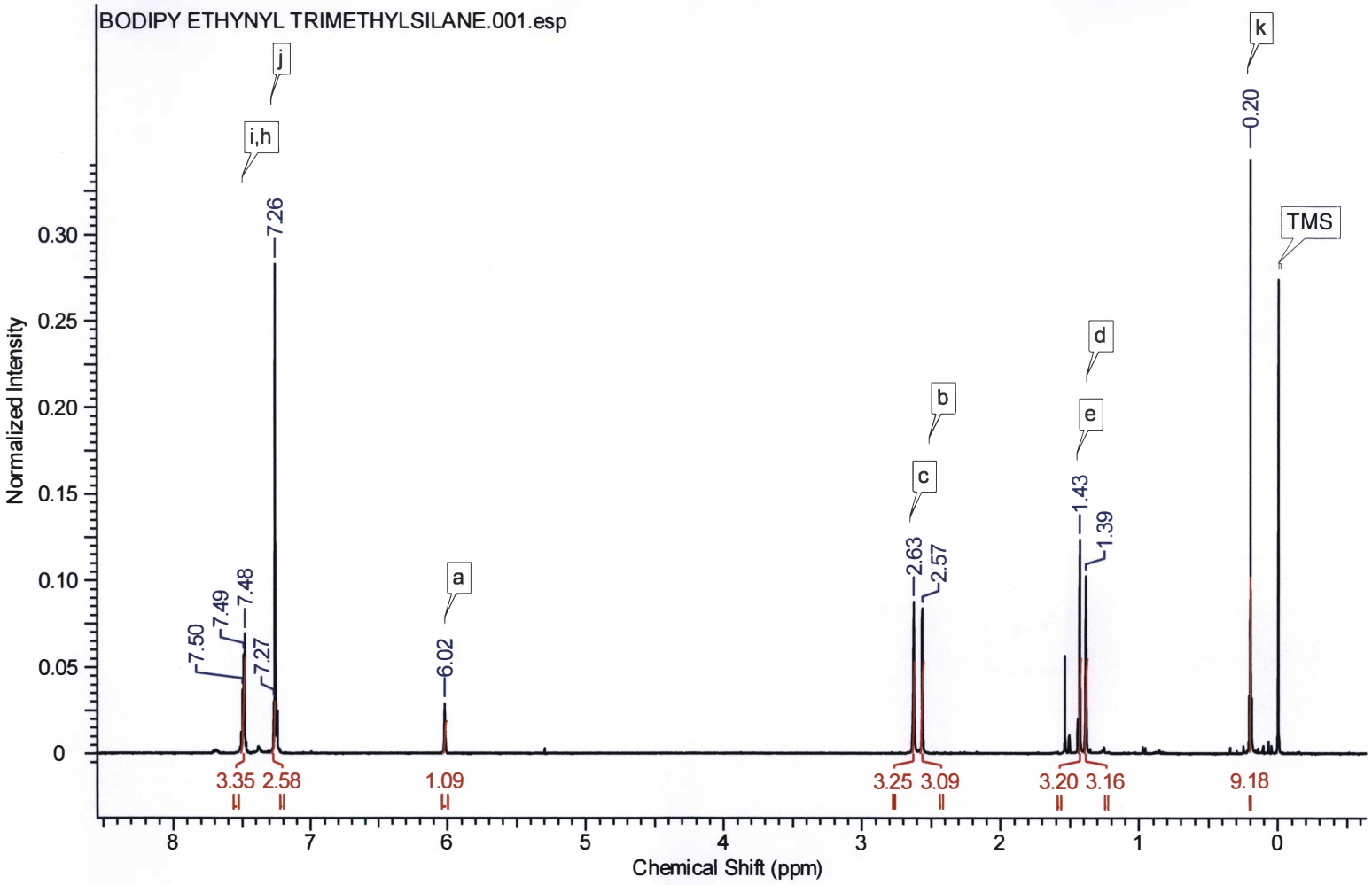

Figure A.9 The 1H NMR spectrum of PS005

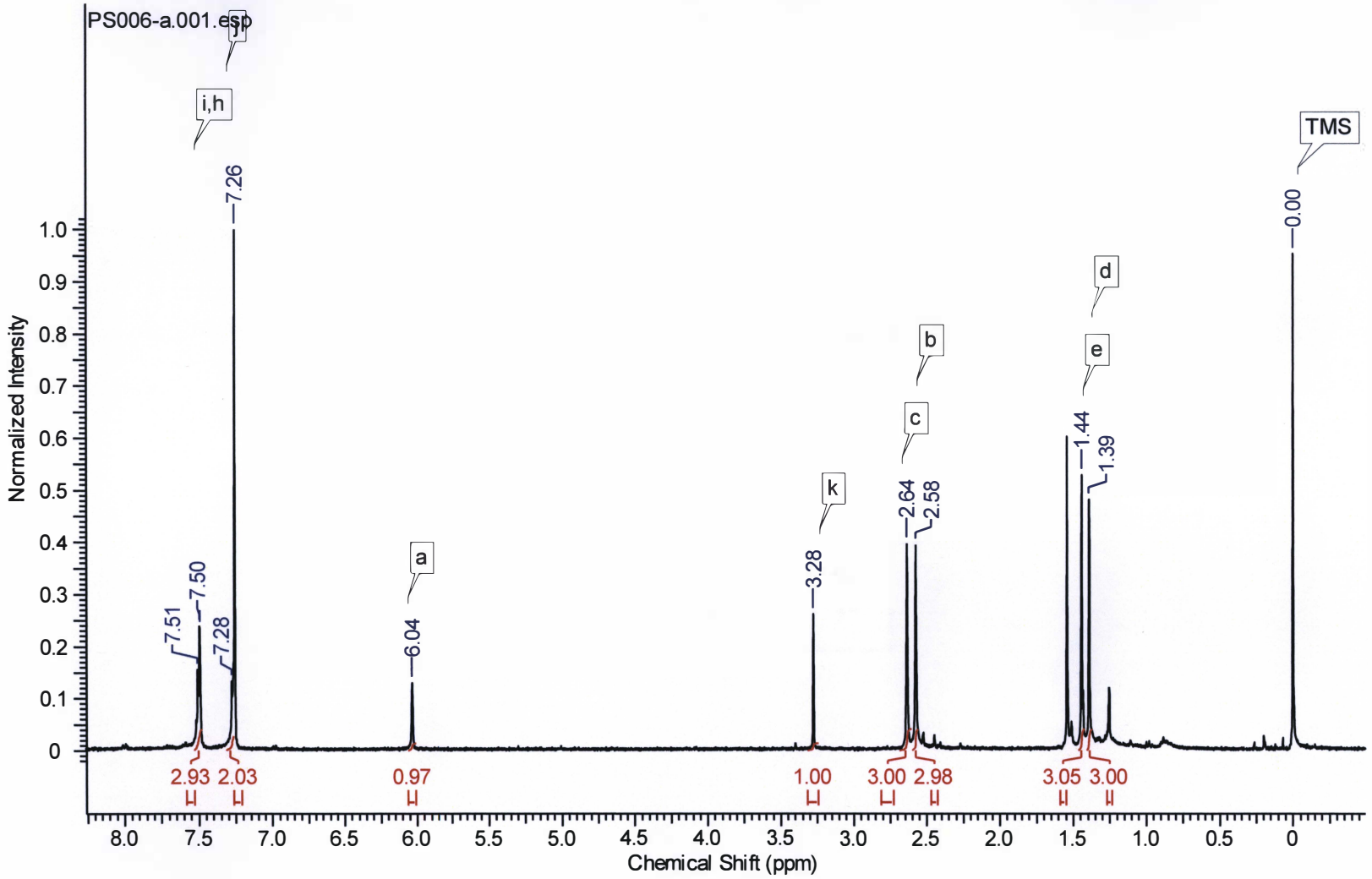

Figure A.10 The 1H NMR spectrum of PS006